Aus der Medizinischen Klinik und Poliklinik IV

Klinik der Universität München

Direktor: Prof. Dr. med. Martin Reincke

DKK3 Driven Wnt Pathway in Radiation-induced Inflammatory

and Fibrosing Skin Injury

Dissertation

zum Erwerb des Doktorgrades der Humanbiologie

an der Medizinischen Fakultät der

Ludwig-Maximilians-Universität zu München

vorgelegt von

Li Li

aus Sichuan, China

2023

Mit Genehmigung der Medizinischen Fakultät

der Universität München

Berichterstatter:	Prof. Dr. Peter J. Nelson
Mitberichterstatter:	Prof. Dr. Christine Spitzweg
	Prof. Dr. Michael Flaig
Mitbetreuung durch den promovierten Mitarbeiter:	Prof. Dr. Dr. Peter E. Huber
	P. D. Dr. Roger Sandhoff
Dekan:	Prof. Dr. med. Thomas Gudermann
Tag der mündlichen Prüfung:	23.06.2023

Contents

Zusammenfassung

Die Radiodermatitis ist eine häufige unerwünschte Nebenwirkung bei der Strahlentherapie maligner Tumoren. Besonders bei hautnahen Tumoren treten Hautaffektionen auf, die von leichten, vorübergehenden Rötungen und Entzündungen bis hin zu schweren Ulzerationen und Nekrosen reichen können. Für die schwerwiegenden Formen chronischer Strahlendermatitiden und Fibrosen, die eine erhebliche Einschränkung der Lebensqualität bedeuten können, gibt es keine gut wirksame medikamentöse Therapie, was den dringenden Bedarf an neuen Behandlungsstrategien unterstreicht. Vor dieser Arbeit war bekannt, dass der kanonische Wnt-Signalweg eine wichtige Rolle in der Entstehung von strahleninduzierter Dermatitis und Fibrose einnimmt und daher ein potenzielles Ziel für die Behandlung darstellt. Vom löslichen Faktor Dickkopf 3 (WNT Signalweg Inhibitor 3,DKK3) war bekannt, dass er die kanonische Wnt-Aktivität in zellspezifischer Weise moduliert. Eine frühere Studie der eigenen Gruppe, in der die Rolle von DKK3 in der entzündlichen Nierenfibrose beschriebenen wurde, deutete darauf hin, dass epitheliales DKK3 die kanonische Wnt-Signalübertragung aktivieren kann und dadurch eine profibrotische- und immunpolarisierende Rolle bei der Nierenfibrose spielen könnte. Pilotstudien mit bestrahlten Mäusen legten außerdem nahe, dass eine globale Deletion von DKK3, die Tiere möglicherweise vor strahleninduzierter Hyperplasie und Hautfibrose schützen könnten. Aufgrund dieser Vorbefunde wurde die Hypothese aufgestellt, dass nach einer Strahlenschädigung die DKK3-Expression in Verbindung mit der kanonischen Wnt-Aktivierung zu einer kompensatorischen hyperreaktiven epidermalen Hyperplasie, entzündlichen Infiltration und Fibrose führt.

Um diese Hypothese zu untermauern, wurde ein Modell für strahleninduzierte Hauthyperplasie und entzündliche Fibrose entwickelt, in dem eine einmalige Strahlendosis von 20Gy bei C57BL/N-Wildtyp-Mäusen eine reproduzierbare chronische Strahlendermatitis auslöste. Vier bis acht Wochen nach der Bestrahlung wurde in der Haut der bestrahlten Mäuse im Vergleich zu den nicht bestrahlten

Kontrollen eine signifikante Hyperplasie, myeloische Infiltration und Fibrose festgestellt. Um den zellulären Ursprung von DKK3 zu identifizieren und seine Aktivität in der kanonischen Wnt-Signalübertragung in bestrahlter Mäusehaut zu verfolgen, wurde eine DKK3-Promotor-basierte (Dkk3-LCh) und kanonische Wnt (TCF/LEF)-exprimierende Doppelreporter-Maus (DKK3-LCh x TCF/LEF) verwendet. Die Aktivierung der DKK3-Expression und die Aktivität des Wnt-Signalwegs wurden nach einer einmaligen Dosis von 20Gy untersucht. 6 bzw. 14 Tage nach der Bestrahlung wurden in basalen Keratinozyten der behandelten Haut eine erhöhte DKK3-Expression und eine erhöhte Aktivität des kanonischen Wnt-Signalwegs festgestellt.

Um den Einfluss von DKK3 auf strahleninduzierte Dermatitis und entzündliche Fibrose in vivo zu untersuchen, wurde eine Reihe von gewebespezifischen DKK3-Knockout Modellen verwendet. Es zeigte sich, dass sowohl eine globale DKK3-Depletion, als auch eine Keratinozyten-spezifische DKK3-Depletion partiell vor epithelialer Hyperplasie und Fibrose schützten. Interessanterweise zeigte sich in beiden Modellen eine noch stärkere myeloide Infiltration in der Bestrahlungsstelle als die bereits erhöhte Infiltration, die bei WT-Mäusen beobachtet wurde. Die Ergebnisse deuten darauf hin, dass die keratinozytäre Expression von DKK3 und die damit einhergehende Aktivierung des kanonischen Wnt-Signalwegs die Entstehung einer pro-fibrotischen Umgebung begünstigt. Im Gegensatz dazu führte eine fehlende DKK3-Expression in Keratinozyten zu einem weniger-fibrotischen Gewebemilieu.

Die myeloischen Zellinfiltrate wurden mittels FACS-Analyse näher untersucht. Hierfür wurden Zellen, die aus der Haut von globalen DKK3-Knockoutmäusen und Keratinozyten-spezifischen DKK3 Knockouts 4 Wochen nach der Bestrahlung isoliert wurden, mit den Zellen von WT-Mäusen verglichen. Die Charakterisierung der extrahierten Zellen erfolgte mittels FACS-Analyse durch das Staining von Leukozyten- und Myeloiden-Untergruppenmarkern. In beiden Modellen, im globalen- und im Keratinozyten-spezifischen DKK3-Knockout wurde eine verringerte Anzahl von CD206+ und CD163+ Makrophagen gefunden. Von diesen Oberflächenmarkern ist bekannt, dass sie sowohl beim Menschen als auch bei Mäusen M2-ähnliche profibrotische Phänotypen repräsentieren. Um die potenzielle Wirkung von DKK3 auf das Sekretom

der Keratinozyten und die damit einhergehenden Auswirkungen auf die myeloische Differenzierung und Polarisierung besser zu charakterisieren, wurden ein Chemokin/Wachstumsfaktor-Array und eine RT-qPCR-Analyse an menschlichen Keratinozyten (N/TERT-1) nach DKK3-Modulation durchgeführt. Die N/TERT-1-Zelllinie wurde mit einer selbst entwickelten Vektorplattform unter Verwendung eines Doxycyclin-induzierbaren DKK3-Überexpressionsplasmids hergestellt. Der Knockdown von DKK3 durch siRNA-Transfektion führte zu erhöhter Expression des M1-ähnlichen Aktivierungsfaktors GM-CSF sowie der proinflammatorischen Faktoren CXCL8, CXCL10 und TNF-α, während die Überexpression von DKK3 in Keratinozyten zu einer Erhöhung des M2-ähnlichen und profibrotischen Faktors TGF-β1 führte.

Das konditionierte Medium aus den N/TERT-1-Zellen, die entweder DKK3 überexprimierten oder in denen die DKK3-Expression runterreguliert worden war, wurde zur Differenzierung humaner mononukleärer Zellen aus peripherem Blut (PBMC) verwendet. Nach sieben Tagen wurden die ausdifferenzierten, Keratinozyten-konditionierten Makrophagen (KcMφ) mittels FACS Analyse charakterisiert. Es zeigte sich, dass eine Überexpression von DKK3 in den Keratinozyten die Expression der M2-ähnlichen Oberflächenmarker CD206 und CD163 erhöht, während eine Erniedrigung von DKK3 die Expression dieser Marker verringert. Im Gegensatz dazu war die Expression von MHCII, CD80 und CD86 in KcMφ in allen Reifestadien der Monozyten erhöht und wurde durch eine Erhöhung oder Erniedrigung der DKK3-Expression nicht wesentlich verändert.

Die N/TERT-1-Zelllinie wurde zur Verfolgung der Aktivierung des kanonischen Wnt-Signalwegs zusätzlich mit einem TCF-basierten Reportergen modifiziert. In diesem Zellsystem konnten hier gezeigt werden, dass die Strahlenbehandlung der Zellen sowohl zu einer erhöhten endogenen DKK3-Expression als auch zu einer erhöhten kanonischen Wnt-Aktivität führte. Desweiteren wurde gefunden, dass strahleninduzierte reactive oxygen species (ROS) und chemische ROS-Stimulation die DKK3-Expression und folglich die Aktivität des kanonischen Wnt-Signalwegs erhöhen können, was auf einen Second-Messenger-Weg hindeutet.

Fibroblasten sind ebenfalls wichtige Treiber der entzündlichen Fibrose.

Interessanterweise zeigten Fibroblasten-spezifische DKK3 Knockout-Mäuse eine stärkere strahleninduzierte Hyperplasie und Fibrose als WT-Mäuse. In vitro wurde entsprechend nachgewiesen, dass die Überexpression von DKK3 in einer dermalen Fibroblasten-Zelllinie die kanonische Wnt-Aktivität wirksam hemmt. Dies scheint eine plausible Erklärung für den stärkeren Strahlenschaden in Fibroblasten-spezifischen DKK3 Knockout-Mäusen zu sein, und zeigt die pleiotrope Natur des DKK3-Proteins und seine hochgradig gewebespezifische Wirkungsweise.

Zusammenfassend zeigt die vorliegende Studie, dass strahleninduzierte ROS zu einer verstärkten DKK3-Expression mit Aktivierung der kanonischen Wnt-Aktivität führen können. Diese Aktivierung in basalen Keratinozyten ist für die strahleninduzierte epitheliale Hyperplasie und die anschließende Gewebefibrose wichtig, da der Verlust von DKK3 in Keratinozyten ausreicht, um Mäuse erheblich vor chronischer Strahlendermatitis zu schützen. Die Mäuse mit jedem untersuchten DKK3 Status hatten eine erhöhte myeloide Infiltration im bestrahlten Hautareal. Interessanterweise war das Ausmaß der myeloiden Infiltration bei den globalen und den Keratinozyten-spezifischen DKK3-Knockout-Mäusen sogar noch höher als bei den WT-Mäusen, was mechanistisch betrachtet darauf hin deutet, dass das Vorhandensein von DKK3 in Keratinozyten mit begleitender Epithelhyperplasie die Makrophagenpolarisation eher in Richtung eines M2-ähnlichen pro-fibrotischen Phänotyps treibt, wenn der Prozess mit 20Gy angestossen wird. Demgegenüber führt das Fehlen von DKK3 zu Makrophagen, die einen eher M1-ähnlichen pro-inflammatorischen Phänotyp aufweisen. Insgesamt kann man aus den Ergebnissen schließen, dass DKK3 eine wichtige Rolle bei der strahleninduzierten Dermatitis und Fibrose hat, dass die Inhibierung von DKK3 den Krankheitsverlauf mildern kann, und dass damit DKK3 ein potenzielles therapeutisches Ziel für strahleninduzierte Dermatitis und Fibrose sein könnte.

Summary

Radiation dermatitis is a common side effect of cancer radiotherapy. To some extent radiation dermatitis occurs in many patients, in particular if the lesion is close to the skin. The skin affections can range from mild and transient redness to severe inflammation, fibrosis, ulceration or necrosis, and may severely reduce the patients' quality of life. The treatment of chronic radiation dermatitis and fibrosis is difficult, underscoring then unmet need for novel targets and treatment strategies. Previous studies have shown that the canonical Wnt signaling pathway plays an important role in driving fibrosis and represents a potential target for the treatment of radiation-induced dermatitis and fibrosis. The soluble factor Dickkopf WNT Signaling Pathway Inhibitor 3 (DKK3) modulates canonical Wnt activity in a cell-specific manner. Our group's previous study (non-radiation) in inflammatory renal fibrosis suggested that epithelial DKK3 may activate canonical Wnt signaling, and through this, play a profibrotic and immune-polarizing role in renal fibrosis. Moreover, our group's pilot studies of irradiated skin suggested that a global knockout of DKK3 may partially protect mice from radiation-induced hyperplasia and skin fibrosis. It was thus hypothesized for this thesis that following radiation damage, DKK3 expression in concert with canonical Wnt activation are linked to a compensatory hyper reactive epidermal hyperplasia, inflammatory infiltration and fibrosis.

To test this hypothesis, a model of radiation-induced skin hyperplasia and inflammatory fibrosis was developed based on previous experiments of the group investigating radiation-induced lung fibrosis. A single dose of 20Gy radiation delivered to C57BL/N wildtype mice was found to induce reproducible chronic radiation dermatitis. Four to eight weeks after radiation, significant hyperplasia, myeloid infiltration and fibrosis was seen in irradiated skin as compared to non-irradiated controls. To identify the relevant cellular source of DKK3, and to monitor the cellular activity of canonical Wnt signaling in irradiated mouse skin, a DKK3 promoter based, and canonical Wnt (TCF/LEF) dual reporter mouse (DKK3-LCh x TCF/LEF) was used. The

activation of DKK3 expression and Wnt pathway activity was evaluated following a single dose of 20Gy. At 6 days and 14 days after radiation, increased DKK3 expression and canonical Wnt pathway activity was detected in basal keratinocytes of irradiated skin and in many instances was found to be coincident.

To investigate the effect of targeted DKK3 depletion on radiation-induced dermatitis and inflammatory fibrosis *in vivo*, a series of DKK3 tissue-specific knockouts were evaluated following radiation injury. Both DKK3 global and DKK3 keratinocyte specific knockout mice were shown to be significantly protected from epithelial hyperplasia and fibrosis. Interestingly, both the DKK3 global knockout and DKK3 keratinocyte specific knockout mice showed even more myeloid infiltration at the radiation site than the already increased infiltration seen in WT mice. The results suggested that keratinocyte expression of DKK3 and accompanying activation of canonical Wnt pathway signaling may be linked to a tissue milieu conducive toward the establishment of a pro-fibrotic environment. By contrast, the absence of DKK3 expression by keratinocyte was linked to a non-fibrotic tissue environment.

To evaluate the myeloid phenotypes seen in the presence or absence of DKK3, cells were isolated from the skin of both DKK3 global knockouts and DKK3 keratinocyte-specific knockouts and compared to the cells present in WT mice skin at 4 weeks after radiation. FACS analysis of leukocyte and myeloid sub-group markers was employed to characterize the phenotype of the extracted cells. Both DKK3 global knockout and the keratinocyte-specific knockout mice exhibited a decreased CD206$^+$ and CD163$^+$ surface marker expression on macrophages that are known to represent M2-like profibrotic phenotypes in both human and mouse settings. To better characterize the potential effect of DKK3 on the keratinocyte secretome with accompanying effects on myeloid differentiation and polarization, a chemokine/growth factor array and RT-qPCR analysis was performed on human keratinocytes (N/TERT-1) after DKK3 modulation. The N/TERT-1 cell line was engineered using an in house developed vector platform using a doxycycline-inducible DKK3 over expression plasmid. DKK3 knockdown performed via siRNA transfection was found to increase expression of the M1-like

phenotype activation factor of GM-CSF, and also increased expression of the pro-inflammatory factors CXCL8, CXCL10, and TNF-α, while over expression of DKK3 led to increased keratinocyte expression of the M2-like and profibrotic factor TGF-β1.

The conditioned media from N/TERT-1 cells with DKK3 modulation was then used to mature human peripheral blood mononuclear cells (PBMC) from healthy donors. After seven days the resultant keratinocyte conditioned macrophages (KcMϕ) were collected for FACS analysis. DKK3 over-expression in the keratinocytes increased expression of the M2-like phenotype surface markers CD206 and CD163, while DKK3 knockdown decreased the expression of these markers in KcMϕ. By contrast, expression of MHCII, CD80 and CD86 in KcMϕ was increased in all settings with maturation of the monocytes, and was not significantly altered by modulation of the DKK3 expression status of the keratinocyte line.

The N/TERT-1 cell line was further modified to include a synthetic TCF-based reporter gene to monitor activation of canonical Wnt pathway signaling. Using this system it was demonstrated that radiation increased both endogenous DKK3 expression and canonical Wnt activity. Radiation also induced ROS and chemical ROS stimulation was able to increase DKK3 expression and canonical Wnt signaling activity suggesting a second messenger path for the phenomena.

Fibroblasts are important drivers of inflammatory fibrosis. Interestingly, DKK3 fibroblast-specific knockout mice showed increased radiation-induced hyperplasia and fibrosis over that seen in WT mice. In line with this in vivo data, it could be demonstrated *in vitro*, that DKK3 over-expression in a dermal fibroblast cell line effectively inhibited canonical Wnt activity. These results further indicated the pleotropic nature of the DKK3 protein and its tissue specific mode of action.

The present study thus shows that radiation-induced ROS can lead to enhanced DKK3 expression with activation of canonical Wnt activity. This activation in basal keratinocytes caused radiation-induced epithelial hyperplasia and subsequent tissue fibrosis, while loss of DKK3 in keratinocytes protected mice partially against chronic radiation dermatitis. Interestingly, while radiation increased myeloid infiltration in all mice under study, the level of infiltrate in the DKK3 global and keratinocyte specific

knockout animals was even enhanced over that seen in the WT mice. Mechanistically, the results suggest that the presence of DKK3 in keratinocytes with accompanying epithelial hyperplasia drives macrophage polarization more towards a M2-like pro-fibrotic phenotype, while the absence of DKK3 leads to macrophages showing a more M1-like pro-inflammatory phenotype. Overall, the results suggest that DKK3 has an important role in radiation-induced dermatitis and fibrosis, that blocking DKK3 may attenuate the disease, and that DKK3 may serve as a potential therapeutic target for radiation-induced dermatitis and fibrosis.

List of figures

List of Tables

List of abbrevations

3DCRT	3D Conformal radiotherapy
APC	Adenomatosis polyposis coli
CAFs	Carcinoma associated fibroblast
CAFs	carcinoma associated fibroblasts
CNS	The central nervous system
CTGF	Connective tissue growth factor
DKK	Dickkopf
DKK3$^{-/-}$	DKK3 global knockout
DNA	Deoxyribonucleic acid
Dox	Doxycycline
DSBs	Double-strand breaks
Dsh	Dishevelled
DTT	Diethiothreitol
ECM	Extracellular matrix
EDTA	Ethylenediaminetetraacetic acid
ELISA	Enzyme-Linked ImmunoSorbent Assay
EORTC	European Organization for Research and Treatment of Cancer
FACS	Flow cytometry
Fz	Frizzled
GSK3-β	Glycogen synthase kinase 3-ß
H 2 DCFDA	Cell-permeable 2 ', 7'-dichlorodihydrofluorescein diacetate
HCl	Hydrochloric
HEK293	Human embryonic kidney cells
IFN-γ	Interferon gamma
IGRT	Image-guided radiotherapy
IHC	Immunohistochemistry
IL-6	Interleukin-6
IL-8	Interleukin-8
IMRT	Intensity modulated radiation therapy
K14	DKK3 keratinocyte specific knockout
K4	Human immortalized dermal fibroblasts
LEF	Lymphoid-enhancing binding factor
LET	Low linear energy transfer
LRP5/6	Low density lipoprotein related protein 5/6
N/TERT-1	Immortalized human dermal keratinocytes
NF-κβ	Nuclear factor-kappa-lightenhancer of activated β-cells
PBL	Peripheral blood lymphocytes
PC12	Rat pheochromocytoma cells
PCP	Planar cell polarity
PDGF	Platelet-derived growth factor
RIF	Radiation-induced fibrosis

RIPA	Radioimmunoprecipitation assay buffer
ROS	Reactive oxygen species
RT	Room teparature
RTOG	Radiation Therapy Oncology Groups
RT-qPCR	Real-time quantitative polymerase chain reaction
SBRT	Stereotactic body radiation therapy
SDS	Sodium Dodecyl Sulfate
TCF	T-cell factor
TGF-β1	Transforming growth factor beita-1
WA	Working agent
WT	Wildtype
Wnt	Wingless/Int
α-SMA	Alpha smooth muscle actin

1. Introduction

1.1 Inflammatory fibrosis

Effective tissue repair after injury is crucial for the survival of all living organisms [1]. Wound repair is thought to follow four general overlapping but distinct stages: the hemostasis stage, inflammation stage, new tissue formation stage, and remodeling stage [2]. The first stage, hemostasis involves the formation of a provisional wound matrix that occurs immediately after injury and is usually completed after a few hours (coagulation phase). Early injury activates the inflammatory response leading to the recruitment of neutrophils, monocytes, and other innate immune cells to the damaged tissue to help clear pathogens and dead cell debris. Subsequently, the infiltrating cells help initiate the tissue repair response. The degree and duration of the inflammatory response ultimately influences the final outcome of the injury. There are advantages of an enhanced inflammatory response. However, there are also disadvantages, including the over-activation of an inflammatory fibrotic response resulting in chronic tissue damage [3].

Tissue fibrosis is defined as a pathological overgrowth, tissue hardening with scar formation caused by the excess deposition of extracellular matrix (ECM) proteins largely secreted by myofibroblasts generally in response to chronic inflammation. Various types of tissue damage are associated with the development of chronic inflammation and tissue fibrosis, including those resulting from radiation damage, infectious disease, chemical toxins, mechanical stress and autoimmune reactions. Fibrosis can affect virtually all tissues and organs of the body and if uncontrolled can lead to end stage diseases, organ failure and death [4].

Myofibroblasts are key cellular mediators of wound repair. These cells produce the ECM and collagen associated with fibrosis. Previous studies have suggested that myofibroblasts are derived from a variety of sources, including resident pericytes, mesenchymal cells, or blood-born mesenchymal stem cell progenitors with a fibroblast/myofibroblast-like phenotype referred to as fibrocytes [5]. Under normal

conditions, wounds undergo healing by the replacement of dead cells with original cell types in the injury area. However, persistent insult and injury can lead to dysregulation of the pro-fibrotic program, resulting in the over-production of ECM proteins. Over-activated myofibroblasts can also help foster a cyclic chronic inflammation by further driving immune cell infiltration. In this context, a diverse series of growth factors and cytokines are produced including important factors linked to the fibrotic process such as members of the transforming growth factor-beta (TGF-β) family and Wingless/Int-1 (Wnt1). The presence of these and related factors activate pathways associated with a fibrotic phenotype further driving myofibroblast recruitment and differentiation accompanying with ECM deposition [6].

The efficient targeting of fibrotic processes remains an important challenge in clinical medicine necessitating further studies of the cellular and molecular mechanisms underlying the biology of fibrosis. An over-activation of the canonical Wnt signaling pathway is strongly linked to the biology of fibrosis. Many of the factors driving fibrosis such as ECM proteins and growth factors are downstream targets of the canonical Wnt signaling pathway [7-10]. Thus, targeting canonical Wnt signaling may help prevent or treat chronic fibrosis.

1.2 Radiation-induced inflammatory fibrosis

1.2.1 Radiation biology

Cancer remains the leading cause of death worldwide. Treatment approaches include surgery, radiation therapy, chemotherapy, hormonal and immunotherapy. Radiation therapy is an important modality of cancer treatment. Approximately 50% of cancer patients receive radiation therapy during their illness, and it represents around 40% of the treatments given for the treatment of cancer. The main goal of radiation therapy is to target cancer cell division [11].

Different forms of radiation can be applied in the context of cancer therapy. These include photon radiation and particle radiation. X-rays and gamma-rays are the most commonly used photons in radiation therapy, which is represented by sparsely

ionizing radiation and is considered to be low linear energy transfer (LET) electromagnetic rays [11]. Particle radiations have higher LET and higher biological effectiveness, at least if heavier than protons, than that seen in photon radiation. For this reason it may be more effective for some radio-resistant and hypoxic cancers including chordoma, (chondro-) sarcoma, salivary gland tumors, and eventually may be also be more effective for glioblastoma, pancreatic cancer, renal cell carcinomas, melanomas and others [11,12]. However, the higher cost and expense of equipment for the production of proton particle radiation, and more so for heavy ion therapy, makes wider application of these approaches more problematic than photon radiation [11,13].

An important target of radiation therapy is genomic DNA. Radiation can either directly damage cellular DNA, or indirectly cause DNA damage through the side reaction of free radicals or radical oxygen species (ROS) derived from ionization of water present in cells. DNA double-strand breaks (DSBs) are responsible for most of the cell death seen during radiation therapy. Cancer cells with DNA damage caused by radiation therapy stop proliferation and die when the damage is beyond their ability to repair [11]. Apoptosis and mitotic catastrophe are common types of cell death caused by radiation [14,15]. In recent years, additional cell death mechanisms such as necrosis, senescence and autophagy have been identified as important processes linked to radiation therapy [16-18].

The goal of cancer radiation therapy is to improve clinical outcomes and to minimize the radiation therapy related toxicities of normal tissues. Technological advances such as three-dimensional conformal radiotherapy (3DCRT), intensity modulated radiation therapy (IMRT), image-guided radiotherapy (IGRT), stereotactic body radiation therapy (SBRT) are used to help achieve this goal [11].

In addition, ionizing radiation can affect diverse cell functions by modulating proteomic, transcriptomic or epigenetic events through mechanisms that are only partly understood. Radiation treatment also causes significant changes in immune responses that are dose dependent. Low dose radiation is sometimes associated with M1-like polarized macrophages [19], while higher doses have been shown to induce more M2-like polarization [20].

1.2.2 Radiation-induced fibrosis

Efforts to minimize radiotherapy related toxicities to normal tissues make use of medical physics, computer science and engineering, along with diagnostic radiology. These approaches have led to significant progress since the 1990s through the development of methods that can better deliver the physical radiation dose to the tumor target while sparing the surrounding healthy tissues. While this physical precision radiotherapy has increased selectivity of the radiation dose gradient towards the tumor and away from normal tissue, external beam radiotherapy must still travel through many layers of healthy tissue resulting in some level of radiation dose. In fact, despite the steep dose gradient, the normal tissue directly adjacent to the tumor receives - due to the safety margins of the radiation field - the same dose as the tumor. Therefore, tissue toxicity complications remain an important clinical problem for all radiotherapy applications. Normal tissue complications are clinically classified as acute (days after radiation), sub-acute (weeks) and chronic/late (months-years). An important late side effect seen is radiation-induced fibrosis (RIF) leading to scarring and loss of function of the respective organ, and potentially reduced quality of life for the cancer patient. RIF can involve all normal tissues in the radiation field, including skin, lung, heart, gastrointestinal and genitourinary tracts, nerves, etc.

As discussed above, fibrogenesis is associated with a series of cellular and pathway signaling events. Clinically relevant RIF occurs 3-12 months after radiation and may progresses over several years. The risk factors of RIF include the total dose of radiation, the dose per fraction of radiation, the volume of tissue treated, and the time frame of treatment delivery [21].

As seen in other chronic fibrosis settings, RIF is associated with an inflammatory response followed by fibroblast recruitment and activation leading to an excess deposition of extracellular matrix. The first inflammatory cells (acute phase) recruited to the site of radiation injury are neutrophils [22], followed by the migration of monocytes and lymphocytes into the injury area [23]. These two cell types interact and help in the differentiation of monocytes into different subsets of macrophages. These

macrophages are thought to broadly include pro-inflammatory M1-like macrophages, or alternatively activated anti-inflammatory and pro-fibrotic M2-like macrophages [24-27].

Radiation-induced fibrosis is a complex process. The most important and most investigated prototypical profibrotic factor is transforming growth factor β1 (TGF-β1), which can convert fibroblasts into ECM producing myofibroblasts as well as drive macrophage polarization. However, after myofibroblast activation, inflammation and continuous stimulation by TGF-β1 is no longer necessary for the maintenance of collagen production. Fibrosis can also be perpetuated for example by autocrine induction of a cytokine called connective tissue growth factor (CTGF, or CCN2) [28]. Many drugs and strategies have been shown preclinically to attenuate radiation-induced fibrosis, but are not as yet approved for clinical use. These include strategies to block TGF-β (both antibodies and receptor kinase inhibitors), recombinant platelet-derived growth factor (PDGF) and statins. Our group has previously shown that blocking PDGF and TGF-β attenuates radiation-induced pulmonary fibrosis, and that blocking CTGF using antibodies can attenuate and reverse the remodeling process and restore lung function [29-31]. One important outcome observed after CTGF antibody treatment was a reduction in M2-like polarized macrophages in fibrosing lung suggesting that the absolute number, as well as functional status of the M2 polarized macrophages may be responsible for pulmonary fibrosis [32]. Another promising concept to address radiation-induced normal tissue fibrosis is the use of mesenchymal stem cell therapy, which may be effective in dermal radiation damage [33].

1.2.3 Radiation-induced inflammatory skin fibrosis

As discussed, radiation dermatitis is a side effect of cancer radiotherapy that can be seen in practically all radiotherapy treatments. The tumor entities where it can occur include tumors in the breast, head and neck region, lung, lymphatic system, extremities (e.g. sarcoma), and the skin itself [34]. It remains an important issue during

radiation treatment of all tumors in close proximity to the skin. Up to 95% of patients who receive radiotherapy may develop some skin affections ranging from mild and transient redness to severe fibrosis, ulceration and necrosis [11,35].

Acute skin reactions after radiation therapy occur within hours to days, followed by sub-acute effects weeks later and manifest similar to what is seen during general tissue damage and wound repair. Chronic radiation dermatitis is seen months to years following exposure, and is described as an ongoing inflammatory fibrosis with hyper- and hypo-pigmentation, atrophy, necrosis and ulceration [36]. The Radiation Therapy Oncology Groups (RTOG) and the European Organization for Research and Treatment of Cancer (EORTC) have established common toxicity criteria for radiation-induced acute and late morbidity. The criteria for skin injury is shown in Table 1.1 where 0 represents no radiation effects seen and 5 represents effects leading to death [37].

Table 1.1 RTOG/EORTC radiation morbidity scoring criteria [37]. The Radiation Therapy Oncology Groups (RTOG), the European Organization for Research and Treatment of Cancer (EORTC).

Scores / Morbidity	Acute morbidity	Chronic morbidity
0	None	None
1	Follicular, faint or dull erythema/epilation/dry desquamation/decreased sweating	Slight atrophy; pigmentation change; some hair loss
2	Tender or bright erythema, patchy moist desquamation/moderate edema	Patch atrophy; moderate telangiectasia; total hair loss
3	Confluent, moist desquamation other than skin folds, pitting edema	Market atrophy; gross telangiectasia
4	Ulceration, hemorrhage, necrosis	Ulceration
5	Death	Death

The pathophysiology of chronic radiation skin fibrosis is poorly understood. It is thought that radiation damages the basal layer stem cells in the skin, which initially shows reduced mitotic activity. The basal stem cells that survive then undergo hyper-activation to repopulate the damaged monolayer, all of which occurs in the context of an inflammatory infiltrate. The process can lead to ulcer formation and fibrosis [38-43]. The pathophysiology of this disease is thought to be driven primarily by a Th2/M2-like immune response [44]. While the interdependence and interactions, as well as the respective roles remain unclear, radiation-induced free radicals along with reversible and irreversible DNA damage are thought to contribute to the acute inflammation and the cascade of sub-acute and chronic processes leading to radiation-induced dermatitis (Figure 1.1) [45].
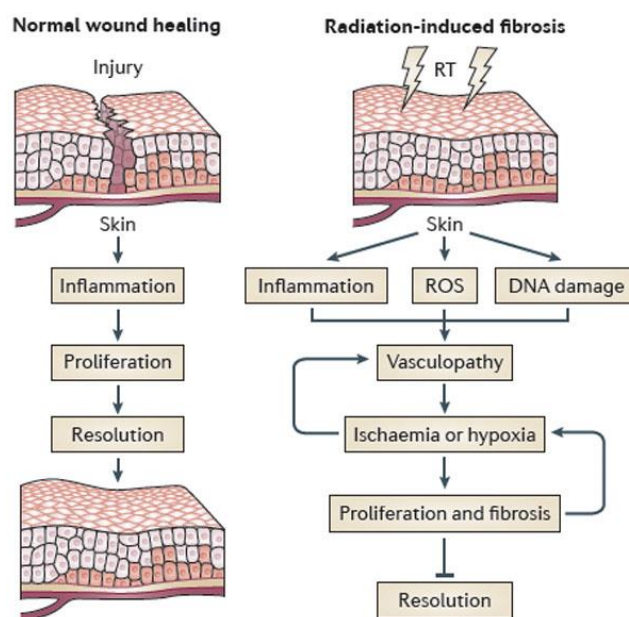
Figure 1.1 The mechanism of radiation-induced skin injury and normal would healing
(Source Nature Reviews Cancer 15:409, 2015)

As discussed, the cytokine TGF-β1 plays an essential role in the initiation of fibrosis. Alfiya *et al.* reported that activation of canonical Wnt signaling is linked to the activation of fibroblasts [6]. Transgenic overexpression of the Wnt inhibitor Dickkopf-1 (DKK1) was found to attenuate skin fibrosis in TGF-β dependent animal models. Their findings suggest that canonical Wnt signaling is necessary for TGF-β dependent fibrosis

and highlight the importance of the crosstalk between both pathways in fibrotic disease [6]. Treatment of chronic radiation dermatitis and fibrosis is difficult, underscoring the need for novel treatment strategies such as modulation of canonical Wnt signaling [35].

1.3 Canonical Wnt signaling and the Dickkopf family

1.3.1 Wnt signaling

The Wnt signaling pathways are highly conserved over evolution. The name Wnt derives from a combination of the Drosophila segment polarity gene wingless and the vertebrate homolog int-1 [46]. The Wnt family ligands consist of 19 highly conserved glycoproteins in mice and humans that play diverse roles in developmental and cellular processes, including regulation of cell fate determination, control of stem cell homoeostasis, cellular proliferation and differentiation [47-49]. Wnt ligands function by binding to the Frizzled (Fz) receptor family comprised of ten Fz receptors in humans. In addition, the interaction of Wnt ligands with Fz receptors is dependent upon co-receptors such as the low density lipoprotein related protein 5/6 (LRP5/6) [50]. Wnt signaling is represented by three distinct signaling cascades: the canonical Wnt/β-catenin pathway, the Wnt/planar cell polarity (PCP) pathway and the Wnt/Ca2+ pathway. Among these, the canonical Wnt/β- catenin pathway is the best characterized and has been shown to be involved in a variety of normal cellular processes as well as diseases [48].

In canonical Wnt/β- catenin pathway activation, a select set of Wnt ligands bind to a receptor complex comprised of a Fz receptor and the co-receptor LRP5/6. β -catenin is a key regulator of canonical Wnt signaling. Intracellular β-catenin protein is constitutively produced and present in the cytoplasm, but rapidly degraded. In the absence of Wnt ligand binding, cytoplasmic β-catenin is turned over following its phosphorylation by the β-catenin destruction complex consisting of Axin, adenomatosis polyposis coli (APC) and glycogen synthase kinase 3- β (GSK3-β) [46,50,51]. Upon Wnt ligand binding, cytoplasmic Dishevelled (Dsh) and Axin proteins are

recruited to the plasma membrane while GSK-3β is inhibited. This results in the destruction Axin-APC-GSK3-β complex falling apart. Degradation of β-catenin is inhibited, the stabilized β-catenin can then enter the nucleus where it binds to members of the T-cell factor/lymphoid-enhancing binding factor (TCF/LEF) family of transcription factors and thereby drives target gene expression (Figure 1.2) [52]. The downstream target genes of the canonical Wnt pathway include genes that play central roles in apoptosis, proliferation, differentiation and polarity as well as ECM-related factors and cytokines.
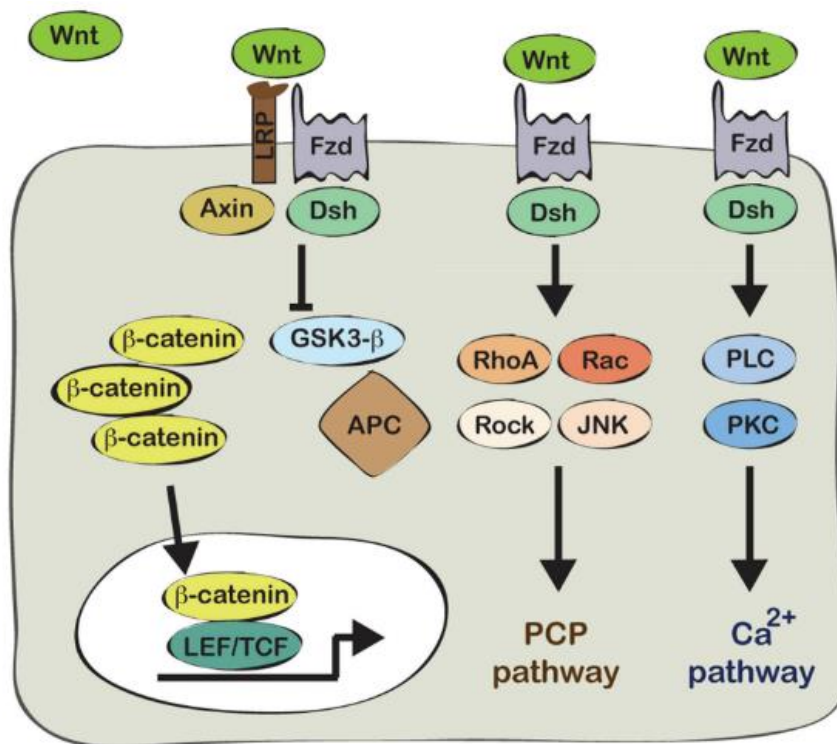
Figure 1.2 Wnt signaling (Source *J Dtsch Dermatol Ges* **13**, 302-306). Three distinct Wnt signaling cascades: the canonical Wnt/β- catenin pathway, the Wnt/planar cell polarity (PCP) pathway and the Wnt/Ca2+ pathway.

1.3.2 DKK family

The DKK protein family is comprised of secreted factors that regulate Wnt pathway signaling [42]. The human DKK family consists of five members, DKK1, DKK2, DKK3, DKK4, and the unique DKK3-related protein Soggy (DKKL1 or SGY-1) [52]. DKK proteins are secreted glycoproteins with a molecular weight between 25 kDa and 38 kDa. All DKK

members with the exception of Soggy share two conserved cysteine-rich domains called Cys1 and Cys2. Within the DKK family, DKK3 exhibits a divergent structure characterized by a short linker region, a larger overall protein size, and high N-terminal sequence with similarities to Soggy. However, not much N-terminal sequence similarity is seen between DKK1, DKK2 or DKK4. DKK3 has four putative posttranslational N-glycosylation sites, while DKK1 and DKK2 have only one site [48]. Figure 1.3 shows the general structure of human DKK protein family members. The unique structure of DKK3 relative to the other DKK family members suggests a different set of biologic functions associated with regulation of Wnt signaling.
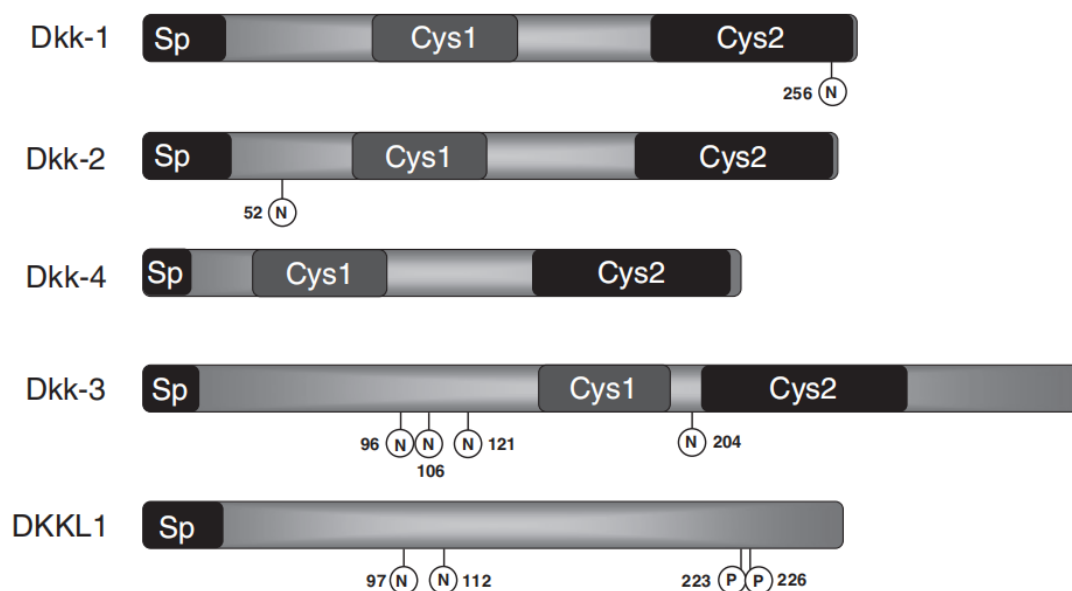
Figure 1.3 Structure of the human DKK protein family (Source *Biochim Biophys Acta* 1825, 18-28). Sp, N-terminal signal peptide; Cys, cysteine-rich domain; N, N-acetylglucosamine; P, phosphoserine. Numbers refer to the modified amino acid residue.

1.3.3 The DKK family and canonical Wnt signaling

DKK1, DKK2, and DKK4 have been shown to inhibit canonical Wnt signaling by binding to the transmembrane receptors kremen 1 and kremen 2, as well as the Wnt co-receptor LRP5/6 [53,54]. DKK3 appears to exhibit divergent biological features and has been shown to either activate or inhibit canonical Wnt pathway signaling depending on the specific cellular or tissue context [55]. The potential roles of the DKK family

members in regulating the Wnt signaling pathway is shown in Figure 1.4. Previous studies have found that DKK3 can enhance canonical Wnt signaling in human Muller glia cells (MIO-M1) and human embryonic kidney cells (HEK293) [56]. In carcinoma associated fibroblasts (CAFs), DKK3 has been described to activate canonical Wnt signaling by interacting with the negative regulator kremen 1 and kremen 2 and thereby increase levels of LRP6 on cell surface [57]. However, DKK3 has also been shown to inhibit canonical Wnt signaling in the rat pheochromocytoma cell line PC12 and in human osteosarcoma Saos-2 cells [58,59].

Our group has previously demonstrated a functional interaction between DKK3 and canonical Wnt signaling in damaged renal epithelial cells where a key role for DKK3 was identified in promoting renal tubular atrophy, interstitial fibrosis and T cell polarization. Tubular epithelial cells were shown to be a major source of DKK3 in damaged kidneys. Importantly, this expression was shown to be associated with enhanced canonical Wnt signaling within the tubular epithelial cells [60]. The results further suggested that DKK3 may also act via parallel signaling pathways that give rise to downstream effects leading to immune regulation and tissue fibrosis [60].
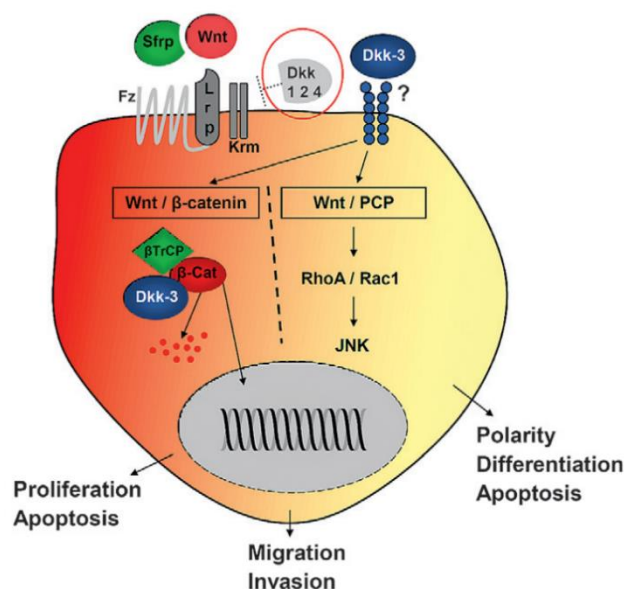
Figure 1.4 DKK family and canonical Wnt signaling (source *Biochim Biophys Acta* **1825**, 18-28). DKK1, DKK2, and DKK4 have been shown to inhibit canonical Wnt signaling by binding to the transmembrane receptors kremen 1 and kremen 2, as well as the Wnt co-receptor LRP5/6, while DKK3 affect canonical Wnt signaling in a cell and tissue dependent manner.

1.4 DKK3 in immunity and chronic fibrosis

DKK3 can also influence immune regulation [61-64]. As discussed above, chronic inflammation is a hallmark of progressive fibrosis where macrophages and T cells are thought to play important roles. Our previous work has shown that protection of renal morphology in the absence of DKK3 was accompanied by T cell accumulation with a bias toward IFNγ-producing Th1 and Tregs. Th1 cells, and IFNγ in particular, may exert antifibrotic effects, while Th2 cells are thought to be profibrotic. The observed T cell phenotype seen paralleled previous findings reported in a mouse model of multiple sclerosis, showing increased accumulation of IFNγ-producing CD4^{+} and CD8^{+} T cells within the central nervous system (CNS) of DKK3-deficient mice [65]. The role of Tregs in fibrosis is still controversial, but the increase in these cells seen after genetic deletion or antibody-mediated blockade of DKK3 might limit Th1 activity. While the observed T cell phenotype could also result in part from a direct effect of DKK3 on T cells.

Wnt signaling has been further shown to modulate immune responses via effects on proinflammatory pathways such as the NF-κB signaling cascade that is essential for stress-triggered cytokine and chemokine expression [63]. Melanoma-intrinsic Wnt/β-catenin signaling can regulate T cell infiltration into the tumor, emphasizing the potential role of Wnt signaling in parenchymal/tumor cells on T cell behavior [61]. DKK3 has also been shown to influence the polarization of macrophages and influence development of dendritic cells in certain tissue settings [66-68]. DKK3 biology has also been associated with general aspects of chronic skin disease and immunity [42,43,69,70].

1.5 Canonical Wnt signaling and skin

1.5.1 Skin structure

Skin is the largest organ of the body and plays an important role in physical protection and immunity. The basic structure of skin is comprised of three layers: the epidermis, dermis and subcutaneous tissue. The topmost layer directly exposed to the environment is the epidermis consisting of keratinocytes, corneocytes and

melanocytes. The layer directly under the epidermis is the dermis and consists of fibroblasts and different appendages including sweat glands, hair follicles and sebaceous glands. Below the dermis is a subcutaneous layer of adipocytes and vessels [71]. Figure 1.5 shows the general structure of skin.
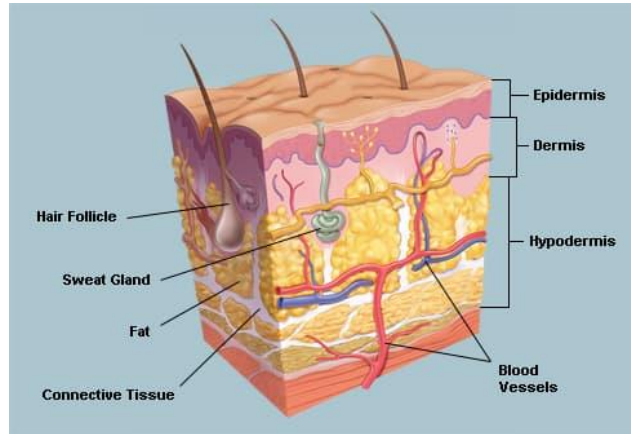
Figure 1.5 Skin anatomy (Source 2014 WedMD, LLC). Three basic layers of skin: the epidermis, dermis and subcutaneous tissue.

1.5.2 Canonical Wnt signaling, skin homeostasis and pathology

Skin is a complex dynamic organ with high cellular regeneration during normal tissue renewal. Canonical Wnt signaling plays a role in the maintenance of skin progenitor cell populations and during skin development and regeneration. Canonical Wnt signaling controls skin homeostasis by regulating stem cell maintenance [71-73]. Lim X *et al.* [74] showed that sustained canonical Wnt activity in the interfollicular epidermis leads to hyperplastic epithelia, suggesting that canonical Wnt signaling increases the proliferation of interfollicular keratinocytes. In addition, canonical Wnt signaling linked to myofibroblast activation enhances the proliferation of dermal fibroblasts and leads to dermal thickening [75]. Depletion of the Wnt-secretion factor Evi/Wls in mouse keratinocytes resulted in a chronic inflammatory phenotype with damaged barrier function and infiltration of immune cells. In addition, skin-specific dendritic epidermal T cells which are thought to help balance epidermal immune homeostasis were lost [75]. Canonical Wnt signaling is important in the communication between skin epithelium and immune system [71].

1.6 Preliminary data: the effect of DKK3 on radiation-induced dermatitis and fibrosis

As we have seen, canonical Wnt signaling plays a role in skin homeostasis and pathology and that DKK3 can modulate canonical Wnt activity in a cell-specific manner. Our renal study suggested that epithelial DKK3 could activate canonical Wnt signaling and play a profibrotic and immune-polarizing role in renal fibrosis. To date, the role of epithelial DKK3 in other fibrotic processes such as inflammatory fibrosis of the skin was unknown. As outlined above, radiation-induced skin inflammation and fibrosis are complications of cancer radiotherapy that can markedly affect the quality of life of patients. Since no satisfactory treatment options exist as of today, it would be of great benefit to find a druggable target for treatment of radiation inflammatory fibrosis. In a preliminary study, a mouse radiation dermatitis model was used to evaluate the role of DKK3 in skin inflammatory disease: C57BL/N wildtype (WT) and DKK3 global knockout (DKK3$^{-/-}$) mice were irradiated with a single dose of 20Gy to the thorax. At 3 months after the radiation, clinical observation generated the hypothesis that DKK3$^{-/-}$ protect mice in part from hair loss, desquamation and ulceration. However, the pilot study was not statistically powered to allow robust conclusions to be drawn.

1.7 Hypothesis and the goals of this study

The preliminary data in irradiated skin generated the hypothesis that DKK3 might play a pivotal role in radiation-induced dermatitis and fibrosis, as a global knockout of DKK3 appeared to protect mice from radiation-induced hyperplasia and skin fibrosis. The goal of the present project was therefore to systematically investigate the role of DKK3 in radiation-induced skin damage and identify the cell types and molecular mechanisms behind DKK3-associated dermal inflammation and fibrosis. Building upon our previous renal study it was hypothesized that DKK3 expression in concert with canonical Wnt activation in basal keratinocytes drives inflammatory infiltration, followed by fibrosis. It was further proposed that acute radiation damage to the skin, potentially mediated by ROS or related processes, could modulate DKK3 expression.

The specific goals for this thesis were to:

(1) Identify the relevant cellular source of DKK3 in irradiated mice skin, and in parallel, the cellular activity of canonical Wnt signaling using DKK3 and canonical Wnt dual reporter mice.

(2) Investigate the importance of tissue-specific targeted deletions of DKK3 in radiation-induced skin hyperplasia and inflammatory fibrosis using DKK3 keratinocyte-specific and DKK3 fibroblast-specific knockout mice.

(3) Characterize the role of DKK3 expression on myeloid infiltration and immune cells polarization in radiation-induced skin hyperplasia and inflammatory fibrosis.

(4) Validate relevant biology using human *in vitro* models.

2. Materials

2.1 Devices and disposable instruments

Table 2.1 Devices and disposable instruments

Devices and disposable instruments	Manufacturer
15ml Polystyrene conical tubes	Life technologies, Carlsbad, USA
6 well plates from Nunc	Thermo Fisher Scientific, Darmstadt, Germany
Amersham 680 Imager	Cell Signaling Technology, Frankfurt, Germany
BD Microlance™ Stainless Steel Needles	Becton Dickinson, NJ, USA
BD Plastipak™ Syringes	Becton Dickinson, NJ, USA
Blotting chamber	Bio-Rad, Hercules, USA
Cell incubator	Heraeus Sepatech, Osterode, Germany
Cell Culture flasks 175 cm²	Becton Dickinson, Heidelberg, Germany
Cell Culture flasks 25 cm² and 75 cm²	Nunc, Wiesbaden, Germany
Centrifuge Rotina 38R	HettichLab, Tuttlingen, Germany
Corning Costar Cell Culture Plates (6-,96-well)	Sigma-Aldrich, Deisenhofen, Germany
Corning Costar Stripettes (5,10,25 ml)	Sigma-Aldrich, Deisenhofen, Germany
CryoTubes	Sigma-Aldrich, Munich, Germany
Easystrainer	Greiner bio one, Frickenhausen, Germany
Electric multipipett	Eppendorf AG, Hamburg, Germany
electrophoresis apparatus	Bio-Rad, Hercules, USA
Eppendorf Tubes (1.5ml, 2ml)	Eppendorf, Hamburg, Germany
Filter paper, extra thick	Bio-Rad, Munich,Germany
Flow cytometer Canto II	BD, Franklin, USA

Flow cytometer Fortessa	BD, Franklin, USA
Flow cytometer LSRII	BD, Franklin, USA
Heraeus Pico 17 Centrifuge	Thermo Fisher Scientific, Darmstadt, Germany
Histology embedding cassettes	NeoLab, Heidelberg, Germany
Incubator CO2-AUTO-ZERO	Heraeus Instruments, Hanau, Germany
LightCycler 480 Instrument	Roche, Mannheim, Germany
Lightcycler 480 PCR plate with 96 wells	Sarstedt, Munich, Germany
Leica TCS SP5 confocal microscope	Leica Biosystems, Wetzlar, Germany
MACS separator	Miltenyi Biotech, Köln, Germany
Manual multipipett	Eppendorf AG, Hamburg, Germany
Manual pipette aid (10µl, 20µl, 100µl, 200µl, 1000µl)	Eppendorf AG, Hamburg, Germany
Microcentrifuge Heraeus Pico 17	Thermo Fisher Scientific, Darmstadt, Germany
Microtome	Microm, Munich, Germany
MultiRad 225	Precision, North Branford, USA
NanoDrop™ Spectrophotometer	Biotechnologie, Erlangen, Germany
Neubauer Counting Chamber	Roth, Karlsruhe, Germany
Operation table	Medax, Germany
Optical lid strip for 96-well plates	Sarstedt, Munich, Germany
Pipette tips Rainin (20, 200, 1000µl)	Mettler-Toledo, Gießen, Germany
Pipette tips with Low Retention LTS Filter (10µl, 200µl, 1000µl)	Mettler-Toledo, Gießen, Germany
Pipettes Rainin (10, 20, 100, 1000 µl)	Mettler-Toledo, Gießen, Germany
Platform shaker, Polymax 1040	Heidolph, Schwabach, Schwabach
Special gel loading tips	Thermo Fisher Scientific, Darmstadt, Germany
Spectramax M5e Microplate Reader	Molecular Devices, Biberach an der Riss, Germany
Surgical scissors and forceps	Integra LifeSciences, France
Syringes (10 und 20 ml)	Becton-Dickinson, Heidelberg, Germany
Thermomixer 5436	Eppendorf AG, Hamburg, Germany
Tubes, 15ml und 50ml	Greiner bio-one, Frickenhausen, Germany
Vertical Laminar Flow Workbench	Heraeus, Hanau, Germany
Vortex MS2 Minishaker	IKA, Staufen, Germany
Water bath M20	Lauda Wobser, Lauda-Königshofen, Germany

2.2 Reagents, chemicals and solutions

Table 2.2 Reagents, chemicals and solutions

Devices and disposable instruments	Manufacturer
10x Taq Buffer without Detergent	New England BioLabs, Ipswich, USA
20x LumiGLO reagent	Cell Signaling Technology, Frankfurt, Germany
2-mercaptoethanol	Sigma-Aldrich, Munich, Germany
2N H2SO4S	Sigma-Aldrich, Munich, Germany

96% Ethanol	Merck, Darmstadt, Germany
Acetic acid	Roth, Karlsruhe, Germany
Acrylamide	Ambion, Darmstadt, Germany
AIM-V medium	Thermo Fisher Scientific, Darmstadt, Germany
Antibody Diluent	DAKO Real, Waldbronn, Germany
Aquatex	Merck, Darmstadt, Germany
ATP Luminescent Cell Viability assay	Merck, Darmstadt, Germany
Avidin/Biotin Blocking Kit	Vector, Burlingame, USA
Bepanthen Eye and Nose Ointment	Bayer, Leverkusen, Germany
Biocoll Separating Solution	BioSell, Nürnberg, Germany
Bladticidin	InvivoGen, San Diego, USA
BSA PCR grade	Thermo Fisher, MA, USA
Collagenase IV	Thermo Fisher Scientific, Darmstadt, Germany
Crystal violet	Serva, Heidelberg, Germany
DAPI	Roche, Mannheim, Germany
Dimethyl sulfoxide (DMSO)	Merck, Darmstadt, Germany
Dispase® II	Sigma-Aldrich, Munich, Germany
Dithiothreitol (DTT)	Invitrogen, Karlsruhe, Germany
Dkk3 antibody	Abcam, Cambridge, UK
DKK3 siRNA	Qiagen, Hilden, Germany
DMEM/F-12 mit Glutamax	Gibco Thermo Fisher Scientific, Waltham , USA
DNase and RNase free water	Thermo Fisher, MA, USA
dNTP	GE Healthcare, Munich, Germany
Doxycycline Hyclate	Santa Cruz, Heidelberg, Germany
DPBS	Gibco Thermo Fisher Scientific, Waltham , USA
Ethanol denaturated, 70%	Roth, Karlsruhe, Germany
FACS™ Accudrop Beads	BD Biosciences, San Jose, USA
Fetal bovine serum (FBS)	Merck/Biochrom GmbH, Berlin (Germany)
Formalin 4 %	Merck, Darmstadt, Germany
Gaussia Luciferase Assay Kit (BioLux)	GeneCopoeia, MD, USA
Glycin	Sigma-Aldrich, Munich, Germany
H2DCFDA assay	Thermo Fisher, MA, USA
Haemalaun	Roth, Karlsruhe, Germany
Hanks' Salzlösung (HBSS)	Sigma-Aldrich, Munich, Germany
Heparin	Miltenyi Biotech, Köln, Germany
Hexanucleotide Mix 10x	Roche, Mannheim, Germany
High Perfect transfection reagent	Qiagen, Hilden, Germany

Homogenizer Ultra-Turrax® T25	IKA GmbH, Staufen, Germany
Human DKK3 ELISA kit	R&D system, Minneapolis, USA
Human serum	Sigma-Aldrich, Munich, Germany
Hydrochloric powder	Sigma-Aldrich, Munich, Germany
Hydrogen peroxide	Merck, Darmstadt, Germany
Ketamine	Bayer, Leverkusen, Germany
K-SFM medium	Gibco Thermo Fisher Scientific, Waltham, USA
LEGENDplex custom Panel chemokines	Biolegend, San diego, USA
LEGENDplex custom Panel growth factors	Biolegend, San diego, USA
Liquid Substrate System for ELISA	Merck, Darmstadt, Germany
Loading buffer 4x	Bio-Rad, Munich, Germany
Methanol	Roth, Karlsruhe, Germany
MgCl2 25mM	Thermo Fisher, MA, USA
Micro beads, CD14	Miltenyi Biotech, Köln, Germany
Mo-DC differentiation medium	Miltenyi Biotech, Köln, Germany
Paraffin	Merck, Darmstadt, Germany
PCR Optimizer	Biomol, Hamburg, Germany
Penicillin	Life technologies, Carlsbad, USA
PFA	Merck, Darmstadt, Germany
Phosphatase inhibitor mini tablets	Thermo Fisher, Waltham, MA / USA
Pierce BCA Protein assay kit	Thermo Fisher, Waltham, MA / USA
Protease inhibitor cocktail tablets	Thermo Fisher, Waltham, MA / USA
Puffer5x	Invitrogen, Karlsruhe, Germany
PureLink™ RNA Mini Kit	Ambion, Darmstadt, Germany
PVDF Membrane	Millipore, Darmstadt, Germany
rhWnt-3a	Bio-Techne, Wiesbaden, Germany
RIPA buffer (10X)	Cell Signaling Technology, Frankfurt, Germany
RNase AWAY® spray	Sigma-Aldrich, Munich, Germany
RNase-Free DNase Set	Qiagen, Hilden, Germany
Rnasin	Promega, Mannheim, Germany
Rotenone	Sigma-Aldrich, Munich, Germany
Silence siRNA	Qiagen, Hilden, Germany
Sodium Dodecyl Sulfate (SDS)	Thermo Fischer, Waltham, MA / USA
Sucrose	Sigma-Aldrich, Munich, Germany
Superscript II	Invitrogen, Karlsruhe, Germany
SYBRgreen I	Sigma-Aldrich, Munich, Germany
Thermomixer 5436	Eppendorf, Hamburg, Germany
Tissue-Tek	Science services, Munich, Germany
Tris buffer	Sigma-Aldrich, Munich, Germany

Trisodium citrate	Merck, Darmstadt, DE
Trypan Blue 0.4% Solution	Lonza AG, Basel (Switzerland)
Trypsin/EDTA Solution (T/E)	PAN-Biotech GmbH, Aidenbach (Germany)
Tween 20	Sigma-Aldrich, Munich, Germany
Xylazine	CliniPharm CliniTox, Zurich, Switzerland
Xylene	Merck, Darmstadt, Germany
Zombie Aqua™ Fixable Viability Kit	Biolegend, San Diego, USA

2.3 Antibodies

2.3.1 Immunohistology

Table 2.3 Antibodies for immunohistology

Name	Manufacturer
Alpha Smooth Muscle Actin (α-SMA)	Sigma-Aldrich , Munich, Germany
F4/80	Origene, MD, USA
HR3	Origene, MD, USA
Ki67	Bethyl, Hamburg, Germany
Goat anti mouse IgG	Dianova, Hamburg, Germany
Rabbit anti rat IgG	Vector, Burlingame, USA

2.3.2 FACS

Table 2.4 Antibodies for flow cytometry analysis

Name	Manufacturer
Anti-human γH2AX	Biologend, San Diego, CA/USA
Anti-human active caspase-3 antibody	BD Biosciences, Heidelberg, Germany
Anti-human CD206	BD Biosciences, Heidelberg, Germany
Anti-human CD163	BD Biosciences, Heidelberg, Germany
Anti-mouse Ly-6C	Biolegend, San Diego, USA
Anti-mouse Ly-6G	Biolegend, San Diego, USA
Anti-mouse CD11b	Biolegend, San Diego, USA
Anti-mouse CD11c	Biolegend, San Diego, USA
Anti-mouse F4/80	Biolegend, San Diego, USA
Anti-mouse MHC -II(I-A/I-E)	Biolegend, San Diego, USA
Anti-mouse iNOS	Thermo Fisher, Waltham, MA / USA

Anti-mouse Arg-1	Thermo Fisher, Waltham, MA / USA
Anti-mouse CD206	Biolegend, San Diego, USA
Anti-mouse CD163	Biolegend, San Diego, USA
Anti-mouse CD45	Biolegend, San Diego, USA

2.3.3 Western Blot

Table 2.5 Antibodies for western blot

Name	Manufacturer
Anti-human DKK3	Proteintech, Rosemont, USA
Anti-human β-Actin	Cell Signaling Technology, Frankfurt, Germany
Anti-rabbit IgG	Cell Signaling Technology, Frankfurt, Germany

3. Methods

3.1 Cell culture

3.1.1 Thawing and freezing of cells

All cell lines were frozen in Dulbecco's Modified Eagle Medium (DMEM) + 10% FCS+ 1% penicillin + 10% DMSO in cryo-tubes. The tubes were placed in an isopropanol container and cooled to -80°C overnight. Afterwards, the cryo-tubes were transferred to a liquid nitrogen container.

To thaw frozen cells, the cryo-tubes were rapidly thawed using a 37°C water bath and immediately transferred into a 75cm^2 sterile cell culture flask with 12ml of relevant growth medium. The medium was changed after 24h to remove DMSO.

3.1.2 General cell culture

All cells were cultured at 37°C with 95% humidity and 5% CO_2. All cell culture work was performed in a laminar flow hood to avoid potential contamination. For sub-culturing of adherent cells, culture medium was discarded and the cells were washed with PBS. The cells were then detached with 0.5% Trypsin-EDTA solution at room temperature (RT) for 5-8 minutes. Detachment of cells was confirmed under the microscope. The

subsequent reaction was stopped by adding quadruple volume of DMEM medium containing 10% FCS. The cell suspension was then moved to a 50ml sterile falcon tube. Cells were pelleted by centrifuging at 180 x g (rt) for 3 minutes. The cell pellets were resuspended using a 5ml sterile syringe. To count cells, 10µl of the cell suspension was mixed with 10µl of Trypan Blue solution to stain dead cells. 10µl of the cell mixture was immediately added into a Neubauer chamber. Only living cells were counted in the chamber. The number of cells/ml suspension was then calculated. The count (x) multiplied by 2 and divided by the quadrants gives a number of $x10^4$ cells/ml cell suspension. Then appropriate fraction of cell suspension (1:5 to 1:2) was distributed to $75cm^2$ sterile flasks containing 12ml of relevant growth medium.

3.1.3 Immortalized human keratinocyte (N/TERT-1) cell line and immortalized human dermal fibroblast (K4) cell line culture

N/TERT-1 cells (human keratinocyte cells immortalized by over expression of terminal transferase) were provided by Prof. Dr. Birgit Schittek, University of Tübingen. The cells were maintained in K-sfm medium supplemented with 1% penicillin, human recombinant epidermal growth factor (rEGF) and bovine pituitary extract (BPE). K4 cells (SV40 Large T antigen-immortalized human dermal fibroblast cells) were cultured in Dulbecco's Modified Eagle Medium (DMEM) supplemented with 10% FCS and 1% penicillin.

3.2 Cell irradiation

Radiation of N/TERT-1 cells was performed using a Multirad 225 X-ray radiation system. The cells were irradiated with a dose rate of 2.15 Gy/min, a tube voltage of 200kV and a tube current of 17.8mA. A filter composed of 0.5mm copper was used to increase the hardness of the photon beam.

3.3 Clonogenic assay

N/TERT-1 cells were seeded in $25cm^2$ flasks with different numbers in each group. The

groups and cell number for each group is shown in Table 3.1.

Table 3.1 Numbers of N/TERT-1 cells seeded in 25cm² flasks for clonogenic assay

Radiation dose	N/TERT-1 Cell number
0Gy	500
1Gy	500
2Gy	1500
4Gy	3000
6Gy	4000
10Gy	5000

24h after cell seeding radiation was delivered. The cells were then placed in an incubator at 37℃ and 5% CO_2 and left until colonies formed. Crystal violet staining was used to identify colonies for counting. Crystal Violet solution was prepared by diluting 1 gram of crystal violet in 10ml of EtOH followed by addition of 490ml of milliQ water. Medium was removed from the 25cm² flasks and 3ml of crystal violet was added for 5 minutes, then the crystal violet was discarded. The flasks were rinsed 3 times with tap water and allowed to dry at RT for one day. The colonies were then counted using a light microscope. Only colonies with more than 50 cells were counted.

Plating efficiency (PE) and surviving fraction (SF) was calculated using the following formulas:

$$PE = \frac{number\ of\ colonies\ formed}{number\ of\ cells\ seeded}$$

$$SF = \frac{PE\ (irradiated\ group)}{PE\ (unirradiated\ controls)}$$

To test the effect of DKK3 expression on clonogenic survival, three different groups were designed: control, nonsense siRNA, DKK3 siRNA. N/TERT-1 cells were seeded in 25cm² flasks in triplicate. 24h later siRNA (20nM) transfection (see Methods 3.11) was performed. After 48h of treatment (DKK3 modulation), radiation was delivered to the cells. The cells were then placed in an incubator at 37℃ and 5% CO_2 until colonies formed. Staining, counting and survival fractions were determined as described above.

3.4 Proliferation assay

5×10^4 N/TERT-1 cells were seeded in $25cm^2$ flasks with triplicates in each group. 24h later the cells were irradiated with increasing doses of radiation (1Gy, 2Gy, 4Gy, 6Gy, 10Gy). Three days after irradiation, the number of living cells in each flask were counted. To perform this, the culture medium was removed and collected in a 15ml tube, then 2ml of PBS was added to rinse the cells. 1ml of 0.05% trypsin-EDTA was then added to detach the cells. 5 minutes later, 8ml of medium with 10% FCS was added to stop the digestion. Cells were then gently suspended and transferred into tubes. The cells were centrifuged at 180 x g (rt) for 3 minutes. The supernatant was discarded and the cell pellets were resuspended in 500µl of medium. The living cells were counted with a cytometer under an inverted microscope as described.

To further test the effect of DKK3 expression on cell proliferation, three different groups were designed: control, nonsense siRNA, DKK3 siRNA. N/TERT-1 cells were seeded in $25cm^2$ flasks in triplicate. 24h later siRNA (20nM) transfection (see Methods 3.11) was performed. 48h later radiation was delivered to the cells. Proliferation assays for each group was performed as described above.

3.5 Chemical ROS stimulation and ATP assay

Cell viability after chemical ROS stimulation was determined by ATP luminescent cell viability assay. N/TERT-1 cells engineered with a TCF/canonical Wnt pathway reporter vector (see Methods 3.14) were seeded in 96 well plate in triplicate in K-sfm medium (without penicillin or growth factors) with 5000 cells/well. 48h later, different concentrations (0nM, 500nM, 1000nM, 2000nM, 4000nM) of the chemical ROS inducer rotenone were added. 12h later, rotenone was gently washed out using PBS, then fresh K-sfm medium (without penicillin or growth factors) was added. 12h after stimulation, part of the medium was collected for ELISA measurement of DKK3 and *Gaussia* luciferase measurements (see Methods 3.14) of canonical Wnt activity. 100µl medium was left in each well. 50µl of ATP luminescent cell viability assay was added to each well, and the plate was gently shaken at RT for 20 minutes. Results were read

using a plate reader.

3.6 Cell cycle, apoptosis and DNA damage measurements

3.6.1 Sample preparation

N/TERT-1 cells with inducible DKK3 (generation of this cell line see Methods 3.14) were seeded in 25cm^2 flasks with 2×10^5 cells/flask in 5ml of K-sfm medium (without penicillin or growth factors) in triplicate. Groups are described in Table 3.2.

Table 3.2 Groups for N/TERT cell cycle, apoptosis and DNA damage measurements

0Gy	1Gy	4Gy
Con	Con	Con
Dox 0.4 µg/ml	Dox 0.4 µg/ml	Dox 0.4 µg/ml
DKK3 siRNA	DKK3 siRNA	DKK3 siRNA

24h later the growth medium was exchanged, and DKK3 knockdown with 20nM DKK3 siRNA (see Methods 3.11) or DKK3 over expression with 0.4µg/ml doxycycline (see Methods 3.12) were performed. 48h later the cells were irradiated using a MultiRad 225 machine with a single dose of 1Gy and 4Gy. 4 days after radiation, samples were collected for FACS and microscopy analysis.

3.6.2 Sample collection

Solution used in this procedure is shown in Table 3.3.

Table 3.3 Solution used for sample collection of N/TERT cell cycle, apoptosis and DNA damage measurements

Name	Solution	Volume/sample
Fixation solution	4.5% PFA/PBS	2 ml
Permeabilization	70% ethanol/ H$_2$O	3 ml
Washing solution	0.5% BSA/PBS	7 ml
Antibody diluent	3% BSA/PBS	100 µl
DNA staining PBS	1 µg/ml DAPI/PBS	200 µl

Medium from each flask was collected in a 15ml tube. Cells were detached using the method described above. All washing solutions and cell suspension was collected in 15ml tubes with the conditioned medium collected in the beginning. Centrifugation was performed at 200 x g 7°C for 5 minutes. Afterwards the supernatant was discarded and cell pellet was resuspended in 1ml of PBS. The cell suspension was transferred to a tube with 2ml of fixation solution and incubated for 10 minutes at RT. Centrifugation was performed at 200 x g 7°C for 5 minutes. The supernatant was discarded and the cell pellet was loosen by tapping onto the tubes and eventually resuspended in 3ml of 70% ethanol. Further analysis was performed using FACS and microscopy.

3.6.3 FACS staining

Cell suspensions were centrifuged at 200 x g 7°C for 5 minutes. Supernatants were discarded and cell pellets were loosen by tapping on the tube followed by resuspension in 3ml of washing solution. Centrifugation was performed at the same settings as before. Supernatant was discarded. The same washing step was repeated one time with 3ml of washing solution, then one time with 1ml of washing solution. In the last step, the supernatant was discarded carefully by pipetting. γH2AX antibody (for double DNA strand breaks, DSBs) was diluted at 1:20, and active caspase-3 antibody (for apoptosis) was diluted at 1:20 with antibody diluent. Cell pellets were loosen by tapping on the tubes and resuspended in 100 µl of antibody solution. The cells were then incubated with antibodies in the dark for one hour at RT. Centrifugation was performed at the same setting as above and the supernatant was discarded. Cell pellets were loosen by tapping on the tube and resuspended in 200µL of DNA staining solution. Samples were pipetted through the filter cap of FACS tubes, and placed on ice in the dark for subsequent FACS analysis.

3.6.4 FACS analysis

FACS measurements were performed using a LSRII flow cytometer and data analysis performed using FlowJo 7.6.5 software (in collaboration with Ramon Lopez Perez, Molecular Radiooncology, DKFZ, Heidelberg). Three independent experiments were carried out on N/TERT-1 cells with triplicate samples for each experiment. During the FACS measurements, 10,000–20,000 cells were acquired from each sample.

3.6.5 Microscopic evaluation of γH2AX induction

Slides were prepared with the same samples used for FACS analysis. 20μL of sample was put onto glass slides and a cover glass was carefully placed on top of the slide without bubbles. The slides were dried at RT avoiding light. Slides were imaged and analyzed using a motorized fluorescence microscope with Metafer software (MetaSystems) in collaboration with Ramon Lopez Perez (Molecular Radiooncology, DKFZ, Heidelberg). For each sample at least 500 cells were acquired.

3.7 ROS measurement after irradiation

N/TERT-1 cells were seeded in 96 well plates in K-sfm medium (without penicillin or growth factors) in triplicate with 5000 cells/well. 24h later a single dose of 4Gy radiation was delivered. 2h and 24h after radiation, ROS levels were measured by the cell-permeable 2',7'-dichlorodihydrofluorescein diacetate (H2DCFDA) assay. Briefly, medium was removed and the cells were gently washed with 1x PBS. 100μL of H2DCFDA ROS assay solution was added to each well. The cells were incubated in a 37°C incubator with 5% CO_2 for 30 minutes. The results were read using a plate reader (luminescence).

3.8 Quantitative Real Time PCR

3.8.1 RNA isolation

10µl of 2-mercaptoethanol was added to 1ml of lysis buffer taken from a PureLink RNA Mini Kit. Medium was discarded, and the cells were washed 2 times with cold PBS. 350µl of lysis buffer work solution was then added to the cells in one well of a 6 well plate. After incubating for 3 minutes, the cells were scratched lose and the lysate was transferred into an Eppendorf tube for RNA isolation. RNA was isolated using the PureLink RNA Mini Kit following the manufacturer's instructions. RNA was eluated in 35µl of RNase free water.

3.8.2 Reverse Transcription

30µl of isolated RNA was added to 15µl of a RT+ reaction mix. To exclude a PCR signal from genomic DNA contamination, and to check the specificity of the primers, a reverse transcriptase negative (RT-) sample was included. 3µl of RNA was diluted to 1:10, then 30µl of diluted RNA was added to 15µl of the RT- reaction mix. The reagents for RT+ and RT- reaction mix is shown in Table 3.4 (volume for each sample):

Table 3.4 The reagents for RT+ and RT- reaction mix (volume for each sample)

Reagents	RT+	RT-
Hexanucleotides (10x)	0.5µl	0.5µl
Acrylamid(15µg/ml), linear	0.5µl	0.5µl
Rnasin 40U/µl	1µl	1µl
DTT 0.1M	2µ	2µ
dNTP 25mM	1µl	1µl
First-strand buffer (5x)	9µl	9µl
Superscript 200U/µl	1µl	-

The reaction mix was incubated at 42 °C for 1.5h on a thermal shaker for reaction. Then a short centrifugation was performed and the samples were stored in a -20 °C freezer until further use.

3.8.3 Quantitative PCR (qPCR)

Real-time quantitative polymerase chain reaction (RT-qPCR) was performed using the SYBR Green method. 2µl of RT+ (1:10) dilution or 2µl RT- samples were added to the master mix to form a total volume of 20µl per well. Each sample was analyzed in duplicates. The reagent master mix is shown in Table 3.5.

Table 3.5 The reagent of master mix of qPCR (volume for each sample)

Reagents	Volume
SYBRgreen	10µl
Forward primer (300nM)	0.6µl
Reverse primer (300nM)	0.6µl
Taq DNA Polymerase	0.12µl
H2O	6.68µl

18S rRNA was used for reference gene. A no template control for target and reference gene was carried out by adding 2µl of water instead of diluted cDNA. Both reference gene and template controls were carried out under the same reaction components and the same conditions.

Plates were sealed and centrifuged briefly to spin down reagents from the walls of the reaction tubes. DNA amplification was performed using a Light Cycler 480 detection system. For Pre-incubation, samples were held at 50°C for 2 minutes and 95°C for 10 minutes. Amplification was carried out with 40 cycles, at each cycle the samples were held at 95°C for 15 seconds, and at 60°C for 60 seconds. A melting step was determined by holding the samples for 5 seconds at 95°C, then for 5 seconds at the second target 65°C.

For calculation: cycle threshold (CT) values for 18s rRNA (CT_{ref}) and target gene (CT_{target}) were measured by Light Cycler 480. Results were shown with target mRNA/18s rRNA.

$$\text{Relative mRNA/18s rRNA} = 2\char`^ CT_{target} - CT_{ref}$$

3.8.4 Primers used for target genes

The mRNA level of chemokines and growth factors secreted by N/TERT-1 cells after DKK3 modulation were measured by RT-qPCR. The sequences of primers used were shown in Table 3.6.

Table 3.6 Primer sequences

Gene	Forward primer	Reverse primer
18s	GCAATTATTCCCCATGAACG	AGGGCCTCACTAAACCATCC
DKK3	GTGCATCATCGACGAGGACTGT	TGGTCTCCACAGCACTCACTGT
TGF-β1	TACCTGAACCCGTGTTGCTCTC	GTTGCTGAGGTATCGCCAGGAA
GM-CSF	GGAGCATGTGAATGCCATCCAG	CTGGAGGTCAAACATTTCTGAGAT
IL-1 β	CCACAGACCTTCCAGGAGAATG	GTGCAGTTCAGTGATCGTACAGG
TNF-α	CTCTTCTGCCTGCTGCACTTTG	ATGGGCTACAGGCTTGTCACTC
CXCL8	TATCCAGAGGCTGGAGAGCTAC	TGGAATCCCTGACCCATCTCTC
CXCL10	GGTGAGAAGAGATGTCTGAATCC	GTCCATCCTTGGAAGCACTGCA
PDGFA	CAGCGACTCCTGGAGATAGACT	CGATGCTTCTCTTCCTCCGAATG

3.9 Western blot

3.9.1 Protein extraction

RIPA buffer work solution was prepared in advance: 9ml ddH2O, one tablet protease inhibitor and one tablet phosphatase inhibitor were added to 1ml of RIPA buffer and mixed well. All procedures were performed on ice. The centrifuge was pre-cooled to 4°C.

Medium was discarded and cells were washed 2 times with cold PBS. 60μl of cold RIPA buffer work solution was added to cells in one well of 6 well plate with 80% confluence. After incubation for 10 minutes, the cells were scratched free and lysate was added to an Eppendorf tube. The samples were then centrifuged at 13000rpm 4° for 20 minutes, supernatant was collected, then aliquoted into Eppendorf tubes and stored at -80 °C for further use.

3.9.2 Protein quantification

Protein concentration was determined using a Pierce BCA Protein assay kit. A protein

standard curve was created using BCA solution. BCA (dilution 1:4) was prepared by adding 90µl of ddH$_2$0 to 30µl of BCA (2mg/ml). The BCA solution for the standard curve was prepared as shown in Table 3.7.

Table 3.7 The preparation of BCA solution for protein quantification standard curve

Conc (µg/ml)	BCA	H$_2$O
0	0 µl (1:4)	60 µl
50	6 µl (1:4)	54 µl
100	12 µl (1:4)	48 µl
250	30 µl (1:4)	30 µl
500	60 µl (1:4)	0 µl
750	22.5 µl	37.5 µl
1000	30 µl	30 µl
2000	60 µl	0 µl

Samples and RIPA buffer work solution were thawed on ice and subsequently diluted by 1:5 with ddH$_2$0. RIPA buffer work solution was used to subtract background. BCA working agent (WA) was prepared by mixing 50 parts of BCA Reagent A with 1 part of BCA Reagent B. 25µL of each standard or sample was pipetted with replicates into a 96 microplate well. 200µl of the WA was added to each well and mixed on a plate shaker for 30 seconds. The plate was covered and incubated at 37°C for 30 minutes. The plate was then cooled before measurement. The results were read out using a plate reader at the absorbance wavelength of 562 nm. A standard curve was produced and protein concentration calculated.

3.9.3 Sample preparation

Based on the results of protein quantification, a corresponding volume of 10µg protein was supplemented with 4x loading buffer and filled to 15µl with water. 1µl DTT per 10µl sample was added as reducing reagent and the samples were vortexed, heated in a thermomixer at 95°C for 10 minutes and centrifuged at 2500rpm for 3 minutes. Afterwards the samples were used for western blot, or stored at -20°C for further use.

3.9.4 Buffer preparation

Buffers needed for gels and blotting were prepared as below:

Separating Gel buffer:

1.5M Tris-HCl pH 8.8 + 0,4%SDS*(*electrophoresis grade)

Stacking Gel buffer:

0.5M Tris-HCl pH 6.8 + 0.4%SDS*

10x Tris-Glycine-SDS Running buffer:

Tris-base   30.3g

Glycine   144g

SDS*   10g (*electrophoresis grade)

Fill using ddH2O to 1L

1x Running Buffer (Tris-Glycine-SDS)

10x Tris-Glycine-SDS Running buffer   100ml

ddH2O   900ml

Mix well and store at RT until usage

10x Tris-Glycine Transfer buffer:

Tris-base   30.3g

Glycine   144g

Fill to 1 L with ddH2O

1x Transfer buffer (Tris-Glycine Methanol) for BioRad Blot system

10x Tris-Glycine Transfer buffer   100ml

Methanol   200ml

ddH2O   700ml

Mix well and store at -20°C bis until usage

Stripping buffer

1M Tris/HCl pH 6,8   3,1ml

10% SDS   10ml

ddH2O   37ml

100mM beta Mercaptoethanol   390µl

3.9.5 Migration and blotting

Gels were placed in the electrophoresis apparatus. 1x Tris-Glycine-SDS running buffer was filled to the appropriate volume marked on the chamber. Samples (15µl/slot) and markers (5µl/slot) were added to the wells. All unused slots were filled with 1x loading buffer. Gels were run initially at 60V for 15 minutes, then the voltage was increased to 120v and the gels were run for an additional 1.5 hours. Then the gels were removed and placed in the transfer "sandwich".

PVDF Membranes were first activated for 30 seconds in methanol, then washed for 2 minutes in ddH2O and kept in blotting buffer. The sandwich-blot was then placed in the blotting chamber together with a cool pack in ice cold transfer-buffer and current was applied for 75 minutes at constant 100V.

After blotting, the transfer membrane was blocked using a 5% BSA solution (diluted in 1x TBST) for 1h at RT. Anti-DKK3 antibody was diluted with 1:2000 in 5% BSA solution. The membrane was incubated on a roller in a 50ml tube with 5ml diluted primary antibody (Table 3.8) in the 4°C cold room overnight.

Table 3.8 The concentration of antibodies used in western blot

Antibody	Host species	Dilution
Anti-DKK3 antibody	Rabbit	1:2000
Anti-rabbit IgG	Goat	1:2000
β-Actin Rabbit mAb	Rabbit	1:2000

The next day the membrane was washed with 1x TBST buffer for 5 minutes x 3 times. Afterwards the membrane was incubated in a working solution of secondary antibody at RT for 1h. Then membrane was subsequently washed with 1x TBST buffer for 5 minutes x 3 times and incubated with LumiGlo Mix (500µl Reagent A + 500µl Reagent

B + 9ml ddH2O) for 2 minutes. In the end, the membrane was analyzed using an Amersham 680 Imager. Afterwards membranes were washed with 1x TBST buffer for 5 minutes x 3 times, then incubated with stripping buffer at 65°C for 25 minutes. Blocking, incubation of anti-β-Actin antibody and secondary antibody and read out were performed the same as described above. Images were then evaluated using Image J.

3.10 ELISA

3.10.1 Sample preparation

Conditioned medium from cell culture was collected in a 15ml falcon tube and centrifuged at 13000rpm for 10 minutes at 4°C. Supernatant was saved, aliquoted and frozen at -80°C until further use. Repeated thawing and freezing samples was avoided.

3.10.2 Plate preparation

The analysis procedure was performed by following the instructions provided in the human DKK3 ELISA kit (R&D system). Capture antibody was diluted in PBS to 4μg/ml and coated onto a 96 well microplate. The plates were sealed and incubated overnight at RT. On the second day capture antibody was discarded and the plates were washed using wash buffer (0.05% Tween 20 in PBS) x 3 times. 300ul of reagent diluent (1% BSA in PBS) was then added to each well and incubated for one hour to block. Then the liquid was removed and each plate was washed 3 times using washing buffer.

3.10.3 Assay procedure

Samples collected from cell culture were diluted with reagent diluent to 1:10. 100ul of diluted samples was added to each well and incubated at RT for 2h. Then 3 washing steps were performed as detailed above. Detection antibody was diluted to 40ng/ml in reagent diluent. 100μl of diluted detection antibody was then added to each well

and incubated at RT for 2h. 3 washing steps were again performed. Streptavidin-HRP was 200 fold diluted in reagent diluent. 100ul of diluted Streptavidin-HRP was added to each well, and the plate was incubated at RT for 20 minutes. 3 washing steps were performed. Substrate solution was prepared by mixing 1:1 color reagent A (H_2O_2) and color reagent B (Tetramethyblenyidine). 100µl of substrate solution was then added to each well and incubated at RT. Direct light was avoided in the Streptavidin-HRP and Substrate solution procedures. Stop solution (2N H_2SO_4S) was added at a volume of 50µl/well. Results were then read using a reader at the absorbance wavelength of 562 nm.

3.11 DKK3 siRNA transfection

Cells were seeded in 6 well plates at $1x10^5$ cells/well in 2.5ml medium/well. 24h after seeding, the DKK3 siRNA transfection was performed. Transfection complex was prepared by mixing 250ul of serum free medium, 12ul of HiPerfect Transfection Reagent and 2.5ul of DKK3 siRNA (stock solution 20uM). The final working concentration of DKK3 siRNA was 20nM. For negative controls, DKK3 siRNA was replaced by the same concentration of nonsense siRNA. The transfection complex was incubated for 15 minutes at RT before transfection. Medium was changed before transfection, subsequently the transfection complex was added to one well of a 6 well plate and gently mixed with medium. Medium was changed 24h after transfection to reduce the siRNA toxicity. Medium, RNA and protein were collected for validation with ELISA, RT-qPCR and western blot at 48h after transfection.

3.12 DKK3 over expression

N/TERT-1 cells engineered with a doxycycline inducible DKK3 vector (see Methods 3.14) were seeded on 96 well plates. One day after seeding, the cell medium was changed and 0.4µg/ml doxycycline was added to the cells. 24h later doxycycline was removed by changing the medium. Medium, RNA and protein was collected for validation with ELISA, RT-qPCR and western blot at 48h after stimulation.

3.13 Chemokines and growth factor array

3.13.1 Sample preparation

N/TERT-1 cells with inducible DKK3 were seeded in 6 well plates with 1×10^5 cells/well in 2.5ml of K-sfm medium (without PS or growth factors). 24h after seeding, the medium was changed, DKK3 knockdown with siRNA and DKK3 over expression with doxycycline were performed as described. 48h later the treated cells were irradiated by MultiRad 225 machine with a single dose of 4Gy.

Four days after radiation, medium was changed to K-sfm medium with 0.5% BSA. 24h later medium was collected and centrifuged at 1500rpm for 20 minutes at RT. Supernatants were collected, aliquoted and frozen at -80°C until measurement.

3.13.2 Chemokines and growth factor assay

The chemokines and growth factors measured in this assay included human TGF-β1, IL-4, IL-6, IL-10, IL-1β. CXCL8, CXCL10, IFN-ŗ, FGF, G-CSF, GM-CSF, M-CSF, PDGF-AA, PDGF-BB, VEGF and TGF-α. Measurement was carried out using a commercial analysis kit (LEGENDplex custom Panel chemokines and growth factors). A standard was first prepared. The standard cocktail was reconstituted with 250µl of assay buffer and incubated at RT for 10 minutes to generate a stock concentration of 10,000pg/ml. 45µl of reconstituted standard solution was then added to Eppendorf tubes (C7), or aliquoted and stored in -80 ℃ until further use. Another 6 tubes were labeled as C6, C5, C4, C3, C2, C1, C0. 45 µl of assay buffer was added to each of the 6 tubes. 15µl of the higher concentration standard was transferred to the lower concentration as indicated in Table 3.9.

Table 3.9 Standard preparation for chemokines and growth factors array

Standard ID	Serial dilution	Assay buffer to add (µl)	Standard to add (µl)	Final conc. (pg/ml)
C7	--	--	--	10,000
C6	1:4	45	15 µl of C7	2500

C5	1:16	45	15 µl of C7	625
C4	1:64	45	15 µl of C7	156.3
C3	1:256	45	15 µl of C7	39.1
C2	1:1024	45	15 µl of C7	9.8
C1	1:4096	45	15 µl of C7	2.4
C0	--	45	--	0

The tubes were briefly vortexed after each dilution step. Beads mix was prepared by diluting all capture beads in assay buffer (each capture beads was mixed by vortexing for more than one minute). All reagents were brought to RT before use. All standards and samples were run in duplicate. The assay plate was kept upright during the entire assay procedure to avoid losing beads. For all incubation steps, the plate was placed in the dark or wrapped with aluminum foil.

To start the assay, 15µl of assay buffer was added to all wells, 15µl of each standard was added to the standard wells, 15µl of each sample was added to the sample wells, 15µl of mixed beads and 15µl of detection antibodies was added to all wells. Then the plate was sealed with aluminum foil and shaken on a plate shaker for 2h at 800 rpm RT. Afterwards 15µl of SA-PE was added to each well, the plate was again sealed with aluminum foil and again shaken for 30 minutes at 800rpm RT. After incubation, the plate was centrifuged at 250 x g for 5 minutes, and the supernatant was removed by flipping the plate. 200µl of 1x washing buffer was added to all wells. Samples were resuspended by pipetting and the plate was centrifuged at 250 x g for 5 minutes. Supernatant was again removed by flipping the plate. The same washing step was repeated for one more time. At the end, the samples were transferred into FACS-tubes and data acquired at FACS Canto I and analyzed with LEGENDplex Data Analysis Software in collaboration with Joscha Kraske (Molecular Radiooncology, DKFZ, Heidelberg).

3.14 Reporter cell line preparation and validation

For this study, an vector platform generated in house and described by Jackel *et al.* [76] was employed to generate dual inducible DKK3 gene and canonical Wnt reporters, or

Wnt reporters alone, in the N/TERT-1 and K4 (immortalized human dermal fibroblast) cell lines. Cells were transfected with pSB.Z.CMV/TO.DKK3 and pSBTR.Wnt (Addgene nr #79482) pSB.Z.CMV/TO in collaboration with Khuram Shehazd (Medical Clinic and Polyclinic IV, LMU, Munich). DKK3 expression plasmid was made using pSBDEST.Z, pENTR-221-CMV/TO pro and pENTR-221-DKK3 in two fragment Gateway cloning as per manufactures instructions and as described by Jackel *et al*. Cells were co-transfected with pSBTR.Wnt (Addgene nr #79482) pSB.Z.CMV/TO[76].

Validation of inducible DKK3 expression was carried out by 0.4µg/ml doxycycline stimulation and subsequently measuring DKK3 levels with ELISA, RT-qPCR and western blot. Validation of canonical Wnt reporter was done by stimulating the Wnt reporter cells with different concentrations (con, 100ng/ml, 200ng/ml, 400ng/ml and 800ng/ml) of Wnt3a recombinant protein and subsequently collecting the medium and measuring canonical Wnt activity in the cell culture supernatant using a *Gaussia* luciferase kit. 10µl of cell culture supernatant was added to 100µl of pre-prepared substrate/buffer solution. After 30 seconds of incubation measurement was performed using a Berthold Lumat LB 9507 Luminometer.

3.15 Monocyte culturing in keratinocyte conditioned medium

3.15.1 Keratinocyte conditioned medium preparation

N/TERT-1 cells with inducible DKK3 were seeded in 75cm^2 flasks with a number of 4 x 10^5 cells/flask in 15ml of K-sfm medium without penicillin or growth factors. 24h later medium was changed, DKK3 knockdown with siRNA and DKK3 over expression with doxycycline was performed as described above. 24h after DKK3 modulation, medium was changed with 15ml of fresh K-sfm medium without penicillin or growth factors. 7 days afterwards medium was collected, centrifuged at 1500 rpm RT for 20 minutes. Supernatant was collected, aliquoted and frozen at -80°C until monocyte culture.

3.15.2 Monocyte isolation from human full blood

Whole blood was drawn from a healthy donor, mixed 1:1 with PBS, carefully overlayed on 15ml of Ficoll in 50ml falcon tubes, and centrifuged at 2000 rpm RT for 20 minutes without brake. Interfase cells (peripheral blood lymphocytes, PBL) were carefully removed using a 10ml pipette and transferred into a new 50ml tube, and mixed 1:1 with PBS/2mM EDTA. Centrifugation was performed at 1900 rpm RT for 12 minutes with brake. Subsequent procedures were all carried out on ice. Supernatants were removed by carefully pipetting and the PBL pellet was resuspended in 5ml of ice cold MACS buffer (PBS + 0.5% human serum + 2mM EDTA). Tubes were rinsed with another 5ml of MACS buffer. The PBL solution was filtered through a previously moistened 40μm cell strainer. Cells was diluted 1:10 by trypan blue with 3% acetic acid, cell number was determined with the method described earlier. PBL cell samples were filled with MACS buffer to 50ml and centrifuged at 1900rpm 4°C for 12 minutes. The required amount of micro-beads was calculated as 20μl beads per 10^7 total PBL in 80μl buffer. After the second washing step, supernatant was removed and the PBL pellet was resuspended in the calculated amount of buffer and beads, mixed well with pipetting. Incubation was done on ice for 15 minutes. Then 20 times the amount of cold MACS buffer was added and centrifugation was performed at 1200rpm 4°C for 10 minutes. In the meantime, a column was clamped in the MACS separator and equilibrated with 3ml buffer. After centrifugation, supernatant was removed and the cell pellet was resuspended in 5ml of cold MACS buffer. This cell solution was then added to the prepared column and run through completely. Afterwards, the column was rinsed 2 times with 5ml buffer. The column was removed from the magnet, 5ml of MACS buffer was added to the column and the plunger was used to squeeze the cells into a 15ml tube. An aliquot of cells was taken for counting as described above. Centrifugation was performed at 1200rpm 4°C for 10 minutes. Supernatant was removed and the cell pellet was resuspended in AIM-V medium. The cells were seeded in 6 well plates. $5x10^6$ cells were seeded in the control group with 5ml of Mo-DC differentiation medium, 5ml of the same medium was added on day three. $7.5x10^6$

cells were seeded for each condition medium groups with different condition mediums using as detailed in the following text: on day zero 3 ml of AIM-V medium and 1 ml of condition medium prepared before was added. On day two and day five, 1 ml of condition medium was added to related plates to feed the cells. On day seven samples were collected as described below.

3.15.3 Sample collection

Samples were collected for further FACS analysis on day seven. Medium was transferred into 15ml falcon tubes. 2ml AIM-V medium was added, then the keratinocyte-conditioned macrophages (KcMφ) were scratched gently from the edge to the middle and transferred into the tubes. Scratching was repeated one time to make sure all cells were collected. Cells were centrifuged at 300 x g at RT for 10 minutes. Afterwards supernatant was collected, aliquoted and frozen at -80°C for further experiments. Cells were resuspended in 1ml of AIM-V medium. Cell number was determined with the method described above. 2×10^5 cells/group were used for FACS staining.

3.15.4 FACS staining of *in vitro* derived macrophages

Keratinocyte-conditioned macrophages (KcMφ) were washed with 500ul of PBS/2mM EDTA, and centrifuged at 15000rpm at RT for 5 minutes. Supernatant was discarded. The following procedures were all performed on ice in the laboratory of Elfriede Noessner (Helmholtz Center, Munich). Master mix was prepared by adding relevant antibodies to FACS buffer (PBS / 2% FCS / 2mM EDTA / 0.1% NaN3) to a total volume of 33.3μl. The antibodies and volumes used for analysis are shown in Table 3.10.

Marker	Reactivity	Color	Volume/sample (μl)

LIVE/DEAD Fixable Blue	Human	Blue fluorescence	0.3
CD14	Human	A700	3.0
CD163	Human	PerCP Cy5.5/PE	5.0
CD64	Human	PE	5.0
CD206	Human	FITC/PerCPCy5.5	5.0
CD80	Human	FITC/PerCy7	5.0
CD86	Human	FITC/APC	5.0
HLADR	Human	FITC/APCCy7/PeCy7/PE	5.0

Table 3.10 Volumes of antibodies for master mix of FACS analysis *in vitro*

For negative controls, 30µl of FACS buffer instead of antibodies was added to 0.3µl live/dead fixable blue. 33.3µl master mix was added to each sample and incubated for 30 minutes on ice avoiding light. Afterwards the FACS tubes were centrifuged at 15000rpm for 5 minutes. Then the samples were washed with FACS buffer for two times and resuspended in 100µl of FACS buffer for measurement.

Compensation was carried out with beads. First, FACS tubes were prepared for each color. 70µl of FACS buffer was added to each tube (for live/dead cells, buffer without FCS). For antibodies, one drop beads (both positive and negative) was added to 1µl of antibody. For live/dead characterization, one drop beads (here only positive beads were added, negative beads were added after washing) for live/dead was added to 0.3µl of live/dead fixable blue. The compensation mix was incubated on ice for 30 minutes avoiding light. Afterwards the FACS tubes were centrifuged at 15000rpm for 5 minutes. Samples were then washed with FACS buffer 2 times and resuspended in 100µl of FACS buffer for measurements.

3.16 Mouse irradiation

All mouse experiments were carried out at the animal facility and the division of Molecular Radiooncology at the German Cancer Research Center (DKFZ) in Heidelberg with the help of Richard Jennemann (Lipid Pathobiochemistry, DKFZ, Heidelberg) and Alexandra Tietz (Molecular Radiooncology, DKFZ, Heidelberg). All animal experiments were approved by the DKFZ institutional review board (IRB) and governmental authorithies (Regierungspräsidium, Karlsruhe, Germany). The relevant animal care

numbers were G-280/19, G-255/20 and G-113/21 (Roger Sandhoff and Peter Huber, DKFZ, Heidelberg).

Before irradiation, all mice were weighed and anesthetized with 70mg/kg ketamine and 7mg/kg xylazine. 5-10 minutes after anesthesia, the mice were fixed in a radiation device designed for hind limb or thorax radiation as shown in Figure 3.1.

Radiation of the mice was performed using a MultiRad 225 X-ray radiation system. Mice were irradiated with a dose rate of 5.53 Gy/min, a tube voltage of 200 kV and a tube current of 17.8 mA. A filter composed of 0.5 mm copper was used to increase the hardness of the photon beam.

A Hind limb irradiation
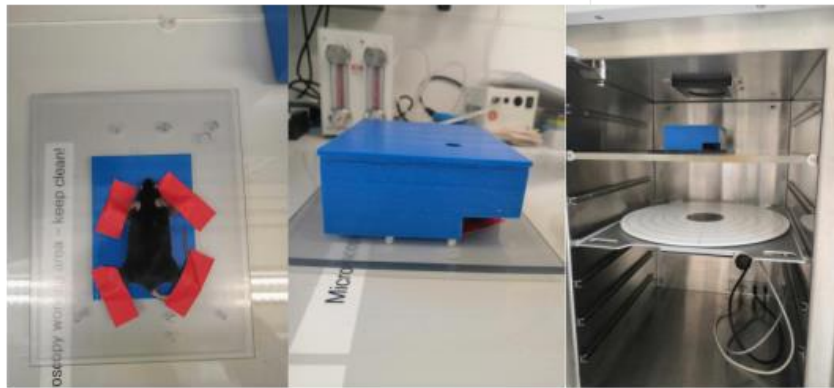
B Thorax irradiation
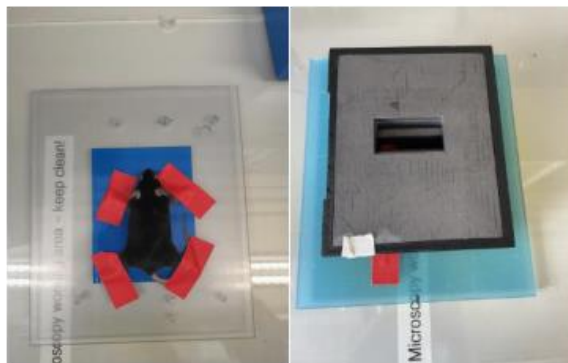
Figure 3.1 The setting up of mice irradiation using a MultiRad 225 X-ray radiation system. (A) Hind limb, (B) Thorax irradiation. Special lead devices were used to shield the not to be irradiated parts of the mouse.

3.17 Mouse line generation

Female 12-week-old mice were used for the experiments. All mice used in this study were generated based on a C57Bl6/N background. All mouse breeding was performed in collaboration with Richard Jennemann (Lipid Pathobiochemistry, DKFZ, Heidelberg). Mice were kept under specific pathogen free conditions in the animal facility of the German Cancer Research Center.

Generation of global DKK3 knockout mice

An embryonic stem cell clone containing a floxed allele of DKK3 (clone EPD0642_3_H05) was purchased from The Knockout Mouse Project (KOMP). The floxed DKK3 line had been bred with Cre-deleter mice to generate global DKK3 knockout mice.

Generation of keratinocytes specific DKK3$^{-/-}$ mice

The floxed DKK3 mice were bred with Cre-recombinase expressing animals under control of the Keratin14 (Krt14) promoter, resulting in a cell-specific knockout of the DKK3 gene in keratinocytes.

Generation of fibroblasts specific DKK3$^{-/-}$ mice

The floxed DKK3 line was paired with Cre-expressing mice under control of the "Platelet Derived Growth Factor Receptor" (PDGFR) promoter, inducing a cell-specific knockout of the DKK3 gene in fibroblasts. All DKK3 lines have been in breeding for many years. No phenotype was observed at any time (i.e. no behavioral changes, no reproductive abnormalities).

Generation of DKK3/Wnt dual reporter mice (DKK3-LCh x TCF/LEF)

The strain combined the mutations Tg (DKK3-luc/mCherry) #Hjg and Tg (TCF / Lef1-HIST1H2BB/EGFP) 61Hadj on a B6 strain background. DKK3-LCh is a luciferase mCherry-expressing reporter which indicates DKK3 promoter activation in the mouse [60]. Tcf-Lef-GFP was used as a reporter for the canonical Wnt signaling pathway[77]. The crossing of these lines resulting in the generation of a reporter mouse line that can be used as a dual reporter for induced DKK3-expression and activation of the canonical Wnt pathway. The established, unencumbered transgenic double transgenic reporter

mice did not present with any stress-induced phenotype.

3.18 Histology

The histology work has been done in collaboration with Gabi Schmidt and Claudia Schmidt (Core facility, DKFA, Heidelberg).

3.18.1 Preparation of slides

Immediately after sacrificing the mice, skin tissue was taken and fixed in 4% formalin for one week. Then the residual water inside tissues was removed by incubating in 70%, 96%, 100% alcohol. The residual alcohol was removed by xylene. Then tissues were embedded in lipophilic paraffin. After the paraffin blocks were cooled down, paraffin-embedded skin sections (4µm) were cut with a microtome. For deparaffinization, paraffin was removed by treating the slides with xylene for 5 minutes x 2 times. For hydration, sections were in alcohol (100% x 3 times, 96% x 2 times, 70% x 1 time), sections were washed with PBS for 5 minutes x 2 times. Then the hydrated sections were proceeded with histological and immunohistological analysis.

3.18.2 Immunohistological staining

Before primary antibody incubation, the sections from the last step were blocked with a mixture of 30 % H_2O_2 (20ml) and methanol (180ml) for 20 minutes in the dark. The slides were then washed in PBS for 5 minutes x 2 times. Afterwards the slides were incubated with 50µl of Avidin for 15 minutes and Biotin for an additional 15 minutes to block the endogenous biotin. After incubation, the slides were washed with PBS for 5 minutes x 2 times. After blocking, the slides were incubated with different primary antibodies at 4°C overnight (the primary antibodies used in our study are described in the materials section). The next day the slides were washed in PBS for 5 minutes x 2 times. Then slides were then incubated with biotinylated secondary antibody for 30 minutes at RT. Washing was performed in PBS for 5 minutes x 2 times. Slides were incubated with substrate solution for 30 minutes at RT followed by 2 times washing

with PBS and Tris-HCl buffer. Then slides were stained in DAB solution, and counter stained with methyl green. Dehydration was carried out by incubation with 96 % ethanol for 10 seconds, 100 % ethanol for 10 seconds, and in the end xylene for 10 seconds. Then slides were mounted with cover lips.

3.18.3 H&E staining

The slides prepared in 3.18.1 were used for H&E staining. The general procedure is as follows:

Dewaxing: Slides were dewaxed with xylene I and II for 10 minutes each.

Rehydration: Slides were treated with alcohol (100% I, 100% II, 96%, 96%, 80%, 70%), 5 minutes for each. Then slides were rinsed with running water for 5 minutes x 3 times.

Hematoxylin staining: Slides were stained with hematoxylin for 2 minutes, afterwards rinsed with running water for 5 minutes.

Eosin staining: Slides were stained with eosin for one minute, and rinsed with running water for 5 minutes x 3 times.

Dehydration: Slides were dehydrated with 70%, 80%, 96%, 96%, 100% alcohol for 10 seconds each, then treated with xylene I and xylene II for 1 minute each. Then the slides were dried and mounted with cover lips.

3.18.4 Goldner staining

The slides prepared in 3.18.1 were used for Goldner staining. The general procedure is as follows:

Buffer preparation: Weigert's iron hematoxylin was prepared by mixing 1g of Merck's hematoxylin dissolved in 100ml 96% alcohol and 1.5 g of iron III chloride from Fluka dissolved in 100ml distilled water. Orange G was prepared by dissolving 20g orange G from Chroma and 20g phosphomolybdic acid in 1L distilled water. Acid fuchsin azophloxin sol was prepared by a mixture of 1% acid fuchsin aqueous 20ml + 2 %

Peanceau de Xylidin aqueous 20ml + 0.5 % azophloxin aqueous 4ml + glacial acetic acid 1.2ml.

Dewaxing: Slides were dewaxed with xylene I and II for 10 minutes each and then washed with tape water.

Staining: Slides were stained with Weigerts iron hematoxylin for 2 minutes and rinsed under running water for 3 minutes. Then slides were treated with Acid fuchsin-azophloxin solution for 5 minutes and rinsed with 1 % acetic acid, and differentiated in orange G solution and rinsed in 1 % acetic acid. Afterwards slides were counterstained with light green 0.15 % aqueous for 5-10 seconds and briefly rinsed in distilled water. Slides were then dehydrated with 96% alcohol, ethanol x 2 times, then treated with xylene I and II for 1 minute each. In the end, the slides were dried and mounted with cover lips.

3.18.5 The quantification of histological and immunohistological stained slides

Quantification of epidermal thickness was performed with H&E-stained skin sections. 5 pictures of each section were taken, for each picture 15 values of epidermis thickness were measured with Image J. An average of 15 values were taken as the epidermis thickness for each picture, the average values of 5 pictures were taken as the epidermis thickness value for each mouse.

Quantification of collagen deposition was done with Goldner-stained skin sections. 5 pictures of each section were taken and measured, dermis is defined manually and collagen positive area/selected area is measured automatically with Image J. The average values of 5 pictures were taken as the collagen positive area (%) for each mouse.

Quantification of Ki-67, F4/80, HR3 and α-SMA positive cells (%) was done with immunohistochemical stained skin sections. 5 pictures of each section were taken and measured, dermis is defined manually and HR3 positive area/selected area is measured automatically with Image J. The average value of 5 pictures were taken as the specific antibody positive area (%) for each mouse.

3.19 Confocal imaging

3.19.1 Sample preparation

Immediately after sacrificing the mice, skin tissue was taken and fixed in 4% formalin for 24h. Then the residual water inside tissues was removed by incubating in 10%, 20%, 30% sucrose. The skin sample was cut in half, frozen quickly in Tissue-Tek on dry ice and kept in -80℃ for further use. Skin sections (4μm) were cut using a microtome before image acquisition.

3.19.2 Image acquisition

Image acquisition was performed using a Leica TCS SP5 confocal microscope (Leica Biosystems) with a 63x oil immersion objective. The tissue samples were excited with a 405 nm UV laser diode, a 405 nm argon multi line and a 488 nm DPSS laser (in collaboration with Elisabeth Grimm, Lipid Pathobiochemistry, DKFZ, Heidelberg).

3.20 FACS analysis of skin tissue

3.20.1 Cell isolation from fresh mice tissue

Fresh skin was taken from mice and placed in 6 well plates in cold PBS. Then PBS was removed and digestion buffer I (1mg/ml Dispase II + 50U/ml DNAse I diluted in PBS) was added to a volume of 2ml/well. Skin was digested at 37ºC for 45 minutes. Afterwards 1ml of FCS was added to stop digestion. Skin was then placed separately in 2ml tubes with 300μl of digestion buffer II (800U/ml Collagenase IV + 50U/ml DNAse I diluted in DMEM with 10% FCS). Samples were cut into small pieces. 1.5ml of digestion buffer II was added to fill up the tube. Incubation was carried out in a thermoshaker at 900 rpm, 37ºC for 1 h. 4μl of 0.5M EDTA was added to samples and incubated for another 10 minutes. After incubation, the samples were passed through a 70μm cell strainer into 50ml falcon tubes and washed with 20ml of HB buffer (Hanks Balanced Salt Solution + 2mM EDTA + 0.5%BSA). Centrifugation was performed at 350

× g, 4ºC for 7 minutes. Supernatant was then removed and the cell pellet was resuspended in 200μl of FACS buffer. FACS staining was immediately followed with cell isolation.

3.20.2 FACS staining

All centrifugation in this FACS staining procedure was performed at 2100 rpm at 5°C for 5 minutes. 100ul of cells were added into a well of 96 well plate for unstained control and zombie for dead cells, 200μl of cells were added to the wells of a 96 well plate for antibodies staining. Cells were centrifuged, then 200μl of FACS buffer was added for washing x 2 times. After washing, centrifugation was performed and supernatant was discarded. All wells were then incubated with 20ul of purified anti-CD16/CD32 antibody (1:50, 0.01μg/μL) in FACS buffer for 10 minutes on ice prior to immunostaining. In the meantime, a master mix was generated by diluting antibodies in FACS buffer for complete staining. The information and concentration of the various antibodies used is shown in Table 3.11.

After incubation, 30μl of FACS buffer was added to unstained and zombie wells. 30μl of master mix was added to the indicated samples. Cells were incubated on ice for 30 minutes under light protection. After incubation 200μl of PBS was added for washing for two times. Zombie aqua dye was 1:100 diluted in PBS in advance. Then cells were resuspended in 50μl of diluted zombie aqua dye and incubated at RT in the dark for 20 minutes. Then cells were washed with FACS buffer x 2 times. Afterwards centrifugation was performed, supernatant was discarded, and intracellular staining was carried out as follows:

Fixation: Cells were fixed with 100μl of 1 x IC Fixation Buffer, resuspension was done after adding the buffer. Cells were then incubated at RT for 40 minutes under protection from light. Centrifugation was performed afterwards and supernatant was discarded.

Permeabilization: Cells were resuspended in 100μl of 1X Permeabilization Buffer and centrifuged.

Blocking: Cells were incubated with 20µl of purified anti-CD16/CD32 antibody in Perm buffer (1:50, 0.01µg/µL) for 10 minutes on ice prior to immunostaining.

Immunostaining: Master mix was prepared by diluting Arg-1 and iNOS antibodies in 1x Permeabilization Buffer. Concentration of antibodies was shown in Table 3.11. 50µL of master mix was added to indicated wells and incubated for 30 minutes.

Cells were washed with commercial 1x permeabilization buffer for 2 times and then resuspended in 200µl of FACS buffer and transferred to FACS tubes and placed on ice under light protection for FACS analysis with single staining samples.

Single staining was done with beads. The beads were vortexed for at least one minute and then 1:10 diluted in FACS buffer. 50µL of diluted beads was added to indicated wells. Each antibody was then added to the indicated well. Beads were then incubated with the antibodies for 30 minutes on ice under light protection. 2 times washing was carried out with FACS buffer. Afterwards the samples were resuspended in 200µL of FACS buffer and transferred to FACS tubes and place on ice under light protection for subsequent FACS measurement. Data was acquired using FACS Fortessa and analyzed with FlowJo 7.6.5 software (in collaboration with Ramon Lopez Perez, Molecular Radiooncology, DKFZ, Heidelberg)

Table 3.11 Information and concentration of antibodies used for FACS analysis *in vivo* from mouse skin tissue

Marker	Reactivity	Color	Concentration
Ly-6C	Mouse	FITC	1:640
Ly-6G	Mouse	PE/Dazzle594	1:320
CD11b	Mouse	Alexa Fluor700	1:640
CD11c	Mouse	Brilliant Violet 785	1:40
F4/80	Mouse	BV605	1:40
MHC -II	Mouse	BV711	1:160
iNOS	Mouse	APC	1:320
Arg-1	Human/Mouse	eFluor450	1:20

CD206	Mouse	PE/Cy7	1:80
CD163	Mouse	PE	1:80
CD45	Mouse	PerCp-Cy5.5	1:100
Zombie aqua			1:100

3.21 Statistical analysis

The quantification of histology and immunohistology data was performed by Fiji software (version of Image J built upon Image J2, National Institutes of Health). FACS data was analyzed by FlowJo 7.6.5 software (FlowJo LLC). All figures and statistical analyses were performed using Microsoft Excel or GraphPad Prism 8.0 software. If not indicated otherwise, data are presented as mean ± standard error of mean (SEM). For parametric distributions, comparisons between two groups were performed by unpaired or paired two-tailed Student's t-test, and comparisons between more than two groups were performed by one-way ANOVA with Tukey's multiple comparisons or two-way ANOVA with Sidak's multiple comparisons test. A p-value of <0.05 was considered to be statistically significant. The linear - quadratic model was used to generate the surviving fitting curves from the clonogenic assay (GraphPad Prism 8.0).

4. Results

4.1 Effects of DKK3 targeted knockout on radiation-induced dermatitis

4.1.1 Radiation-induced dermatitis in C57BL/N wildtype mice

To establish an in house model of radiation-induced chronic dermatitis, 12 week old C57BL/N wildtype (WT) female mice were irradiated with a single dose of 20Gy on the right hind limb. The mice were sacrificed at 4 weeks and 8 weeks after irradiation, and skin tissue was collected for histological and immunohistochemistry (IHC) analysis. Skin taken from left leg was collected as non-irradiated control for each mouse. Histology (H&E staining) and IHC (proliferation marker Ki67) showed radiation-induced epidermal hyperplasia at 4 weeks and 8 weeks as compared to non-irradiated skin (Figure 4.1A-B'). Goldner staining revealed increased collagen deposition in the dermis of irradiated skin at 4 weeks and 8 weeks as compared to non-irradiated skin (Figure 4.1C-C'). While staining for α-smooth muscle actin (α-SMA) at 4 weeks after irradiation showed a trend, no statistically significant increase as compared to non-irradiated skin was seen. However, at 8 weeks after irradiation significantly more α-SMA positive cells were seen in irradiated skin as compared to non-irradiated skin (Figure 4.1D-D'). Staining for macrophages/monocytes (F4/80, HR3) demonstrated that irradiation significantly increased F4/80 and HR3 positive cells at both 4 weeks and 8 weeks as compared to non-irradiated skin (Figure 4.1E-F'). Interestingly, staining for T cells (CD3) showed that irradiation significantly decreased CD3 positive cells at both 4 weeks and 8 weeks as compared to non-irradiated skin.

Together the data in the DKK3 WT mice showed that 20Gy irradiation induces a distinct phenotype of marked dermatitis with epithelial hyperplasia, primarily myeloid immune cell infiltration and signs of tissue remodeling and fibrosis. In the subsequent studies targeted DKK3 knockouts were systematically compared against this model of chronic radiation dermatitis.
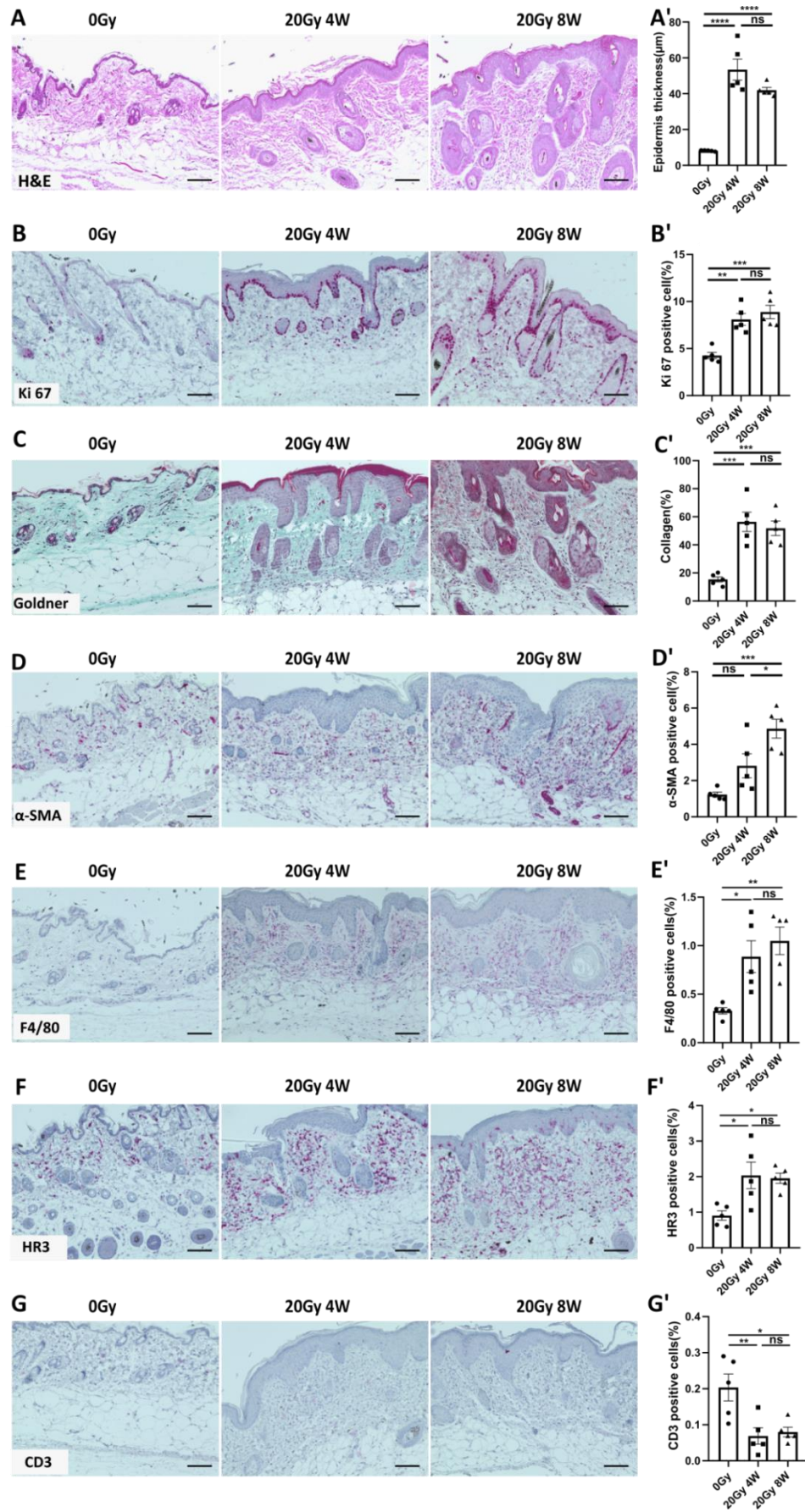
Figure 4.1 Radiation-induced skin changes in histology and immunohistochemistry (IHC) in the hind limb model. Five WT mice in each group were sacrificed at 4 weeks and 8 weeks after a single dose of 20Gy irradiation of the right hind limb. Skin from the irradiated right hind limb and non-irradiated left hind limb (control, 0Gy) were histologically analyzed and quantified (see Methods for details). (A) Representative images of H&E stained skin sections from irradiated and non-irradiated hind limb and quantification (A') of epidermal thickness. (B) Representative images of Ki67 IHC of skin sections from irradiated and non-irradiated hind limb and quantification (B') of Ki67 positive cells (%). (C) Representative images of Goldner stained skin sections showing collagen deposition from irradiated and non-irradiated hind limb and quantification (C') of collagen positive area. (D) Representative images of α-SMA IHC of skin sections from irradiated and non-irradiated hind limb and quantification (D') of α-SMA positive cells (%). (E) Representative images of F4/80 IHC of skin sections from irradiated and non-irradiated hind limb and quantification (E') of F4/80 positive cells (%). (F) Representative images of HR3 IHC of skin sections from irradiated and non-irradiated hind limb and quantification (F') of HR3 positive cells (%). (G) Representative images of CD3 IHC of skin sections from irradiated and non-irradiated hind limb and quantification (G') of CD3 positive cells (%). Scale bars: 50 µm. Data are mean ± SEM, One-Way ANOVA with Tukey's multiple comparisons test, *$P<0.05$, **$P<0.01$, ***$P<0.001$, ****$P<0.0001$.

4.1.2 Effects of global DKK3 knockout on radiation-induced dermatitis in the hind limb model

The DKK family of secreted proteins helps control Wnt pathway signaling. While DKK1, DKK2 and DKK4 have been shown in general to limit canonical Wnt pathway signaling, DKK3 has been found to exhibit divergent biologic features potentially due to the structural differences seen between DKK3 and the other DKK family members [53-55]. To investigate the potential effect of DKK3 expression on radiation-induced dermal hyperplasia, inflammatory infiltration and fibrosis, 12-week-old female C57BL/N WT and C57BL/N mice with a global knockout of DKK3 were irradiated with a single dose of 20Gy on the right hind limb. As found in preliminary experiments, clinical observation showed that DKK3 deficiency (DKK3$^{-/-}$) protected the irradiated skin from hair loss, desquamation and ulceration which was more present in WT mice following radiation treatment (Fig 4.2A). Histology (H&E) and IHC (Ki67) performed on samples collected 4 weeks after irradiation showed that DKK3$^{-/-}$ status significantly reduced the level of radiation-induced epidermal hyperplasia (Figure 4.2B-C') as compared to WT

mice. Goldner staining revealed that the DKK3$^{-/-}$ status also helped protect the irradiated mice from dermal collagen deposition as compared to WT mice 4 weeks after irradiation (Figure 4.2D-D'). Interestingly, staining for macrophages/monocytes (F4/80 and HR3) demonstrated a significantly increased presence of F4/80 and HR3 positive cells in the DKK3$^{-/-}$ mice as compared to the WT mice at the 4 week time point following irradiation (Figure 4.2E-F'). At this early time point, IHC staining of α-SMA again showed no significant difference between WT and DKK3$^{-/-}$ mice (Figure 4.2G-G'). Staining for T cells (CD3) showed no significant differences between WT and DKK3$^{-/-}$ mice, but the overall level of T cells was again dramatically reduced in both WT and DKK3$^{-/-}$ mice relative to non-irradiated controls (Figure. 2H-H').

Consistent with the 4 week data, histology performed on parallel mice but examined at 8 weeks after radiation showed that DKK3$^{-/-}$ mice were markedly protected from clinical skin toxicity, epidermal hyperplasia and collagen deposition (Figure 4.3A-D'). Also consistent with the 4 week data, at 8 weeks after radiation the DKK3$^{-/-}$ mice showed increased myeloid infiltration as compared to WT mice (Figure 4.3E-F'). Importantly, the DKK3$^{-/-}$ mice also showed significantly less α-SMA expression than WT mice (Figure 4.3G-G'). Staining for T cells (CD3) showed no statistically significant differences between WT and DKK3$^{-/-}$ mice, but reduced numbers relative to non-irradiated control mice (Figure 4.3H-H').

In summary, after 20Gy irradiation of the hind limb mice with a global knockout of DKK3 were markedly protected from clinical skin toxicity including hair loss, desquamation and ulceration associated with reduced epidermal hyperplasia and collagen deposition. Irradiation reduced T cell levels but DKK3 status (WT or knockout) had no marked effect on T cell levels. Intriguingly, while the irradiation increased myeloid infiltration in both WT and DKK3$^{-/-}$ mice, but mice with DKK3$^{-/-}$ status showed more irradiation-induced myeloid infiltration in the dermis as compared to WT mice, rather than a reduced myeloid cells as initially expected as these mice showed less fibrosis. These results suggest that the effector status of the immune infiltrate, rather

than the absolute number of the myeloid cells, may dictate the fate of tissue fibrosis in this model. Consequently, it was hypothesized that knockout of DKK3 may help drive macrophage polarization more towards an effector status that does not promote tissue fibrosis – as commonly associated with a "M1-like" phenotype. In contrast, the presence of DKK3 could help drive macrophage polarization more towards a chronic fibrosing process - generally associated with a "M2-like" polarization status. To test this hypothesis, the experimental work plan was expanded. Rather than solely analyzing skin of the hind limb, additionally the skin of the thorax of mice was irradiated in subsequent experiments. This was done as the thoracic skin is thick enough to allow extensive immune cell analysis by flow cytometry (FACS) to characterize the composition and potential polarization of the immune cell infiltrate. In addition, these experiments allowed confirmation of the general findings at a different anatomical skin site.
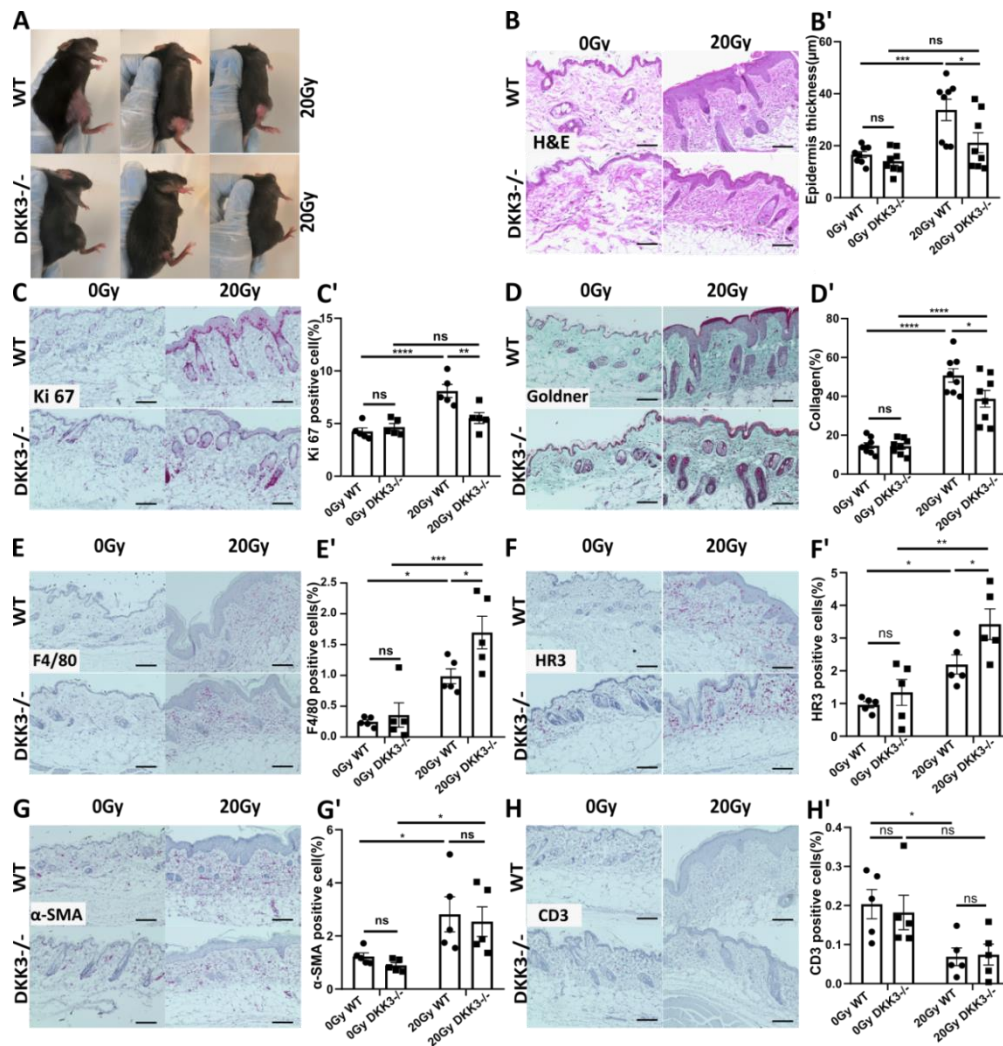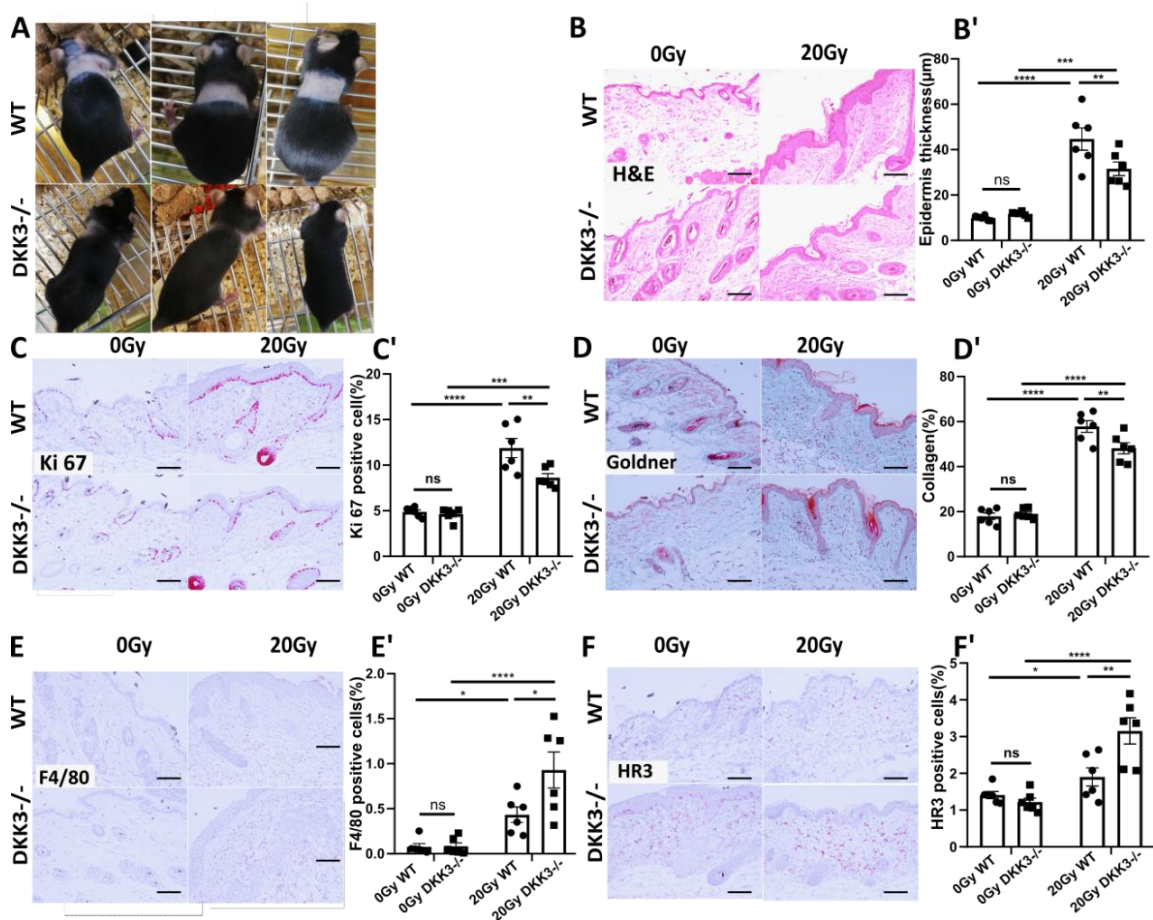
Figure 4.2 Effects of DKK3 global knockout on dermatitis 4 weeks after irradiation in the hind limb model. (A) Representative images of WT (*n* = 5) and DKK3^{-/-} (*n* = 5) mice 4 weeks after radiation. (B) Representative images of H&E stained skin sections from WT and DKK3^{-/-} mice and quantification (B') of epidermis thickness. (C) Representative images of Ki67 IHC of skin sections from WT and DKK3^{-/-}mice and quantification (C') of Ki67 positive cells (%). (D) Representative images of Goldner stained skin sections showing collagen deposition from WT and DKK3^{-/-} mice and quantification (D') of collagen positive area. (E) Representative images of F4/80 IHC of skin sections from WT and DKK3^{-/-} mice and quantification (E') of F4/80 positive cells (%). (F) Representative images of HR3 IHC of skin sections from WT and DKK3^{-/-} mice and quantification (F') of HR3 positive cells (%). (G) Representative images of α-SMA IHC of skin sections from WT and DKK3^{-/-} mice and quantification (G') of α-SMA positive cells (%). (H) Representative images of CD3 IHC of skin sections from WT and DKK3^{-/-} mice and quantification (H') of CD3 positive cells (%). All animals (5 in WT group and 5 in DKK3^{-/-} group) were histologically analyzed and quantified (see Methods for details). Scale bars: 50 μm. Data are mean ± SEM, Two-way ANOVA with Sidak's multiple comparisons test, *P＜0.05, **P＜0.01, ***P＜0.001, ****P＜0.0001 .
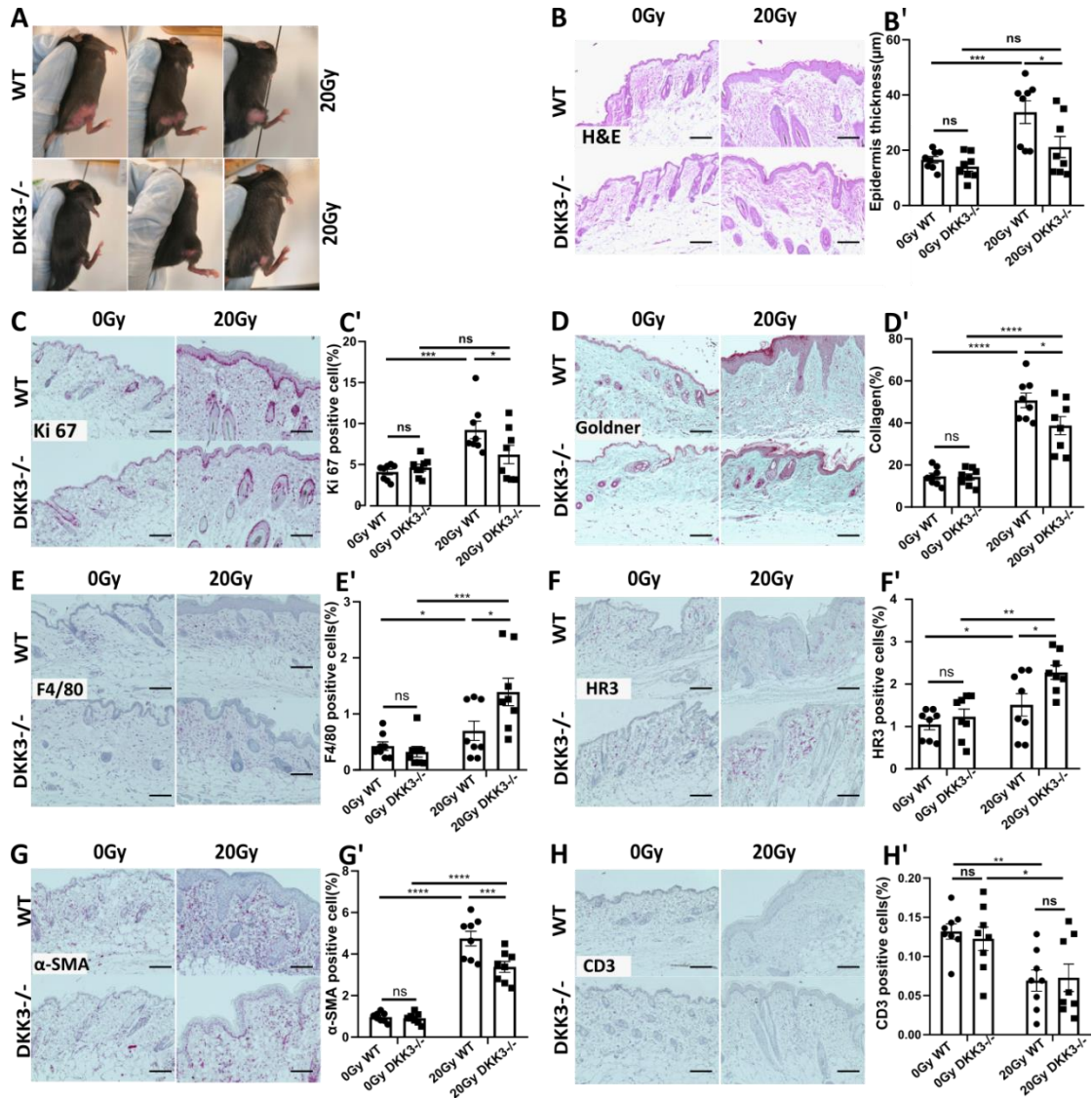
Figure 4.3 Effects of DKK3 global knockout on dermatitis 8 weeks after irradiation in the hind limb model. (A) Representative images of WT (n = 8) and DKK3$^{-/-}$ (n = 8) mice 8 weeks after irradiation. (B) Representative images of H&E stained skin sections and the quantification (B') of epidermis thickness. (C) Representative images of Ki67 IHC and the quantification (C') of Ki67 positive cells (%). (D) Representative images of Goldner stained skin sections showing collagen deposition and quantification (D') of collagen positive area. (E) Representative images of F4/80 IHC and quantification (E') of F4/80 positive cells (%). (F) Representative images of HR3 IHC and quantification (F') of HR3 positive cells (%). (G) Representative images of α-SMA IHC and quantification (G') of α-SMA positive cells (%). (H) Representative images of CD3 IHC of skin sections from WT and DKK3$^{-/-}$ mice and quantification (H') of CD3 positive cells (%). All animals (8 in WT group and 8 in DKK3$^{-/-}$ group were histologically analyzed and quantified (see Methods for details). Scale bars: 50μm. Data are mean ± SEM, Two-way ANOVA with Sidak's multiple comparisons test, *P＜0.05, **P＜0.01, ***P＜0.001, ****P＜0.0001 .

4.1.3 Validation of the effects of DKK3 global knockout on radiation-induced dermatitis in the thoracic model

12-week-old C57BL/N female WT and global DKK3$^{-/-}$ mice were irradiated with a single dose of 20Gy prescribed to the thorax as described in details in Methods. The thoracic model allowed for the generation of larger tissue samples for *ex vivo* analysis. Accordingly, histology from thoracic skin taken at 4 weeks after irradiation again showed that DKK3$^{-/-}$ mice were protected from clinical skin toxicity, epidermal hyperplasia and collagen deposition (Figure 4.4A-D') as compared to WT mice. Also consistent with the hind limb data, at 4 weeks after irradiation the DKK3$^{-/-}$ mice showed increased macrophages/monocytes (F4/80 and HR3) infiltration (Figure 4.4E-F') as compared to WT mice.
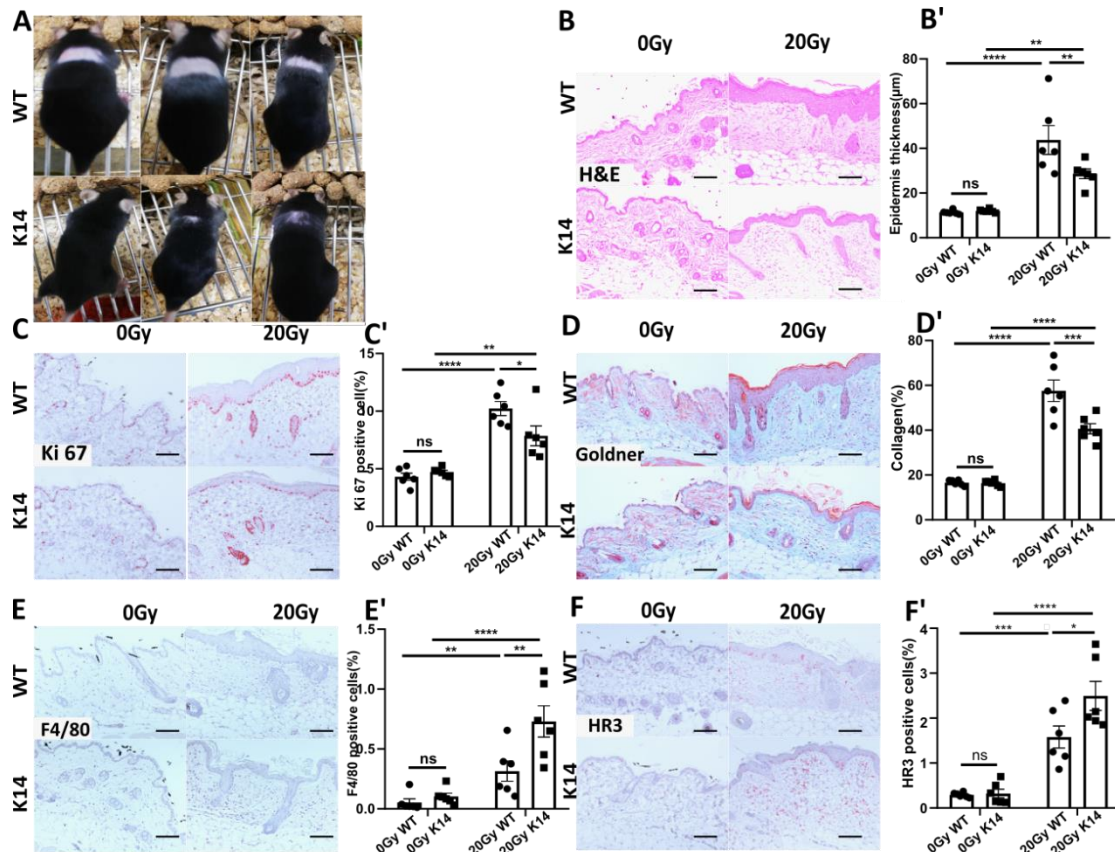

Figure 4.4 Effects of DKK3 global knockout on dermatitis 4 weeks after irradiation in thoracic model. (A) Representative images of WT (*n* = 6) and DKK3$^{-/-}$ (*n* = 6) mice 5

weeks after irradiation. (B) Representative images of H&E stained skin sections and the quantification (B') of epidermis thickness. (C) Representative images of Ki67 IHC and quantification (C') of Ki67 positive cells (%). (D) Representative images of Goldner stained skin sections showing collagen deposition and quantification (D') of collagen positive area. (E) Representative images of F4/80 IHC and the quantification (E') of F4/80 positive cells (%). (F) Representative images of HR3 IHC and quantification (F') of HR3 positive cells (%). All animals (6 in WT group and 6 in DKK3$^{-/-}$ group) were histologically analyzed and quantified (see Methods for details). Scale bars: 50μm. Data are mean ± SEM, Two-way ANOVA with Sidak's multiple comparisons test, *P＜ 0.05, **P＜0.01, ***P＜0.001, ****P＜0.0001 .

4.1.4 Effects of DKK3 keratinocyte specific (K14 Cre X Dkk3$^{fl/fl}$) knockout on radiation-induced dermatitis in the thoracic model

Based on our previous study in the kidney, it was proposed that the DKK3 status of keratinocytes may play a central role in the outcome of the radiation-induced skin fibrosis. To test this hypothesis, mice were generated carrying a DKK3 keratinocyte specific knockout as described in Methods (these mice will be referred as K14 mice). A single dose of 20Gy was delivered to the thoracic region of 12-week-old C57BL/N female WT and K14 mice. Histology performed from samples taken 4 weeks after irradiation showed that analogous to what was found with the global DKK3$^{-/-}$ mice, K14 mice were markedly protected from clinical skin toxicity, epidermal hyperplasia and collagen deposition (Figure 4.5A-D'). Similar to the DKK3 global knockout mice data, at 4 weeks after irradiation the K14 mice also showed increased macrophage/monocyte (F4/80 and HR3) infiltration (Figure 4.5E-F') as compared to WT mice.

Figure 4.5 Effects of DKK3 keratinocyte specific knockout on dermatitis 4 weeks after radiation in the thoracic model. (A) Representative images of WT (*n* = 6) and K14 (*n* = 6) mice 4 weeks after radiation. (B) Representative images of H&E stained skin sections and the quantification (B') of epidermis thickness. (C) Representative images of Ki67 IHC and quantification (C') of Ki67 positive cells (%). (D) Representative images of Goldner stained skin sections showing collagen deposition and quantification (D') of collagen positive area. (E) Representative images of F4/80 IHC and quantification (E') of F4/80 positive cells (%). (F) Representative images of HR3 IHC and quantification (F') of HR3 positive cells (%). All animals (6 in WT group and 6 in K14 group) were histologically analyzed and quantified (see Methods for details). Scale bars: 50μm. Data are mean ± SEM, Two-way ANOVA with Sidak's multiple comparisons test, *P＜0.05, **P＜0.01, ***P＜0.001, ****P＜0.0001 .

4.1.5 Effects of DKK3 fibroblast specific (PDGFR Cre X Dkk3^{fl/fl}) knockout on radiation-induced dermatitis in the hind limb model

Fibroblasts/myofibroblasts are crucial cell types for the process of fibrosis through their proliferation and production of ECM and are known to express DKK3, especially after activation to myofibroblasts[57]. To study whether the DKK3 expression status of

fibroblasts can also influence the outcome of radiation-induced skin fibrosis, mice carrying a DKK3 fibroblast specific knockout were generated as described in Methods (these mice will be referred as PDGFR mice). A single dose of 20Gy was applied to the right hind limb of 12-week-old C57BL/N female WT and the DKK3 fibroblast specific knockout mice. Surprisingly, partially opposite results were obtained for mice with DKK3 fibroblast specific knockout as compared to DKK3 global and keratinocyte specific knockout mice. Histology performed 4 weeks after irradiation showed that PDGFR mice had significantly more epidermal hyperplasia and collagen deposition as compared to WT mice, not less as seen in the DKK3 global and keratinocyte specific knockouts (Figure 4.6A-C).
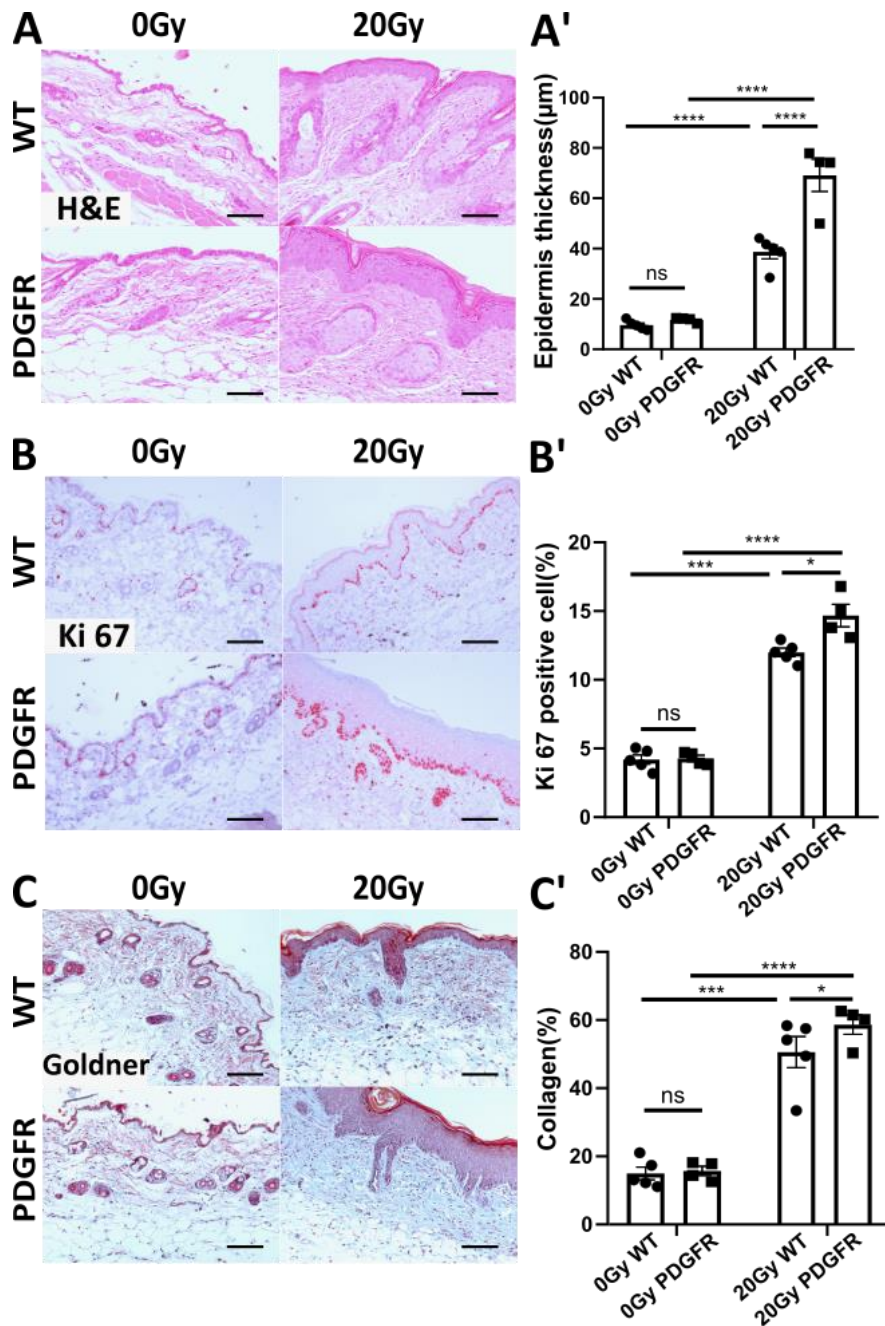
Figure 4.6 Effects of DKK3 fibroblast specific knockout on dermatitis 4 weeks after irradiation in the hind limb model. DKK3 Fibroblast specific knockout mice are referred to as PDGFR mice. 5 in WT group and 4 in PDGFR group were histologically analyzed and quantified (see Methods for details). (A) Representative images of H&E stained skin sections and quantification (A') of epidermis thickness. (B) Representative images of Ki67 IHC and quantification (B') of Ki67 positive cells (%). (C) Representative images of Goldner stained skin sections showing collagen deposition and quantification (C') of collagen positive area. Scale bars: 50μm. Data are mean ± SEM, Two-way ANOVA with Sidak's multiple comparisons test, *P＜0.05, **P＜0.01, ***P ＜0.001, ****P＜0.0001 .

## 4.2 Effects of DKK3 modulation on monocyte differentiation and polarization

The mouse experiments (Results 4.1) showed that global or keratinocyte absence of DKK3 (DKK3$^{-/-}$) led to reduced skin remodeling and fibrosis, but was associated with an increased immune infiltrate. Since this DKK3$^{-/-}$ status also reduced epithelial hyperplasia, therefore it was hypothesized that the presence or absence of DKK3 expression in dermal keratinocytes may help modulate the nature of the immune infiltrate after irradiation injury, which in turn alters the inflammatory fibrogenesis. More specifically, keratinocyte expression of DKK3 may act to help establish a tissue milieu conducive toward the establishment of a pro-fibrotic environment. By contrast, the absence of DKK3 expression by keratinocytes could lead to a non-fibrotic/proinflammatory tissue environment. Classically pro-fibrotic myeloid cells have been referred to as M2-like while a M1-like polarization has been more associated with a pro-inflammatory, but non-fibrotic phenotype [78]. Strict M1/M2 designations have fallen out of favor as the myeloid biology seen *in vivo* has proven to be too complicated to assign to global phenotypes [79]. More recently a continuum model for macrophage states was established describing a dynamic plasticity of effector functions [80]. In the present work, the myeloid phenotypes analyzed will be referred to as derived from either fibrotic or non-fibrotic tissues and associated with M2-like or M1-like polarization status.

To evaluate the myeloid phenotypes seen in the presence or absence of DKK3 *in vivo*, cells were isolated from thoracic skin of DKK3 global knockouts, DKK3 keratinocyte specific knockouts and WT mice at 4 weeks after 20Gy irradiation. An *ex vivo* FACS analysis using different leukocyte sub-group markers was employed for these cells. DKK3 global knockout resulted in a decreased percentage of CD206^{high}, CD163^{high} and CD163^{high}&CD206^{high} macrophages as compared to WT mice. CD206^{high}, CD163^{high} macrophages represent M2-like profibrotic phenotypes (Figure 4.7A). The DKK3 keratinocyte specific knockout showed a similar effect of decreased CD206^{high} and CD163^{high} positive cells in skin macrophage populations (Figure 4.7B).
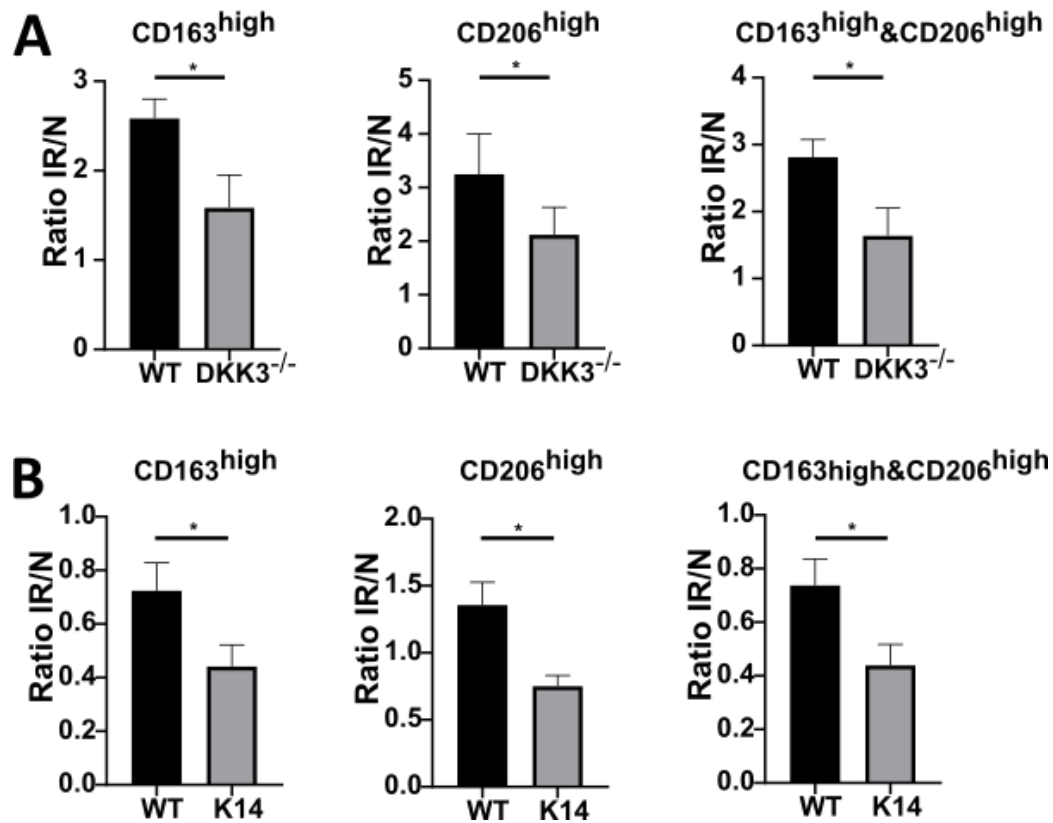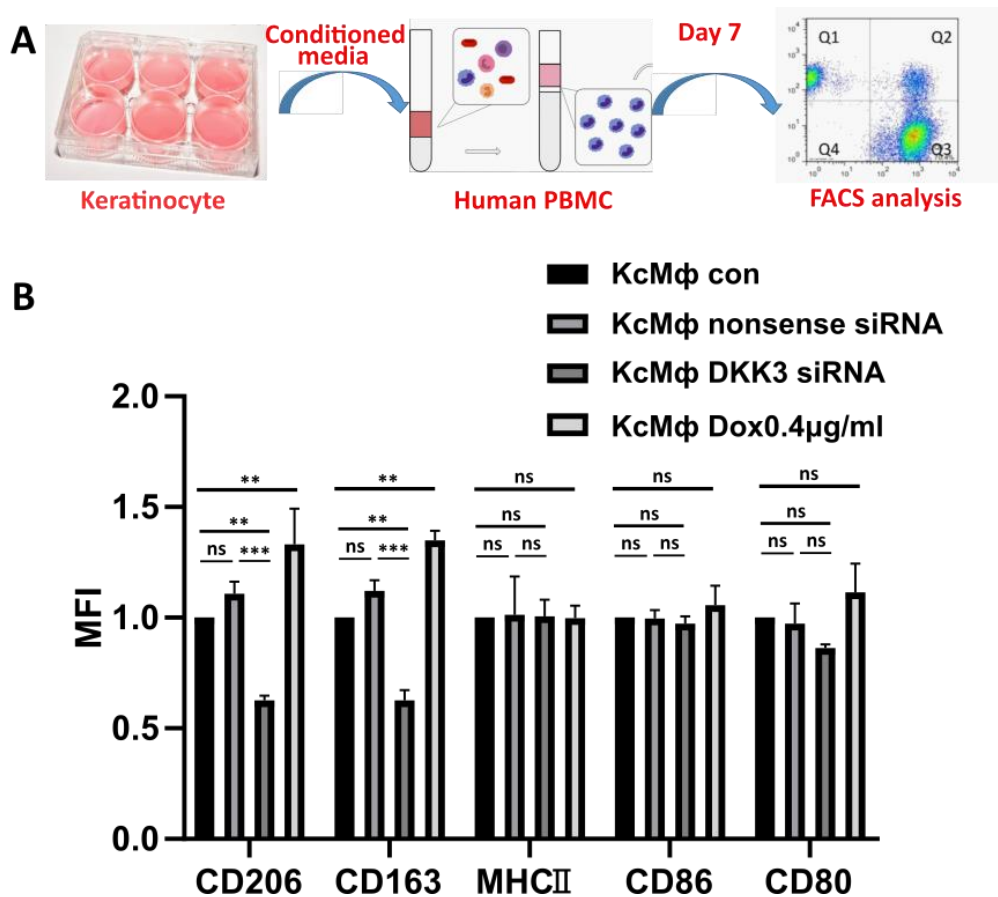
Figure 4.7 Effects of DKK3 modulation on monocyte differentiation and polarization
in vivo. Mice were irradiated with 20Gy at the thoracic region and cells isolated form irradiated skin were taken for FACS analysis at 4 weeks after irradiation. IR: irradiated. N: non-irradiated control. (A) Global DKK3 knockout decreased the expression of pro-fibrotic markers CD206 and CD163 as compared to WT. (B) DKK3 keratinocyte specific knockout also decreased the expression of pro-fibrotic markers CD206 and CD163 as compared to WT. Data are mean ± SEM, Student t-test, *P＜0.05.

To further characterize the effect of keratinocyte expression of DKK3 on myeloid differentiation and polarization, an *in vitro* DKK3 modulation system was established by introducing a doxycycline-inducible DKK3 overexpression plasmid into the immortalized human keratinocyte cell line N/TERT-1 as described in Methods. In separate N/TERT-1 cells, DKK3 siRNA was used to reduce endogenous DKK3 expression. A human DKK3 ELISA, RT- qPCR and western blot were used to validate modulation of DKK3 expression levels. Treatment by siRNA transfection resulted in more than 90% reduction in endogenous DKK3 expression, while a more than ten-fold over-expression of DKK3 was measured following doxycycline induction (Figure 4.8A-C).
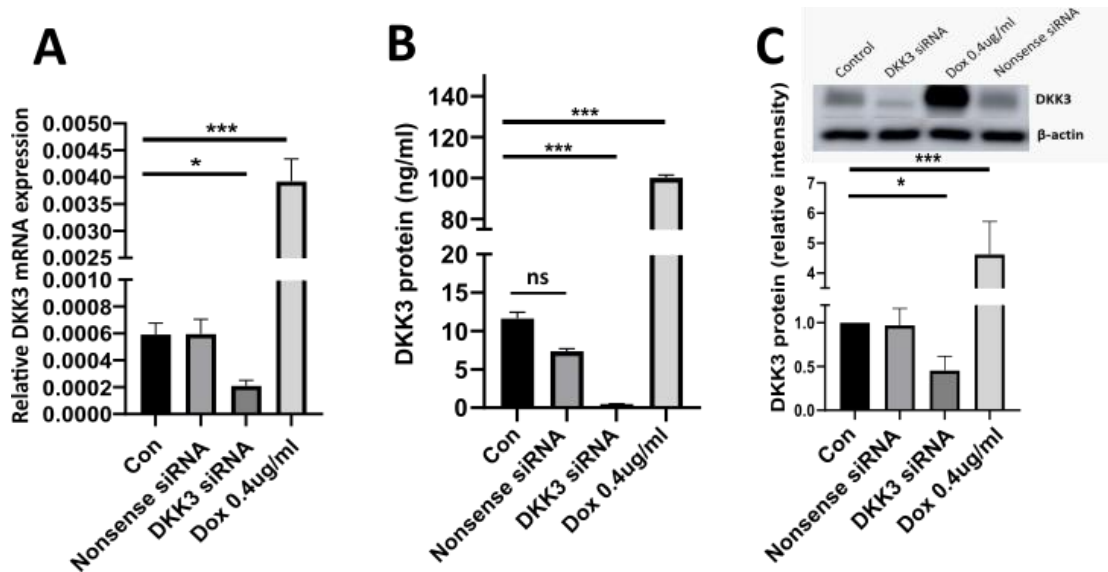
Figure 4.8 *In vitro* DKK3 modulation system in immortalized human keratinocytes (N/TERT-1) (A) DKK3 mRNA level measured by RT-qPCR after treatment with DKK3 siRNA or induction with doxycycline 0.4µg/ml. DKK3 mRNA was calculated with the relative DKK3 mRNA/18s rRNA. (B) DKK3 protein levels in supernatant measured by ELISA after DKK3 modulation. (C) Total cell DKK3 protein levels measured by Western Blot and quantified after modulation of DKK3 expression. Data are mean ± SEM, one way ANOVA with Tukey's multiple comparisons test, *P＜0.05, ***P＜0.001.

To study the interplay of DKK3 expression in keratinocytes and the potential activation of myeloid cells by keratinocyte-secreted factors, keratinocyte-conditioned media was used to "mature" human peripheral blood monocytes as described in Methods. After 7 days of treatment with the conditioned media, FACS analysis for macrophage surface markers was performed on the keratinocyte-conditioned macrophages (KcMφ) (Figure 4.9A). The results revealed that DKK3 over-expression conditioned keratinocyte media increased surface expression of the M2-like/fibrosis markers CD206 and CD163 in KcMφ, while DKK3 knockdown conditioned keratinocyte media decreased the expression of CD206 and CD163 in KcMφ. By contrast, surface expression of MHCII, CD80 and CD86 was increased in the KcMφ as they matured from monocytes, but were not significantly altered by modulation of the DKK3 expression status of the keratinocyte line (Figure 4.9B).

Figure 4.9 Effects of conditioned media taken from human keratinocytes with DKK3 modulation on human macrophage polarization *in vitro*. (A) The conditioned media was used to drive maturation of human peripheral blood monocytes (PBMC) to macrophages over a seven days period. (B) DKK3 over-expression conditioned keratinocyte media was found to increase the expression of the M2-like/fibrosis surface markers CD206 and CD163 in keratinocyte conditioned machrophages (KcMφ), while DKK3 knockdown conditioned keratinocyte media decreased the expression of CD206 and CD163 in KcMφ. MFI, mean fluorescence intensity. Data are mean ± SEM, one way ANOVA with Tukey's multiple comparisons test, *$P < 0.05$, ***$P < 0.001$, ****$P < 0.0001$.

To characterize the potential effect of DKK3 expression status of the N/TERT-1 cells on the production of relevant proteins, conditioned media from the keratinocyte cell lines with modulated DKK3 expression was then analyzed using a dedicated chemokine/growth factor array. DKK3 modulation tended to change the secretion of various proteins including TGF-β1, IL-4, IL-6, IL-10, IL-1β, CXCL8, CXCL10, VEGF, GM-CSF, G-CSF, PDGF-AA, PDGF-BB, M-CSF and TGF-α(Figure 4.10A). RT-qPCR was subsequently performed to validate the effect of DKK3 modulation on the level of transcription.

These results suggest that modulation of DKK3 expression in keratinocytes effectively changes their secretome. DKK3 overexpression increased keratinocyte expression of the M2-like factor and profibrotic factor TGF-β1[81]. DKK3 knockdown increased the expression of key M1-like activation factor GM-CSF[82] and the pro-inflammatory factors CXCL8, CXCL10 and TNF-α (Figure 4.10B).

Thus, the *in vivo* and *in vitro* results strongly suggest that the presence of DKK3 in keratinocytes helps drive macrophage polarization towards a more pro-fibrotic phenotype, while the absence of keratinocyte DKK3 leads to a more non-fibrotic polarized phenotype.
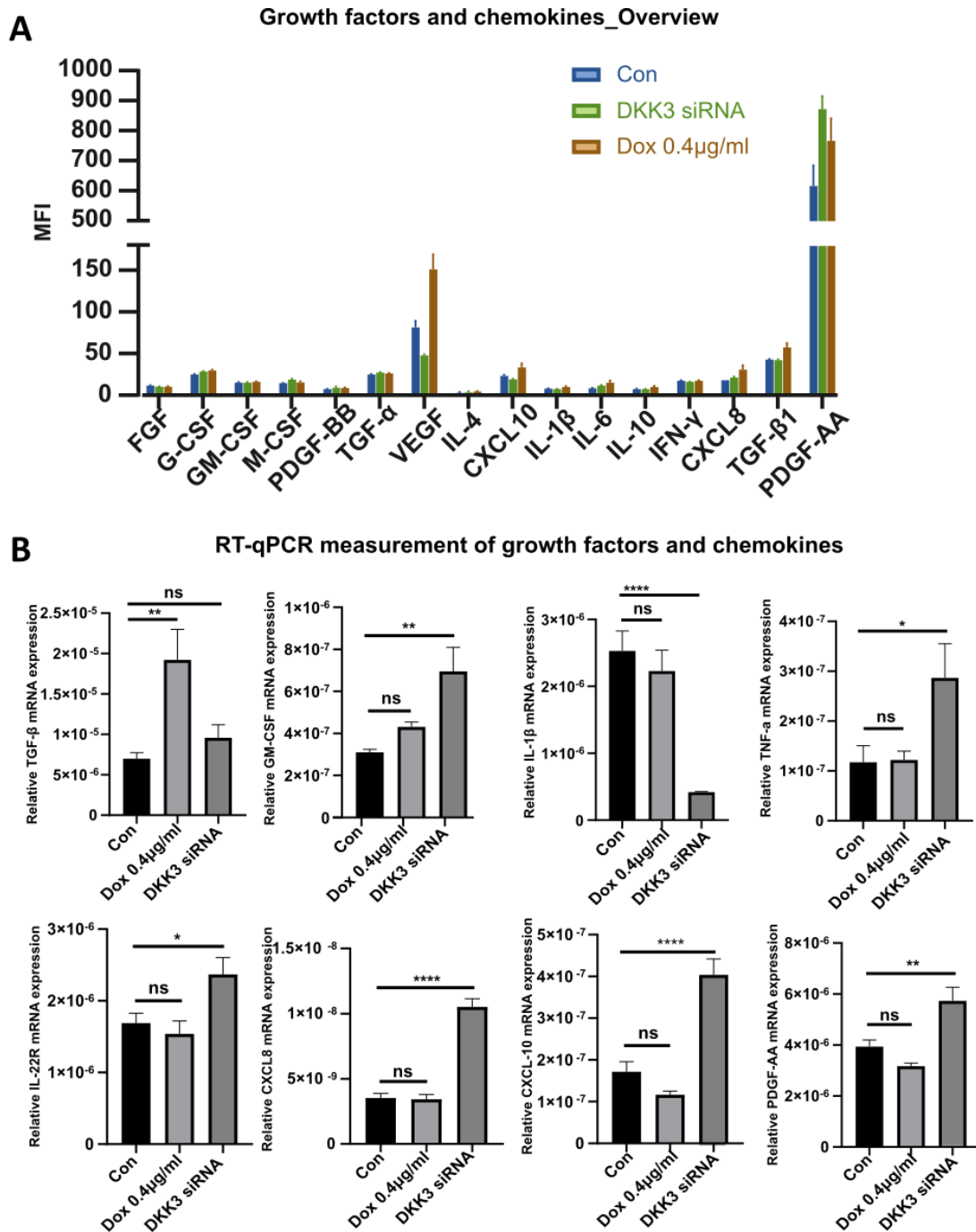
Figure 4.10 Effects of keratinocyte DKK3 modulation on expression of chemokines and growth factors *in vitro*. (A) Overview of the effects of DKK3 modulation on protein secretion in keratinocyte measured by growth factor/chemokine array. MFI, mean fluorescence intensity. (B) Validation via RT-qPCR analysis of factors altered by DKK3 modulation in keratinocytes. The mRNA levels were calculated with the relative target gene mRNA/18s rRNA. Data are mean ± SEM, one way ANOVA with Tukey's multiple comparisons test, $*P < 0.05$, $**P < 0.01$, $****P < 0.0001$.

4.3 DKK3 and canonical Wnt biology on keratinocytes in radiation-induced dermatitis

4.3.1 Effects of DKK3 on cell viability and proliferation of N/TERT-1 cells in response to radiation

The nature of the tissue damage that occurs can influence the repair process. In this instance, treatment with 20Gy irradiation was used to induce skin damage. Radiation can directly damage DNA and leads to enhanced production of reactive oxygen species (ROS). Keratinocyte DKK3 expression status as shown above (Figures 4.1. and 4.2) can influence the degree of radiation-induced dermatitis and fibrosis in part through macrophage polarization. To help assess the direct impact of irradiation and DKK3 expression on keratinocyte biology the human keratinocyte cell line (N/TERT-1) was used to establish *in vitro* assays for the evaluation of parameters potentially associated with irradiation-induced tissue damage. Clonogenic and proliferation survival assays were performed on the N/TERT-1 cells to assess the general radiobiological properties of the cell line with and without DKK3 modulation. As expected, irradiation reduced the clonogenic cell survival and cell number/proliferation in a dose dependent manner (Figure 4.11A-B). The clonogenic survival and proliferation assays were then repeated after irradiation following DKK3 knockdown in N/TERT-1 cells. DKK3 knockdown did not significantly influence the clonogenic survival or proliferation of the N/TERT-1 cells up to 10Gy (Figure 4.11C-D). Since 4Gy reduced cell proliferation to ~50% and survival to ~15%, and 4Gy is also a clinically meaningful dose in radiotherapy, 4Gy was chosen as the representative dose of irradiation for subsequent *in vitro* experiments. While clonogenic and proliferation measurements were helpful to assess major effects of irradiation and DKK3 expression, more refined assays were subsequently employed to study the radiobiology in greater detail.
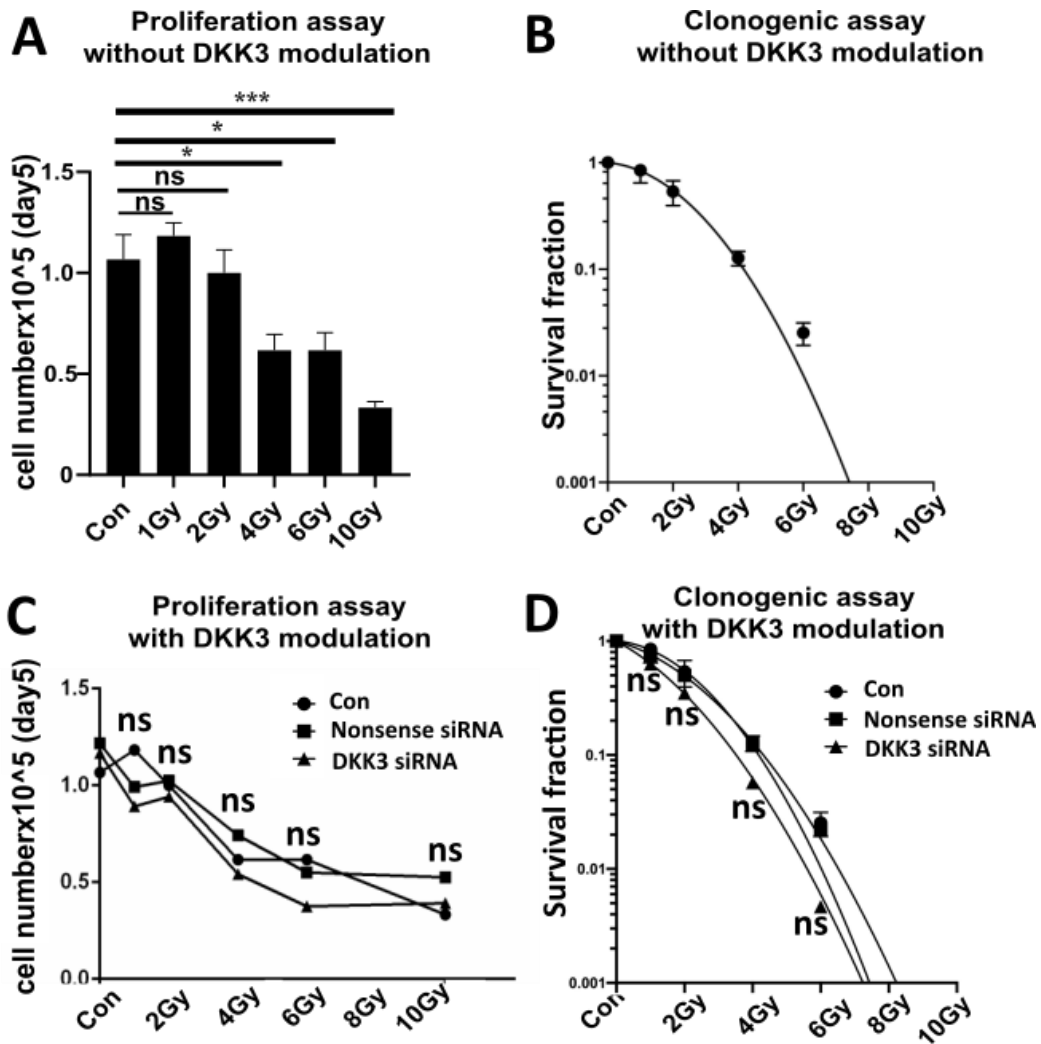
Figure 4.11 Effects of DKK3 on survival fraction and proliferation of N/TERT-1 cells in response to irradiation. Cells were seeded and 24h later irradiated with increasing doses. (A) Cell number on day 5 as a measurement for proliferation. Data are mean ± SEM, one way ANOVA with Tukey's multiple comparisons test, *P＜0.05, ***P＜0.001. (B) Clonogenic survival fraction after irradiation. Data are mean ± SEM, modeled according the linear-quadratic model using Prism. (C-D) N/TERT-1 cells transfected with DKK3 siRNA, nonsense siRNA or controls were irradiated and clonogenic and proliferation assays performed. (C) DKK3 status had no statistically significant effect on proliferation. Data are mean ± SEM, one way ANOVA with Tukey's multiple comparisons test. (D) DKK3 status had no detectable effect on clonogenic survival fraction. Modeled according the linear quadratic model. Data are mean ± SEM, one way ANOVA with Tukey's multiple comparisons test.

4.3.2 Effects of DKK3 on radiation-induced DNA damage and apoptosis in N/TERT-1 cells

Genomic DNA is an important effector target in the radiotherapy of cancer. When radiation-induced DNA damage is beyond the capacity for repair, the cell cycle is interrupted and certain forms of cell death occur, including apoptosis [11]. DNA double-strand breaks (DSBs) are largely responsible for radiation-induced cell death. Measurement of the number and the dynamics of DSBs repair upon irradiation can be used for radiobiological cell characterization.

To determine whether DKK3 expression can influence cell cycle and apoptosis rates after irradiation, FACS analysis of caspase 3 level was performed on DKK3-modulated N/TERT-1 cells. As expected, irradiation markedly increased apoptosis rates as compared to the non-irradiated groups, and irradiation also led to higher levels of cells in G2 phase ("G2 arrest") in particular at the later time points ($\geq$ 24h) indicating DNA damage and ongoing repair processes (Figure 4.11A-B). These results correspond to higher S phase levels in the cells at the earlier time points after irradiation. DKK3 knockdown led to increased apoptosis rates following irradiation as compared to controls and also led to more cells in G2 phase, in particular at the later time points.

The number of DNA double strand breaks (DSBs) as determined by γ-H2AX repair foci is a direct and important parameter of radiation-induced cell damage. To further study the effect of DKK3 status on DNA damage and repair after irradiation two methods were applied: γ-H2AX FACS analysis and direct count of γ-H2AX foci on slides by microscopy. Overall, the γ-H2AX levels and number of foci were induced by the 4Gy irradiation at all time points with an initial increase seen at 30 min, 1h and 3h followed by a gradual decrease that reached the non-irradiated control levels after 24h to 72h post irradiation. These findings are suggestive of full DSB repair with minor residual damage. The differences seen between the DKK3 modulated cells did not reach statistical significance. While the DKK3 siRNA knockdown tended to show slightly higher γ-H2AX levels at 30 minutes, at later time points (1h, 3h, 6h, 24h and 72h) the DKK3 knockdown trended toward (Figure 4.12A-D) slightly lower γ-H2AX levels

indicating accelerated DNA repair after irradiation. The microscopic analysis confirmed these findings (Figure 4.12E-H).

In summary, the classical radiobiological analysis demonstrated that the keratinocyte response to radiation with respect to intrinsic radiosensitivity, DNA DSBs damage, DNA DSBs repair dynamics, apoptosis induction and cell cycle changes were not dominated by DKK3 status. While DKK3 expression had overall only mild radiobiological consequences along these parameters, the slightly increased apoptosis and increased G2 arrest seen in the DKK3 knockdown cells were in line with the initially detected increased γ-H2AX levels that subsided at later time points indicating all together a minor role for DKK3 in the DNA repair process. Therefore, similarly as for the cells *in vitro*, one might conclude that the phenotypical differences observed in mice *in vivo* with different DKK3 status are also not dominated by the radiobiological processes investigated here. Instead, it is supposed that the observed phenotypical differences appear to be more closely linked with specific DKK3 – Wnt signaling processes triggered by radiation.
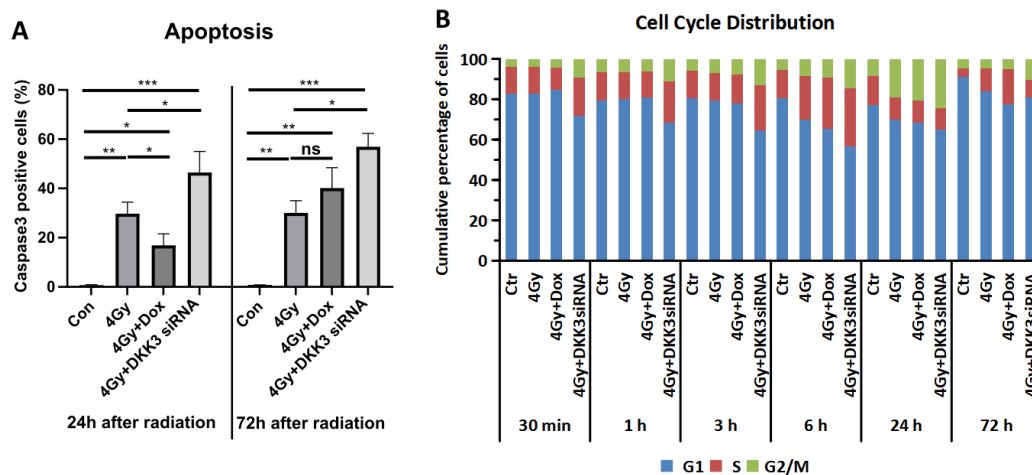
Figure 4.12 Effects of DKK3 on apoptosis and cell cycle in N/TERT-1 cells after irradiation. (A) Apoptosis measured by FACS analysis of caspase 3 level after 4Gy irradiation and DKK3 modulation. Data are mean ± SEM, one way ANOVA with Tukey's multiple comparisons. *$P<0.05$, **$P<0.01$, **$P<0.001$. (B) FACS based cell cycle analysis of N/TERT-1 cells after 4Gy irradiation and DKK3 modulation. The bar charts showed the proportional distribution of cells in different phases (G1, S, G2/M) at different time points.

A γH2AX total N-0Gy

B γH2AX G1 N-0Gy

C γH2AX S N-0Gy

D γH2AX G2 N-0Gy

91
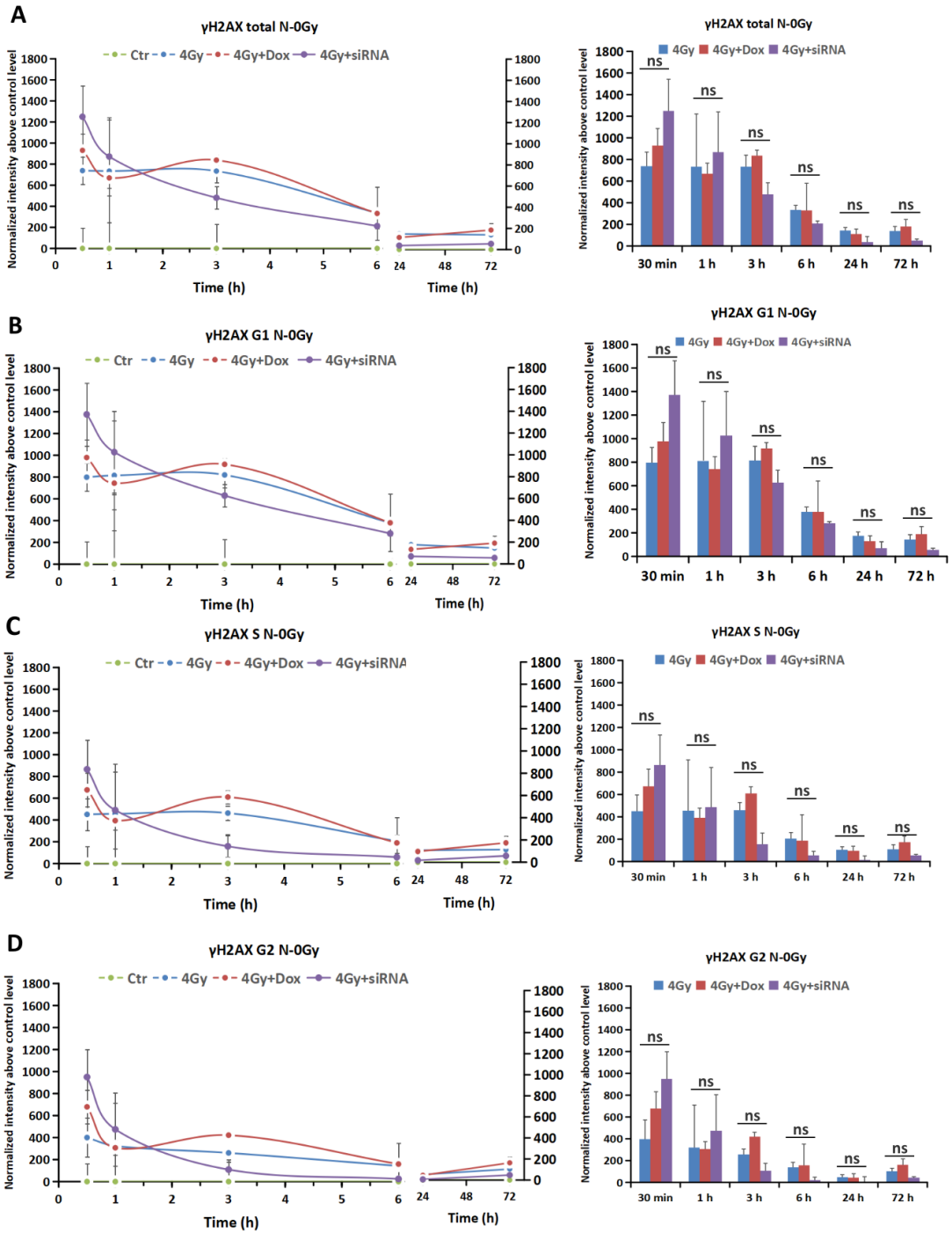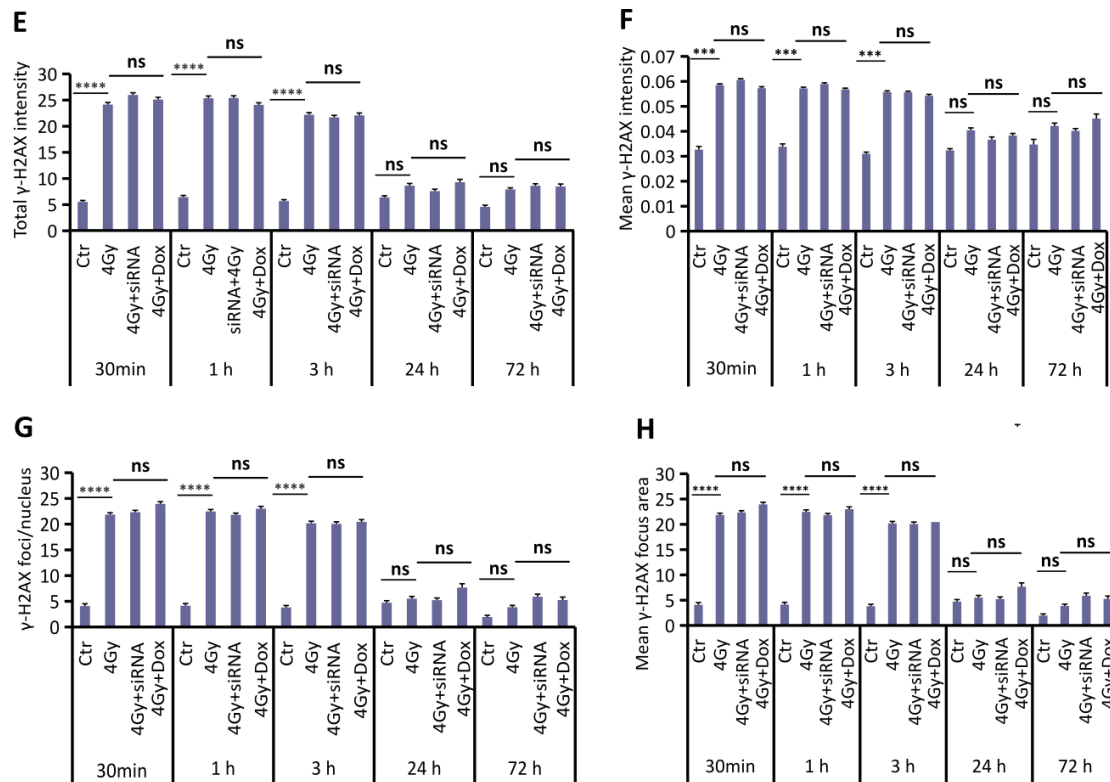
Figure 4.13 Effects of DKK3 on radiation-induced DNA damage and repair in keratinocytes. (A-D) DNA damage measured by FACS analysis of γ-H2AX levels (total, G1, S, G2 cell cycle specific) after DKK3 modulation and 4Gy irradiation. Dynamics over time with interpolation curve (left). Bar charts (right). Irradiation significantly induced DNA damage at 30min, 1h, 3h as compared to non-irradiated control. DKK3 modulation had no significant effect on DNA damage or repair. Control levels were subtracted in the figures. (E-H) DNA damage measured by automatic microscopic slides analysis of γ-H2AX foci after DKK3 modulation and 4Gy irradiation. Total γ-H2AX intensity, mean γ-H2AX intensity, number of γ-H2AX foci/nucleus, mean γ-H2AX focus area. Data are mean ± SEM, one way ANOVA with Tukey's multiple comparisons, ***P＜0.001, ****P＜0.0001.
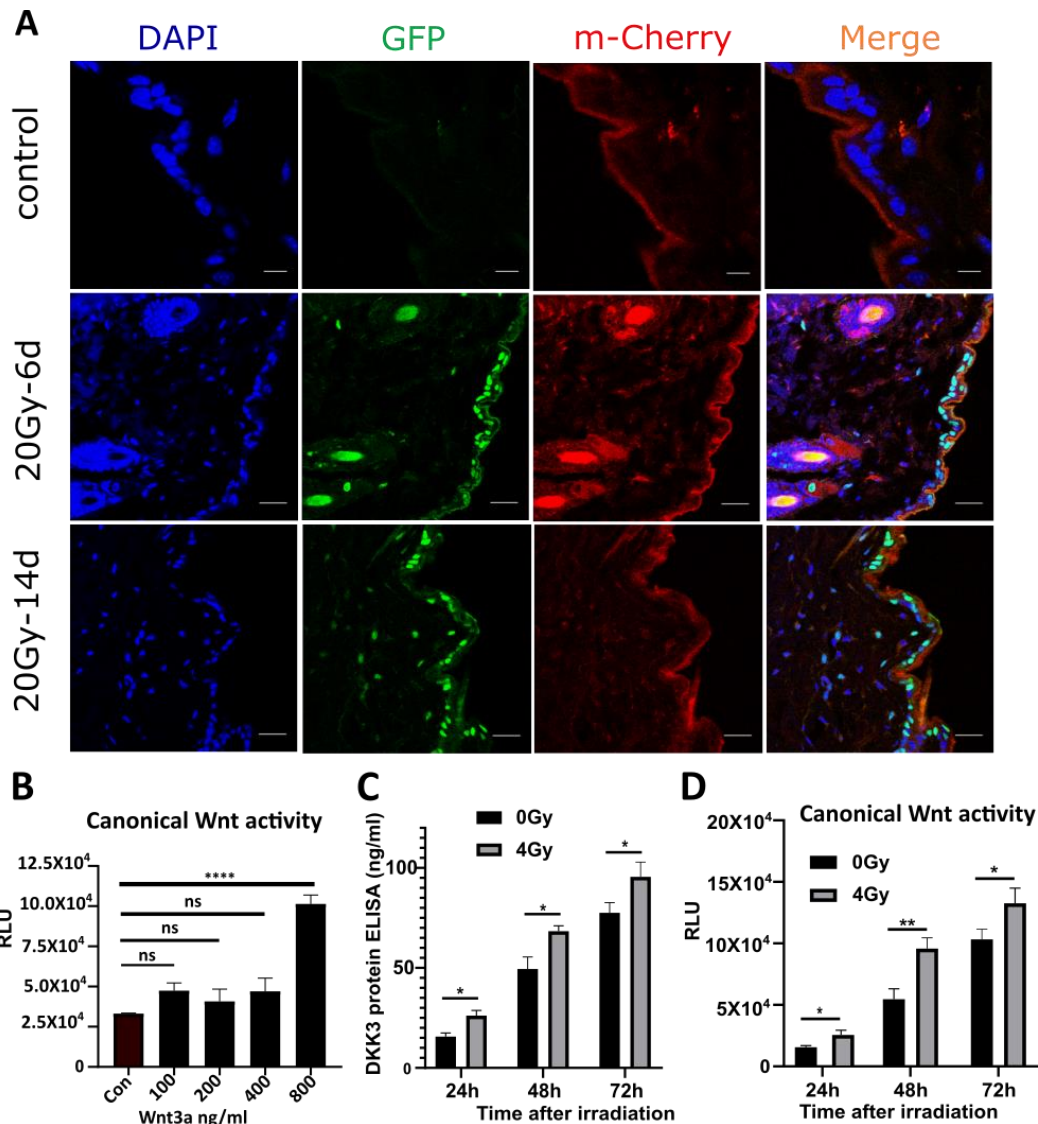
4.3.3 Effects of irradiation on DKK3 expression and canonical Wnt activity in keratinocytes

To further characterize the potential effects of irradiation on DKK3 expression and canonical Wnt pathway activity in keratinocytes and related tissues in the *in vivo* setting, DKK3/Wnt dual reporter mice were generated as described in Methods (DKK3-LCh x TCF/LEF). The mice were irradiated with a single dose of 20Gy on the right hind

limb as described in Methods. Canonical Wnt activity presented with green GFP-reporter signal and DKK3 expression with red m-Cherry signal. Skin samples from right hind limb were taken at 6 days and 14 days after 20Gy irradiation and analyzed via fluorescence microscopy. DKK3 and Wnt reporters were both found to be markedly increased in the basal keratinocyte layer versus non-irradiated controls at each time point and to be largely co-incident in expression (Fig 4.14A).

To model the effects of irradiation on DKK3 expression and canonical Wnt activity in keratinocytes *in vitro*, the N/TERT-1 cells were stably engineered using an in house developed vector platform with a synthetic TCF-based reporter gene. The system allows measurement of canonical Wnt pathway activation by assessing *Gaussia* luciferase reporter activity that is actively secreted into the growth media as described in Methods. To establish positive control levels, the N/TERT-1 canonical Wnt-reporter cells were treated with increasing concentrations of recombinant Wnt3a. Secreted *Gaussia* luciferase reporter activity - measuring activation of canonical Wnt signaling - was determined using a commercial *Gaussia* luciferase kit. The results showed a dose-dependent activation of canonical Wnt signaling in the N/TERT-1 canonical Wnt-reporter cells in response to Wnt3a stimulation (Figure 4.14B).

The N/TERT-1 canonical Wnt-reporter cells were then stimulated with 4Gy irradiation. Endogenous DKK3 secretion and canonical Wnt activity were subsequently measured. ELISA performed on cell culture medium collected at 24h, 48h and 72h after treatment showed that DKK3 expression was markedly increased after irradiation (Figure 4.14C). *Gaussia* luciferase-canonical Wnt-reporter activity measured in the growth media at 24h, 48h and 72h after irradiation further showed radiation-activation of canonical Wnt pathway activity in the N/TERT-1 canonical Wnt-reporter cells (Figure 4.14D).

Figure 4.14 Irradiation increased DKK3 expression and canonical Wnt activity *in vivo and in vitro*. (A) The effect of irradiation on DKK3 expression and canonical Wnt activity in Dkk3/Wnt dual reporter mice. Representative immunofluorescence images of *Dkk3-LCh* x TCF/LEF mouse skin 0 day (Control, *n* = 2), 6 days (n = 2) and 14 days (*n* = 2) after irradiation. Canonical Wnt activity is represented by GFP signal and DKK3 expression as red m-Cherry signal. Nuclei were stained with DAPI (scale bars: 50μm). (B) Validation of canonical Wnt reporter in the N/TERT-1 cell line. N/TERT-1 canonical Wnt-reporter cells were treated with increasing levels of recombinant Wnt3a. 48h after stimulation, cell growth media was collected for *Gaussia* luciferase measurement of canonical Wnt activity. Data represent relative light units (RLU). Wnt3a activates canonical Wnt reporter in a concentration dependent manner. Data are mean ± SEM, One way ANOVA with Tukey's multiple comparisons test, ****P $<$ 0.0001. (C) Irradiation increased DKK3 expression in N/TERT-1 cell culture media measured by ELISA. Data are mean ± SEM, Student t-test. *P $<$ 0.05. (D) Irradiation activated canonical Wnt activity measured by *Gaussia* luciferase reporter in N/TERT-1 cell growth media. Data are mean ± SEM, Student t-test. *P$<$0.05, **P$<$0.01.
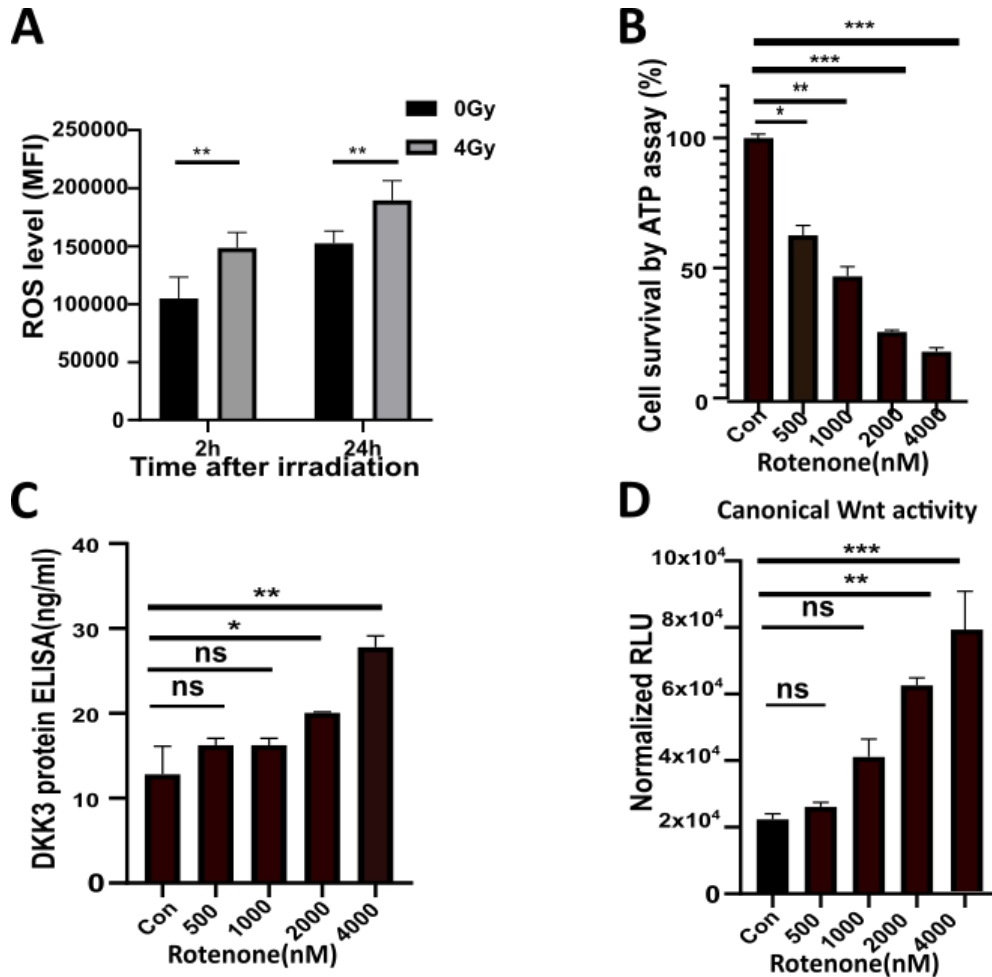
4.3.4 Effects of radiation-induced ROS on DKK3 expression and canonical Wnt activity

The transient generation of reactive oxygen species (ROS) by ionizing radiation has many important consequences in cells and tissues. ROS acts as second messengers and can have diverse effects on cell biology [27,83]. It was proposed that ROS produced following irradiation could influence DKK3 expression and/or canonical Wnt pathway signaling and thus influence the pathophysiology seen. To investigate whether ROS has an effect on DKK3 expression and canonical Wnt activity upon irradiation, N/TERT-1 canonical Wnt-reporter cells were stimulated with either 4Gy irradiation, or the chemical ROS inducer rotenone, and endogenous DKK3 expression and canonical Wnt activity were subsequently measured. The H2DCFDA assay, which detects intracellular ROS, was used to measure ROS levels after irradiation treatment. As expected, irradiation significantly increased ROS levels at 2h and 24h following irradiation (Figure 4.15A).

To model the radiation-induced ROS and eliminate the potential contribution of other radiation-induced events, the chemical ROS inducer rotenone was then used to directly study the influence of ROS on the expression of DKK3 and canonical Wnt activity. Cell viability as measured by ATP assay showed that rotenone treatment decreased cell survival in a concentration dependent manner (Figure 4.15B). ELISA demonstrated that DKK3 expression, when normalized to cell viability, was significantly increased at 12h after rotenone treatment (Figure 4.15C). In addition, *Gaussia* luciferase assay revealed that canonical Wnt activity normalized to cell viability was also significantly increased at 12h after rotenone stimulation (Figure 4.15D).

Taken together, radiation increased DKK3 expression and canonical Wnt activity in the N/TERT-1 cells *in vitro,* which is in line with the *in vivo* results from DKK3/Wnt dual reporter mice showing an early increase in DKK3 expression and canonical Wnt activation in basal keratinocytes after irradiation. Because chemical ROS stimulation was found to increase DKK3 expression and canonical Wnt activity in keratinocytes, it is suggestive of a role for ROS in the observed radiation-induced skin damage *in vivo*

via regulation of DKK3 and canonical Wnt activity. This conclusion is based on the results showing irradiation activated ROS levels in N/TERT-1 keratinocytes *in vitro,* and the general observation that ionizing radiation causes ROS in any living tissue *in vitro* and *in vivo*.


Figure 4.15 Effects of irradiation-induced ROS on DKK3 expression and canonical Wnt activity in N/TERT-1 cells. (A) Irradiation-induced ROS. MFI (mean fluorescence intensity). N/TERT-1 cells were irradiated with 4Gy, 2h and 24h after irradiation ROS levels were measured by H2DCFDA assay. Data are mean ± SEM, Student t-test. **P ＜0.01. For figure B-D, N/TERT-1 cells were stimulated with different concentrations of the chemical ROS inducer rotenone. 12h after stimulation, cell viability, DKK3 expression and canonical Wnt activity were measured. (B) Rotenone reduced cell survival rate measured with ATP assay in a concentration dependent manner. (C) Rotenone increased DKK3 expression (data normalized by cell viability) in a concentration dependent manner. (D) Rotenone activates canonical Wnt pathway (data normalized by cell viability) in a concentration dependent manner. Data represent normalized relative light units (RLU). Data are mean ± SEM, One-way ANOVA with Tukey's multiple comparisons test. *P＜0.05, **P＜0.01, ***P＜0.001.

4.3.5 Effects of DKK3 expression on canonical Wnt activity in N/TERT-1 cells

As discussed earlier, the DKK family of Wnt pathway regulatory proteins are generally associated with a blockade of Wnt signaling, however, in the previous renal study by our group we could show that the expression of DKK3 in tubular epithelial cells was required for canonical Wnt-pathway activation following injury [60]. To investigate whether DKK3 influences dermal keratinocytes in a similar manner, the canonical Wnt-reporter cells discussed above were then engineered to allow induction of DKK3 overexpression by treatment with doxycycline. Importantly, DKK3 over-expression alone led directly to activation of canonical Wnt signaling pathway (Figure 4.16A). To further analyze the potential interplay of DKK3 with canonical Wnt activity after irradiation, DKK3 siRNA knockdown of endogenous DKK3 was performed followed by irradiation of the cells with 4Gy. Canonical Wnt activity was measured 72h after irradiation. While the data recapitulated the results as shown in Fig 4.14, namely that irradiation increased canonical Wnt activity in control cells, DKK3 knockdown abrogated the increase in irradiation-induced canonical Wnt activity seen (Figure 4.16B).

These results further link the expression of DKK3 to the activation of canonical Wnt pathway signaling in dermal keratinocytes. Moreover, DKK3 appears to be necessary and sufficient for radiation-induced Wnt signaling suggesting that radiation-induced DKK3 upregulation presumably via ROS is causative for Wnt activity in the dermis.
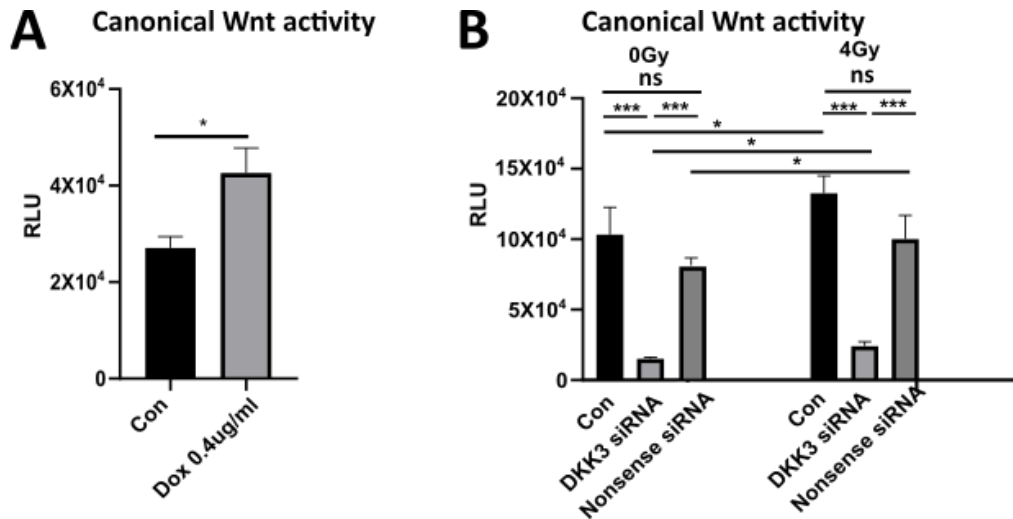
Figure 4.16 Effect of DKK3 on canonical Wnt activity in keratinocyte. (A) DKK3 over-expression using Doxycycline activated canonical Wnt activity. Data are mean ± SEM, Student's t-test. (B) DKK3 knockdown inhibited canonical Wnt activity upregulation in N/TERT-1 cells after irradiation. Data represent relative light units (RLU). Data are mean ± SEM, Two-way ANOVA with Sidak's multiple comparisons test. *P＜0.05, ***P＜0.001.

In summary, our data shows that radiation induces ROS leading to DKK3 upregulation and canonical Wnt activation in keratinocytes. DKK3 in keratinocytes also drives macrophage polarization more toward a M2-like pro-fibrotic phenotype leading to skin fibrosis (Figure 4.17).
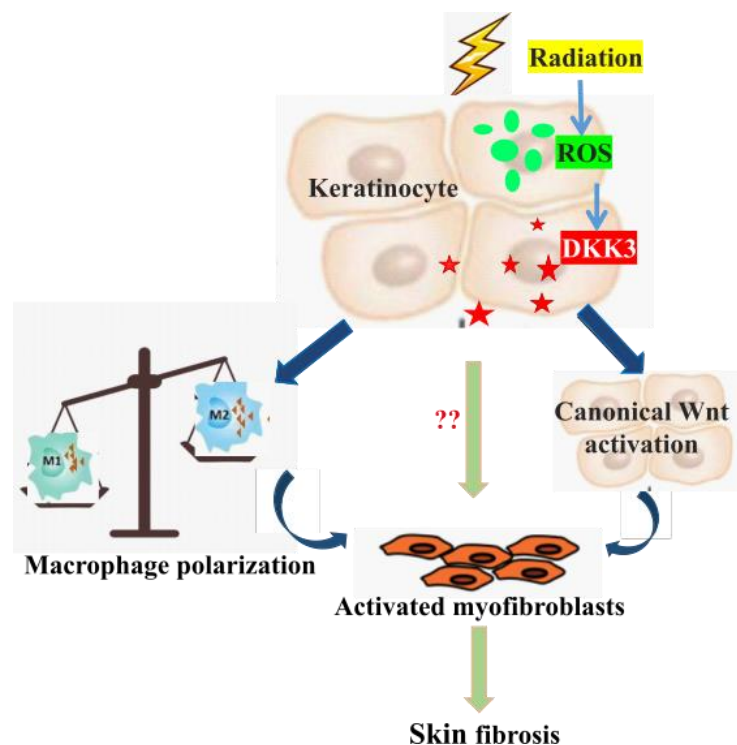
Figure 4.17 Schematic illustration of the hypothetical DKK3 function in the development of radiation-induced skin fibrosis. Radiation induces radical oxygen species (ROS) that leads to enhanced DKK3 expression with activation of canonical Wnt activity in keratinocytes and activated myofibroblasts. Upregulated DKK3 in keratinocytes leads to changes in cytokines expression that drives macrophage polarization more towards a M2-like pro-fibrotic phenotype. This activates myofibroblasts leading to fibrosis.

4.4 Effects of DKK3 on canonical Wnt activity in human immortalized dermal fibroblasts (K4)

Fibroblasts are important drivers of inflammatory fibrosis. Ferrari *et al.* reported that in carcinoma associated fibroblasts (CAFs), DKK3 can activate canonical Wnt signaling by interacting with the negative regulator Kremen and thereby increase levels of LRP6 on the cell surface [36]. In contrast, our *in vivo* data showed increased fibrosis with DKK3 fibroblast specific knockout in the radiation-induced chronic dermatitis model. To examine the potential effect of DKK3 modulation on dermal fibroblasts and canonical Wnt activity in more detail, immortalized dermal fibroblast (K4) cells were engineered with the canonical Wnt reporter and inducible DKK3 vectors used above (as described in Methods). Doxycycline was again used to induce DKK3 expression. ELISA in the supernatant, western blotting from total cell lysates and RT-qPCR confirmed the validity of the system with increased protein and mRNA expression of DKK3 following doxycycline induction in the engineered K4 cells (Figure 4.18A-C). Interestingly, canonical Wnt activity measurements by *Gaussia* luciferase after doxycycline induction showed that DKK3 overexpression led to reduced canonical Wnt pathway activation in the K4 cells (Figure 4.18D).

Taken together, while DKK3 over-expression led to activated canonical Wnt activity in keratinocytes, over-expression of DKK3 inhibited canonical Wnt activity in fibroblasts. These findings demonstrate the pleotropic nature of this regulator in different cell types of the same tissue and help explain the in *vivo* data where DKK3 fibroblast specific knockouts increased irradiation-induced collagen deposition as a consequence of enhanced canonical Wnt signaling as compared to WT or keratinocyte KO mice with

intact DKK3 expression by fibroblasts/myofibroblasts. Together these findings further emphasize the importance of epithelial hyperplasia in the radiation model.
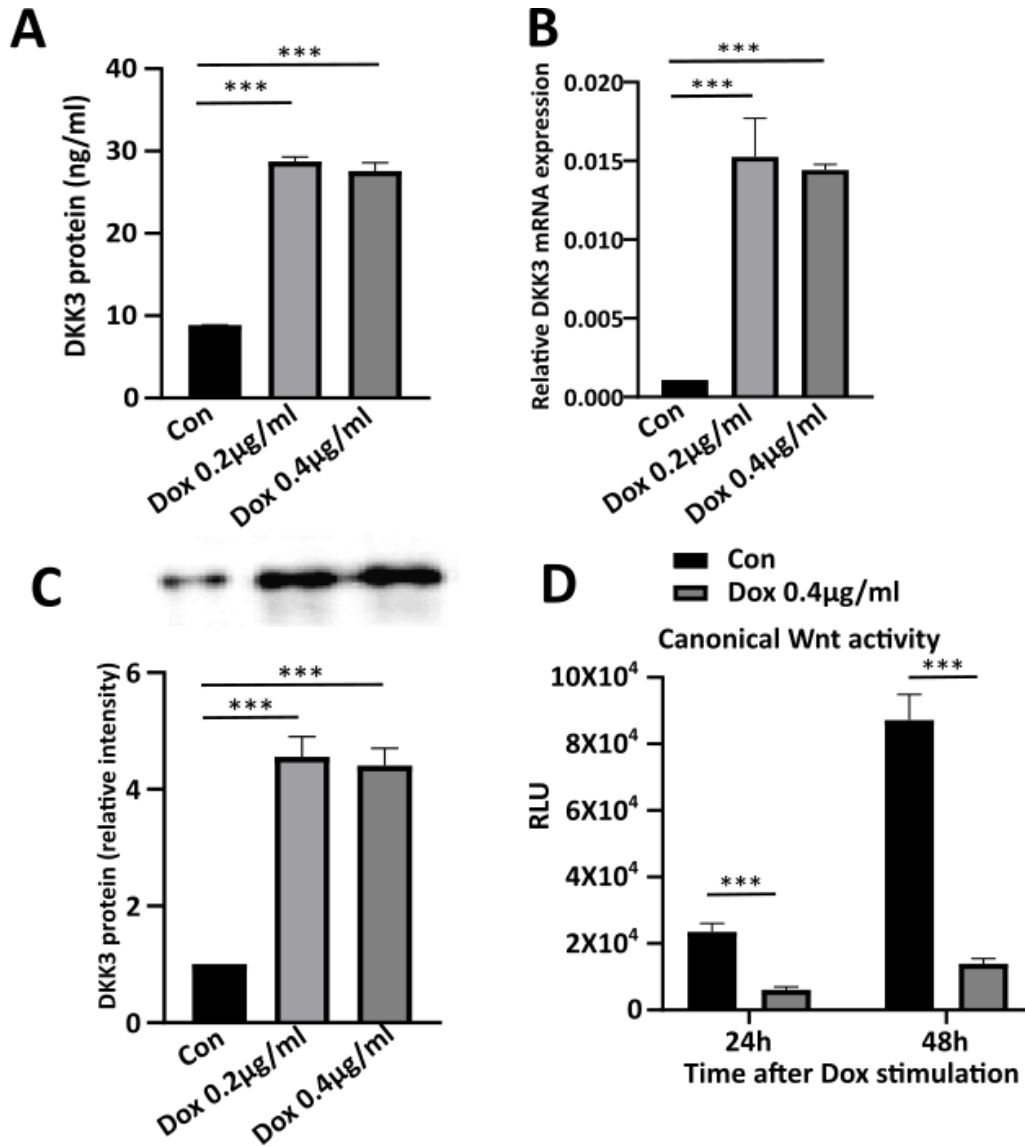
Figure 4.18 Effects of DKK3 on canonical Wnt activity in human immortalized dermal fibroblasts (K14). (A) DKK3 protein level in the supernatant measured by ELISA after DKK3 modulation. (B) DKK3 mRNA level measured by RT-qPCR after DKK3 modulation. DKK3 mRNA was calculated with the relative DKK3 mRNA/18s rRNA. (C) Intracellular DKK3 protein level measured by Western Blot and quantified after DKK3 modulation. A-C: Data are mean ± SEM, one way ANOVA with Tukey's multiple comparisons test. ***P＜0.001. (D) DKK3 over expression using doxycycline inhibited canonical Wnt activity. Data represent relative light units (RLU). Data are mean ± SEM, Student's t-test. ***P＜0.001.

5. Discussion

Radiotherapy using ionizing radiation is a mainstay of cancer therapy and is known to potentially induce severe side effects such as acute (dermatitis) and chronic skin damage (fibrosis). The role of DKK3 was investigated in this context in a model of radiation-induced dermal inflammation and fibrosis *in vitro* and *in vivo*. The project builds upon our earlier preclinical studies of DKK3 in damaged epithelial cells during renal damage and fibrosis in a non-radiation model [60], as well as upon studies in a radiation-induced lung fibrosis model in mice[29-31]. The results presented in this thesis support the hypothesis that epithelial expression of DKK3 can promote inflammatory fibrosis as evidenced here in models of radiation dermatitis. DKK3 deficiency was found to attenuate radiation-induced dermal hyperplasia and fibrosis. It is shown here for the first time that DKK3 can directly activate canonical Wnt signaling in keratinocytes, and that this expression has a direct impact on the proliferation of keratinocytes essentially driving the epithelial hyperplasia evident in the radiation model. In addition, DKK3 expression and the subsequent epithelial hyperplasia seen upon irradiation can also influence the polarization status of inflammatory myeloid cells, and through this, help drive a profibrotic effector status in these cells.

5.1 Radiation induces epithelial hyperplasia, myeloid infiltration and fibrosis in skin models *in vivo*

The most severe complication of the therapeutic application of radiation is an extensive radiation-induced fibrosis that can affect the life quality of tumor patients who receive radiotherapy that in some instances can be life threatening [35]. Chronic radiation dermatitis is seen months to years following exposure, and is described as an ongoing inflammatory fibrosis with hyper- and hypo-pigmentation, atrophy, necrosis and ulceration [35].
In the study of radiation-induced skin injury, various animal models using different strains of mice and rats have been described in the literature. The radiation doses

applied vary from 10Gy to 60Gy, and the observation time ranges from a few days to 6 months depending on the specific question addressed. The dorsal skin and the hind limb skin are the most frequently used irradiation area [84-93]. In the present study, 20Gy single dose were applied to induce radiation injury to the skin of both the thorax and the hind limb in C57BL6/N mice. This model was chosen, as previous studies in the same C57BL6/N mouse model from our group had successfully applied the same type of radiation to induce and investigate radiation-induced lung fibrosis with the mice maintaining an acceptable health status over many weeks without marked weight loss. These prior lung investigations, which had indicated certain tolerable skin damage without ulceration[20,29-31], helped choose the experimental model for the present thesis. In this thesis, in a first round of *in vivo* experiments both the hind limb model and the thoracic model showed that 4 weeks after 20Gy radiation obvious hyperplasia, myeloid infiltration and collagen deposition were reproducibly detected in irradiated skin as compared to non-irradiated skin. By 8 weeks after radiation, signs of fibrosis as identified by increased collagen deposition and α-SMA positive cells was observed in irradiated mouse skin. Thus, 20Gy radiation on either hind limb or thorax in C57BL/N mice was applied throughout this study to model radiation-induced skin injury using 4 to 8 weeks observation time depending upon the experimental context.

5.2 Keratinocytes represent an important cellular source of DKK3 in radiation-induced dermatitis

DKK3 is expressed by many tissues during embryonic development including the neural epithelium, dental follicles, limb bud and the developing heart, it is also found to be expressed in some adults tissues. DKK3 is richly expressed in adult brain and heart muscle tissues, showing cellular specifically in Muller glia cells and cardiomyocytes [94-97]. In adult skin, Brenner *et al*. demonstrated DKK3 expression in the upper epidermal layers of normal skin tissue and skin expression of DKK3 was found to change in response to UV radiation [98]. A study by Du *et al.* revealed that DKK3 expression could be further localized at the transitional area of upper spinous layer

and granular layer in skin. In this study, DKK3 expression in skin cancer cells was described as being reduced relative to normal skin [95]. Moreover, DKK3 expression was shown to be downregulated in the epidermis after treatment with the mitogenic agent TPA, during excisional wound healing in mice, as well as in the epidermis of different human diseases with the common characteristic of epidermal hyperproliferation [94]. The results as presented in this thesis show somewhat contradictory observations relative to the reports highlighted above, as a radiation-induced increase in DKK3 was reproducibly observed in the various *in vitro* studies, as well as in DKK3/Wnt dual reporter mice. In the *in vivo* setting, we could demonstrate that DKK3 expression increased as evidenced by DKK3-reporter activity, and that this increase occurred in basal keratinocytes early (days) after radiation. The results support the contention that basal keratinocytes represent an important early cellular source of DKK3 following radiation damage. The apparent differences found in our studies relative to previous reports may be due in part to the nature of tissue damage driving the epidermal hyperproliferation studied. Importantly, the veracity of our studies could be subsequently validated using the targeted depletion of DKK3 in relevant skin tissues in our murine models of radiation dermatitis and *in vitro* studies.

5.3 Radiation-induced ROS is a potential mediator of enhanced DKK3 expression in basal keratinocytes

Radical oxygen species (ROS) are generated by ionizing radiation in watery solutions ("radiolysis" of water) and are considered important mediators by which ionizing radiation interacts with molecules in cells and tissue. ROS cause biological effects including DNA damage eventually leading also to chronic dermatitis [27]. ROS and free radical scavengers have been reported to be effective treatments for the mitigation of radiation-induced toxicity in preclinical models [99]. In fact, the ROS eliminating prototypical drug amifostine was clinically approved in the 1990s because it could somewhat reduce radiotherapy related side effects when treating cancers of the head and neck region such as dermatitis and xerostomia [100]. Amifostine has been more

effective for acute and subacute symptoms and less effective in preventing fibrosis, and its clinical use has been largely abandoned due to side effects, and in particular, with the advent of precision radiotherapy like intensity modulated radiotherapy (IMRT) by which the salivary glands (parotid gland) can markedly be spared and xerostomia reduced. Since ROS play a central part in radiobiology, and its attenuation might reduce radiation toxicity, the role of ROS in DKK3 activation was evaluated. It was first confirmed *in vitro* that radiation-induced ROS in keratinocytes. Then the chemical ROS inducer rotenone was found to increase DKK3 expression in a dose-dependent manner in keratinocytes. Thus, it is likely that radiation-induced ROS can contribute to the upregulation of DKK3 measured upon radiation. To the best of our knowledge, this is the first report showing that increased ROS can lead to the induction of DKK3 expression in keratinocytes. These findings further suggest that DKK3 may be part of the cellular response mechanism to radiation and ROS-induced stress. This hypothesis is in line with data from Qiu *et al.* who reported that the expression of DKK3 could prevent oxidative stress-induced apoptosis by attenuating xanthine dehydrogenase expression in Li21 hepatoma cells and tPH5CH immortalized hepatocytes [99]. Likewise, a second study using a lung adenocarcinoma model reported that DKK3 expression decreased the intracellular level of ROS and may thus act as an anti-apoptotic molecule [101]. These studies showed that DKK3 inhibited ROS induction and attenuated apoptosis, suggesting that in some tissue settings, DKK3 biology may be part of the cellular defense mechanism against acute radiation damage. This general view was supported by results presented in this thesis. It was found that not only did radiation-induced ROS increase DKK3 expression, but a knockdown of DKK3 in keratinocytes led to increased apoptosis rates following irradiation. These results suggest that radiation damage as evidenced by cellular apoptosis induction via ROS is attenuated by the presence of DKK3. Thus, DKK3 appears to mitigate acute radiation damage in terms of apoptotic cell death, while promoting later and chronic toxicity in form of tissue remodeling and inflammatory fibrosis. This result is also in line with clinical observations that the anti- ROS drug Amifostine was more effective in mitigating acute dermatitis than fibrosis. Importantly, the biologic actions of DKK3 appear to be context

dependent reflecting the pleotropic properties described in the literature and depend on the tissue under study: While the two mentioned preclinical reports and the here presented data are consistent, one other report concluded, by contrast, that DKK3 over expression could induce apoptosis in lung adenocarcinoma cells [102].

5.4 Effects of DKK3 on commonly studied radiobiological processes

Our *in vitro* data demonstrated a keratinocyte response to radiation with respect to the intrinsic radiosensitivity, DNA DSB damage, DNA DSB repair dynamics, apoptosis induction and cell cycle changes. However, these endpoints were not strongly influenced by the DKK3 expression status. The slightly increased apoptosis and ROS level as well as G2 arrest seen in the DKK3 knockdown cells was probably associated with the increased γ-H2AX levels initially detected that then subsided at later time points suggesting a minor role if any for DKK3 in the DNA repair process. To our knowledge, this is the first study evaluation the potential effect of DKK3 on radiosensitivity, DNA damage and repair after irradiation. The results strongly suggest that the phenotypical differences observed in mice and cells with different DKK3 status are not associated with effects on the radiobiological processes investigated here, but rather are more strongly linked to specific DKK3 – canonical Wnt signaling processes triggered by radiation.

5.5 DKK3 activates canonical Wnt signaling in keratinocytes

As discussed, the regulation of canonical Wnt pathway and DKK3 biology depends on the specific cellular or tissue context under study [54]. DKK3 can either activate or inhibit canonical Wnt pathway activity [55-58]. It has been reported that DKK3 can potentiate canonical Wnt signaling by binding to the negative regulator proteins Kremen 1 or Kremen 2 in human neuroblasts and human embryonic kidney 293 cells [101]. However, DKK3 has also been described as an anti-oncogene that inhibits canonical Wnt signaling in some cancer cells [48,102,103]. The previous study from our group examining

the role of DKK3 in chronic kidney damage suggested that DKK3 expression is associated with canonical Wnt signaling activation in tubular epithelial cells [59]. The results as presented in this thesis suggest that in keratinocytes, DKK3 potentiates canonical Wnt activity and tissue fibrosis supporting the earlier findings reported in damaged kidney. Moreover, radiation was found to increase DKK3 expression in keratinocytes and was followed by an activation of canonical Wnt activity. Interestingly, radiation alone was not found to activate Wnt in DKK3 knockout keratinocytes suggesting that functional DKK3 is necessary for radiation to activate canonical Wnt pathway signaling.

5.6 DKK3 inhibits canonical Wnt activity in dermal fibroblasts

Carcinoma associated fibroblasts (CAFs) are an important and somewhat unique cell type found in tumor stroma. Ferrari *et al*. demonstrated that DKK3 in CAFs could also potentiate canonical Wnt signaling through interaction with Kremen and thereby increase cell-surface levels of the Wnt co-receptor LRP6 [56]. Since fibroblasts clearly play a central role in the development of fibrosis, the effect of DKK3 overexpression and canonical Wnt activity was evaluated using a dermal fibroblast cell line (K4). Interestingly, the results suggest that in dermal fibroblasts, DKK3 leads to inhibition of canonical Wnt activity. This observation is in contrast to what was reported in the CAF study, and our findings in the present study in keratinocytes. Intriguingly, these results may also help explain the *in vivo* data as discussed above, where the fibroblast specific DKK3 knockout mice showed increased collagen deposition suggesting over-activated myofibroblast activity and enhanced canonical Wnt pathway activation associated with fibrosis.

5.7 Global and keratinocyte specific knockout of DKK3 attenuates radiation-induced hyperplasia and fibrosis *in vivo*

TGF-β plays a key role in fibroblast activation and in fibrotic diseases in general [104]. Akhmetshina *et al.* reported that interaction between the TGF-β and canonical Wnt

signaling pathways is important for fibroblast activation and ECM accumulation during fibrosis [6]. A series of studies have also shown that increased canonical Wnt signaling activity plays an important role in fibrotic diseases, such as renal fibrosis, pulmonary fibrosis, liver fibrosis, dermal fibrosis, the fibrosis following muscular dystrophy, as well as in scarring after myocardial fibrosis [7-9,105-109]. Our previous report in kidney revealed that epithelial DKK3 plays an important profibrotic role in renal fibrosis. The study showed that genetic depletion of DKK3 or DKK3 antibody treatment attenuated experimental renal fibrosis [59]. Based on the findings described in this thesis, keratinocytes represent an important cellular source of DKK3, and that DKK3 overexpression in keratinocytes can activate canonical Wnt activity. The results further suggest that enhanced DKK3 expression by basal keratinocytes plays a key role in radiation-induced dermal hyperplasia and fibrosis. Unlike depletion in fibroblasts, the global knockout or keratinocyte specific knockout of DKK3 led to protection of mice from epidermal hyperplasia and dermal fibrosis following radiation injury.

5.8 DKK3 drives macrophage polarization more towards a chronic fibrosing process as generally associated with a "M2-like" polarization status

Both genetically global knockout and keratinocyte-specific knockout of DKK3 lead to an increased infiltration of monocytes and macrophages in irradiated mouse skin over the already increased infiltration of these cells seen in WT animals. At first glance, these findings appear in contrast to the current paradigm regarding the role of an inflammatory infiltrate in driving chronic fibrosis. Macrophages are heterogeneous cells with considerable plasticity and diversity that is thought to influence inflammatory fibrosis by shifting between M1-like and M2-like phenotypes. Classically, pro-fibrotic myeloid cells are referred to as M2-like cells while M1-like polarization is associated with a pro-inflammatory/anti-fibrotic status. It has been previously reported that DKK3 can induce the differentiation of human CD14+ monocytes into a novel cell type described as immature dendritic cells, generated with GM-CSF and IL-4. DKK3 present within tumors has been suggested to help activate immune cells and

thus increase the anti-cancer immunity [110,111]. Zhang *et al.* reported that the related DKK family member DKK2, leads to significantly decreased expression of markers related to M1-like macrophages after DKK2 knockdown, while increased M2-like macrophage markers were more associated with DKK2 expression [112]. The *in vitro* and *ex vivo* FACS data from mouse skin provided in the present study has shown that keratinocyte expression of DKK3 appears to drive macrophage polarization more in the direction of a M2-like/pro-fibrotic phenotype, and is a direct result of the epidermal hyperplasia present in our model system. The results further support the idea that the effector status of the infiltrate, rather than the absolute number of the myeloid cells, dictates the fate of tissue fibrosis as global or keratinocyte DKK3 knockouts decreased radiation-induced hyperplasia and fibrosis, while still showing a robust myeloid infiltration. The finding of enhanced M2-like macrophages in the more fibrosis prone DKK3 wildtype animals in response to radiation injury is also in agreement with our previous study in a radiation-induced lung toxicity model using the same C57BL/N mouse background and the same 20 Gy single dose irradiation [20,32]. In that study it was shown that 20Gy irradiation-induced a time dependent acute and subacute pulmonary inflammation leading to lung remodeling and fibrosis that was associated with substantially enriched M2 macrophages in the radiation-injured lungs. Lung remodeling and fibrosis could partially be attenuated and reversed by blocking connective tissue growth factor (CTGF)-driven signaling which decreased M2 activation. Of note, the anti-fibrotic CTGF antibody also markedly decreased Wisp1 (Wnt1 inducible signaling pathway protein 1) in mouse lungs that was upregulated after radiation further strengthening the notion of radiation-induced DKK3/Wnt signaling leading to tissue fibrosis .

5.9 Limitations

There are limitations of the present study. In general, radiation effects on biological systems dependent on the dose and fractionation scheme, both *in vitro* and *in vivo*. The time-frame of the data read out is also relevant, in particular for analysis of *in vivo*

radiation effects on normal tissue as presented here. Due to time limitations the entire spectrum of these parameters could not be covered in this thesis study. This limits the strengths of conclusions that can be drawn from the data presented as it relates to the dose and time frame studied. For example, it would have been interesting to evaluate the very early immediate radiation responses *in vivo*, or observe the mice for longer than 8 weeks. The relatively short time-frame available for observation of tissue fibrosis is also a limitation of the study. Unfortunately, due to time constraints and animal welfare issues, it was not possible to obtain longer time points. Clinically it takes months to years for patients who receive radiation therapy to develop fibrosis. Being able to assess the effects at 3 or 6 months may provide additional information regarding long-term DKK3-mediated effects on the prognosis of tissue fibrosis.

A series of mediators of radiation-induced toxicity and fibrosis have been described. These include: transforming-growth-factor-β (TGF-β), platelet-derived-growth-factor (PDGF), connective tissue growth factor (CTGF), matrix-metallo-proteinases (MMPs), integrins, lysophosphatidic acid receptors, Rho/ROCK signaling and CD73 [113]. The potential interaction of DKK3/Wnt with these signaling nodes at any given time point of the inflammatory fibrogenesis cascade after radiation injury remain open issues. In addition, the molecular mechanism by which radiation-induced ROS leads to increased DKK3 expression, or how DKK3 leads to activation of canonical Wnt activity in keratinocytes remains unclear.

5.10 Summary

Radiation-induced fibrosis is common in tumor patients who receive radiotherapy. When it occurs in skin, it can affect quality of life and influence disease prognosis. Treatment of chronic radiation dermatitis and fibrosis is difficult underscoring the very real need for novel targets and treatment strategies. Canonical Wnt signaling plays an important role in fibrotic diseases and is recognized as a target for radiation-induced dermatitis and the treatment of fibrosis.

The present study shows that radiation-induced ROS in basal keratinocytes can in turn

lead to DKK3 over-expression and activation of canonical Wnt pathway activity. This action was directly linked to the epidermal hyperplasia seen during radiation dermatitis. DKK3 deficiency was found to lead to reduced canonical Wnt activity and reduced dermal hyperplasia and fibrosis upon radiation injury. Interestingly, DKK3 expression by keratinocytes appears to modulate the polarization of the myeloid infiltrate present in the damaged skin tissue. The expression of DKK3 by keratinocytes after radiation appears to help drive macrophage polarization more towards a M2-like pro-fibrotic macrophage phenotype, while the absence of DKK3 in keratinocytes leads to a macrophage polarization more toward a more M1-like pro-inflammatory phenotype.

In conclusion, the study shows that DKK3/Wnt plays an important role in radiation-induced dermatitis and fibrosis, and suggests that DKK3 may serve as a therapeutic target for the treatment of radiation-induced dermal fibrosis and potentially also for fibrotic diseases in other anatomical sites or of different origin.

6. References

1   Eming, S. A., Martin, P. & Tomic-Canic, M. Wound repair and regeneration: mechanisms, signaling, and translation. *Sci Transl Med* **6**, 265sr266, doi:10.1126/scitranslmed.3009337 (2014).

2   Gurtner, G. C., Werner, S., Barrandon, Y. & Longaker, M. T. Wound repair and regeneration. *Nature* **453**, 314-321, doi:10.1038/nature07039 (2008).

3   Eming, S. A., Wynn, T. A. & Martin, P. Inflammation and metabolism in tissue repair and regeneration. *Science* **356**, 1026-1030, doi:10.1126/science.aam7928 (2017).

4   Wynn, T. A. Cellular and molecular mechanisms of fibrosis. *J Pathol* **214**, 199-210, doi:10.1002/path.2277 (2008).

5   Quan, T. E., Cowper, S. E. & Bucala, R. The role of circulating fibrocytes in fibrosis. *Curr Rheumatol Rep* **8**, 145-150, doi:10.1007/s11926-006-0055-x (2006).

6   Akhmetshina, A. *et al.* Activation of canonical Wnt signalling is required for TGF-beta-mediated fibrosis. *Nat Commun* **3**, 735, doi:10.1038/ncomms1734 (2012).

7   Chilosi, M. *et al.* Aberrant Wnt/β-Catenin Pathway Activation in Idiopathic Pulmonary Fibrosis. *The American Journal of Pathology* **162**, 1495-1502, doi:10.1016/s0002-9440(10)64282-4 (2003).

8   Colwell, A. S., Krummel, T. M., Longaker, M. T. & Lorenz, H. P. Wnt-4 expression is increased in fibroblasts after TGF-beta1 stimulation and during fetal and postnatal wound repair. *Plast Reconstr Surg* **117**, 2297-2301, doi:10.1097/01.prs.0000218708.16909.31 (2006).

9   He, W. *et al.* Wnt/beta-catenin signaling promotes renal interstitial fibrosis. *J Am Soc Nephrol* **20**, 765-776, doi:10.1681/ASN.2008060566 (2009).

10   Wei, J. *et al.* Canonical Wnt signaling induces skin fibrosis and subcutaneous lipoatrophy: a novel mouse model for scleroderma? *Arthritis Rheum* **63**, 1707-1717, doi:10.1002/art.30312 (2011).

11   Baskar, R., Lee, K. A., Yeo, R. & Yeoh, K. W. Cancer and radiation therapy: current advances and future directions. *Int J Med Sci* **9**, 193-199, doi:10.7150/ijms.3635 (2012).

12   Schulz-Ertner, D. & Tsujii, H. Particle radiation therapy using proton and heavier ion beams. *J Clin Oncol* **25**, 953-964, doi:10.1200/JCO.2006.09.7816 (2007).

13   Ma, C. M. & Maughan, R. L. Within the next decade conventional cyclotrons for proton radiotherapy will become obsolete and replaced by far less expensive machines using compact laser systems for the acceleration of the protons. *Med Phys* **33**, 571-573, doi:10.1118/1.2150220 (2006).

14   Jonathan, E. C., Bernhard, E. J. & McKenna, W. G. How does radiation kill cells? *Curr Opin Chem Biol* **3**, 77-83, doi:10.1016/s1367-5931(99)80014-3 (1999).

15   Dewey, W. C., Ling, C. C. & Meyn, R. E. Radiation-induced apoptosis: relevance to radiotherapy. *Int J Radiat Oncol Biol Phys* **33**, 781-796, doi:10.1016/0360-3016(95)00214-8 (1995).

16   Hotchkiss, R. S., Strasser, A., McDunn, J. E. & Swanson, P. E. Cell death. *N Engl J Med* **361**, 1570-1583, doi:10.1056/NEJMra0901217 (2009).

17   Roninson, I. B. Tumor cell senescence in cancer treatment. *Cancer Res* **63**, 2705-2715 (2003).

18   Ito, H., Daido, S., Kanzawa, T., Kondo, S. & Kondo, Y. Radiation-induced autophagy is associated with LC3 and its inhibition sensitizes malignant glioma cells. *Int J Oncol* **26**, 1401-1410 (2005).

19   Klug, F. *et al.* Low-dose irradiation programs macrophage differentiation to an iNOS(+)/M1 phenotype that orchestrates effective T cell immunotherapy. *Cancer Cell* **24**, 589-602, doi:10.1016/j.ccr.2013.09.014 (2013).

20   Bickelhaupt, S. *et al.* Effects of CTGF Blockade on Attenuation and Reversal of Radiation-Induced Pulmonary Fibrosis. *J Natl Cancer Inst* **109**, doi:10.1093/jnci/djw339 (2017).

21   Straub, J. M. *et al.* Radiation-induced fibrosis: mechanisms and implications for therapy. *J Cancer Res Clin Oncol* **141**, 1985-1994, doi:10.1007/s00432-015-1974-6 (2015).

22   Andreassen, C. N. *et al.* ATM sequence variants and risk of radiation-induced subcutaneous fibrosis after postmastectomy radiotherapy. *Int J Radiat Oncol Biol Phys* **64**, 776-783, doi:10.1016/j.ijrobp.2005.09.014 (2006).

23   Haston, C. K., Begin, M., Dorion, G. & Cory, S. M. Distinct loci influence radiation-induced alveolitis from fibrosing alveolitis in the mouse. *Cancer Res* **67**, 10796-10803, doi:10.1158/0008-5472.CAN-07-2733 (2007).

24   Gordon, S. & Martinez, F. O. Alternative activation of macrophages: mechanism and functions. *Immunity* **32**, 593-604, doi:10.1016/j.immuni.2010.05.007 (2010).

25   Sica, A. & Mantovani, A. Macrophage plasticity and polarization: in vivo veritas. *J Clin Invest* **122**, 787-795, doi:10.1172/JCI59643 (2012).

26   Varin, A. & Gordon, S. Alternative activation of macrophages: immune function and cellular biology. *Immunobiology* **214**, 630-641, doi:10.1016/j.imbio.2008.11.009 (2009).

27   Travis, E. L. Organizational response of normal tissues to irradiation. *Semin Radiat Oncol* **11**, 184-196, doi:10.1053/srao.2001.25243 (2001).

28   Yarnold, J. & Brotons, M. C. Pathogenetic mechanisms in radiation fibrosis. *Radiother Oncol* **97**, 149-161, doi:10.1016/j.radonc.2010.09.002 (2010).

29   Flechsig, P. *et al.* LY2109761 attenuates radiation-induced pulmonary murine fibrosis via reversal of TGF-beta and BMP-associated proinflammatory and proangiogenic signals. *Clin Cancer Res* **18**, 3616-3627, doi:10.1158/1078-0432.CCR-11-2855 (2012).

30   Abdollahi, A. *et al.* Inhibition of platelet-derived growth factor signaling attenuates pulmonary fibrosis. *J Exp Med* **201**, 925-935, doi:10.1084/jem.20041393 (2005).

31   Dadrich, M. *et al.* Combined inhibition of TGFbeta and PDGF signaling attenuates radiation-induced pulmonary fibrosis. *Oncoimmunology* **5**, e1123366, doi:10.1080/2162402X.2015.1123366 (2016).

32   Sternlicht, M. D. *et al.* Radiation-induced pulmonary gene expression changes are attenuated by the CTGF antibody Pamrevlumab. *Respir Res* **19**, 14, doi:10.1186/s12931-018-0720-4 (2018).

33   Nicolay, N. H., Lopez Perez, R., Debus, J. & Huber, P. E. Mesenchymal stem cells - A new hope for radiotherapy-induced tissue damage? *Cancer Lett* **366**, 133-140, doi:10.1016/j.canlet.2015.06.012 (2015).

34   Alexopoulou, E. *et al.* An Exploratory Study of Radiation Dermatitis in Breast Cancer Patients. *Anticancer Res* **38**, 1615-1622, doi:10.21873/anticanres.12392 (2018).

35   Hegedus, F., Mathew, L. M. & Schwartz, R. A. Radiation dermatitis: an overview. *Int J Dermatol* **56**, 909-914, doi:10.1111/ijd.13371 (2017).

36   Spalek, M. Chronic radiation-induced dermatitis: challenges and solutions. *Clin Cosmet Investig Dermatol* **9**, 473-482, doi:10.2147/CCID.S94320 (2016).

37   Cox, J. D., Stetz, J. & Pajak, T. F. Toxicity criteria of the Radiation Therapy Oncology Group (RTOG) and the European Organization for Research and Treatment of Cancer (EORTC). *Int J Radiat*

Oncol Biol Phys **31**, 1341-1346, doi:10.1016/0360-3016(95)00060-C (1995).

38   Tharmalingam, S., Sreetharan, S., Kulesza, A. V., Boreham, D. R. & Tai, T. C. Low-Dose Ionizing Radiation Exposure, Oxidative Stress and Epigenetic Programing of Health and Disease. *Radiat Res*, doi:10.1667/RR14587.1 (2017).

39   Tibbs, M. K. Wound healing following radiation therapy: a review. *Radiother Oncol* **42**, 99-106 (1997).

40   Salvo, N. *et al.* Prophylaxis and management of acute radiation-induced skin reactions: a systematic review of the literature. *Curr Oncol* **17**, 94-112 (2010).

41   Bickers, D. R. & Athar, M. Oxidative stress in the pathogenesis of skin disease. *J Invest Dermatol* **126**, 2565-2575, doi:10.1038/sj.jid.5700340 (2006).

42   Lim, X. & Nusse, R. Wnt signaling in skin development, homeostasis, and disease. *Cold Spring Harb Perspect Biol* **5**, doi:10.1101/cshperspect.a008029 (2013).

43   Lien, W. H. *et al.* In vivo transcriptional governance of hair follicle stem cells by canonical Wnt regulators. *Nat Cell Biol* **16**, 179-190, doi:10.1038/ncb2903 (2014).

44   Gieseck, R. L., 3rd, Wilson, M. S. & Wynn, T. A. Type 2 immunity in tissue repair and fibrosis. *Nat Rev Immunol* **18**, 62-76, doi:10.1038/nri.2017.90 (2018).

45   Barker, H. E., Paget, J. T., Khan, A. A. & Harrington, K. J. The tumour microenvironment after radiotherapy: mechanisms of resistance and recurrence. *Nat Rev Cancer* **15**, 409-425, doi:10.1038/nrc3958 (2015).

46   Komiya, Y. & Habas, R. Wnt signal transduction pathways. *Organogenesis* **4**, 68-75, doi:10.4161/org.4.2.5851 (2008).

47   Kleber, M. & Sommer, L. Wnt signaling and the regulation of stem cell function. *Curr Opin Cell Biol* **16**, 681-687, doi:10.1016/j.ceb.2004.08.006 (2004).

48   Veeck, J. & Dahl, E. Targeting the Wnt pathway in cancer: the emerging role of Dickkopf-3. *Biochim Biophys Acta* **1825**, 18-28, doi:10.1016/j.bbcan.2011.09.003 (2012).

49   Klaus, A. & Birchmeier, W. Wnt signalling and its impact on development and cancer. *Nat Rev Cancer* **8**, 387-398, doi:10.1038/nrc2389 (2008).

50   He, X., Semenov, M., Tamai, K. & Zeng, X. LDL receptor-related proteins 5 and 6 in Wnt/beta-catenin signaling: arrows point the way. *Development* **131**, 1663-1677, doi:10.1242/dev.01117 (2004).

51   Gordon, M. D. & Nusse, R. Wnt signaling: multiple pathways, multiple receptors, and multiple transcription factors. *J Biol Chem* **281**, 22429-22433, doi:10.1074/jbc.R600015200 (2006).

52   Krupnik, V. E. *et al.* Functional and structural diversity of the human Dickkopf gene family. *Gene* **238**, 301-313, doi:10.1016/s0378-1119(99)00365-0 (1999).

53   Niehrs, C. Function and biological roles of the Dickkopf family of Wnt modulators. *Oncogene* **25**, 7469-7481, doi:10.1038/sj.onc.1210054 (2006).

54   Mao, B. *et al.* Kremen proteins are Dickkopf receptors that regulate Wnt/beta-catenin signalling. *Nature* **417**, 664-667, doi:10.1038/nature756 (2002).

55   Monaghan, A. P. *et al.* Dickkopf genes are co-ordinately expressed in mesodermal lineages. *Mech Dev* **87**, 45-56, doi:10.1016/s0925-4773(99)00138-0 (1999).

56   Nakamura, R. E., Hunter, D. D., Yi, H., Brunken, W. J. & Hackam, A. S. Identification of two novel activities of the Wnt signaling regulator Dickkopf 3 and characterization of its expression in the mouse retina. *BMC Cell Biol* **8**, 52, doi:10.1186/1471-2121-8-52 (2007).

57   Ferrari, N. *et al.* Dickkopf-3 links HSF1 and YAP/TAZ signalling to control aggressive behaviours

in cancer-associated fibroblasts. *Nat Commun* **10**, 130, doi:10.1038/s41467-018-07987-0 (2019).

58   Hoang, B. H. *et al.* Dickkopf 3 inhibits invasion and motility of Saos-2 osteosarcoma cells by modulating the Wnt-beta-catenin pathway. *Cancer Res* **64**, 2734-2739, doi:10.1158/0008-5472.can-03-1952 (2004).

59   Caricasole, A. *et al.* Functional characterization of WNT7A signaling in PC12 cells: interaction with A FZD5 x LRP6 receptor complex and modulation by Dickkopf proteins. *J Biol Chem* **278**, 37024-37031, doi:10.1074/jbc.M300191200 (2003).

60   Federico, G. *et al.* Tubular Dickkopf-3 promotes the development of renal atrophy and fibrosis. *JCI Insight* **1**, e84916, doi:10.1172/jci.insight.84916 (2016).

61   Meister, M. *et al.* Dickkopf-3, a tissue-derived modulator of local T-cell responses. *Front Immunol* **6**, 78, doi:10.3389/fimmu.2015.00078 (2015).

62   Ludwig, J. *et al.* Dickkopf-3 acts as a modulator of B cell fate and function. *J Immunol* **194**, 2624-2634, doi:10.4049/jimmunol.1402160 (2015).

63   Ma, B. & Hottiger, M. O. Crosstalk between Wnt/beta-Catenin and NF-kappaB Signaling Pathway during Inflammation. *Front Immunol* **7**, 378, doi:10.3389/fimmu.2016.00378 (2016).

64   Papatriantafyllou, M. *et al.* Dickkopf-3, an immune modulator in peripheral CD8 T-cell tolerance. *Proc Natl Acad Sci U S A* **109**, 1631-1636, doi:10.1073/pnas.1115980109 (2012).

65   Meister, M. *et al.* Self-Antigen Presentation by Keratinocytes in the Inflamed Adult Skin Modulates T-Cell Auto-Reactivity. *J Invest Dermatol* **135**, 1996-2004, doi:10.1038/jid.2015.130 (2015).

66   Karamariti, E. *et al.* DKK3 (Dickkopf 3) Alters Atherosclerotic Plaque Phenotype Involving Vascular Progenitor and Fibroblast Differentiation Into Smooth Muscle Cells. *Arterioscler Thromb Vasc Biol* **38**, 425-437, doi:10.1161/ATVBAHA.117.310079 (2018).

67   Cheng, W. L. *et al.* Dickkopf-3 Ablation Attenuates the Development of Atherosclerosis in ApoE-Deficient Mice. *J Am Heart Assoc* **6**, doi:10.1161/JAHA.116.004690 (2017).

68   Lu, K. H. *et al.* Dickkopf-3 Contributes to the Regulation of Anti-Tumor Immune Responses by Mesenchymal Stem Cells. *Front Immunol* **6**, 645, doi:10.3389/fimmu.2015.00645 (2015).

69   Lien, W. H. & Fuchs, E. Wnt some lose some: transcriptional governance of stem cells by Wnt/beta-catenin signaling. *Genes Dev* **28**, 1517-1532, doi:10.1101/gad.244772.114 (2014).

70   Fuchs, E. Scratching the surface of skin development. *Nature* **445**, 834-842, doi:10.1038/nature05659 (2007).

71   Augustin, I. Wnt signaling in skin homeostasis and pathology. *J Dtsch Dermatol Ges* **13**, 302-306, doi:10.1111/ddg.12620 (2015).

72   Hsu, Y. C., Li, L. & Fuchs, E. Emerging interactions between skin stem cells and their niches. *Nat Med* **20**, 847-856, doi:10.1038/nm.3643 (2014).

73   Clevers, H., Loh, K. M. & Nusse, R. Stem cell signaling. An integral program for tissue renewal and regeneration: Wnt signaling and stem cell control. *Science* **346**, 1248012, doi:10.1126/science.1248012 (2014).

74   Lim, X. *et al.* Interfollicular epidermal stem cells self-renew via autocrine Wnt signaling. *Science* **342**, 1226-1230, doi:10.1126/science.1239730 (2013).

75   Chen, D., Jarrell, A., Guo, C., Lang, R. & Atit, R. Dermal beta-catenin activity in response to epidermal Wnt ligands is required for fibroblast proliferation and hair follicle initiation. *Development* **139**, 1522-1533, doi:10.1242/dev.076463 (2012).

76   Jackel, C. *et al.* A vector platform for the rapid and efficient engineering of stable complex transgenes. *Sci Rep* **6**, 34365, doi:10.1038/srep34365 (2016).

77   Ferrer-Vaquer, A. *et al.* A sensitive and bright single-cell resolution live imaging reporter of Wnt/ss-catenin signaling in the mouse. *BMC Dev Biol* **10**, 121, doi:10.1186/1471-213X-10-121 (2010).

78   Mills, C. D., Kincaid, K., Alt, J. M., Heilman, M. J. & Hill, A. M. M-1/M-2 macrophages and the Th1/Th2 paradigm. *J Immunol* **164**, 6166-6173, doi:10.4049/jimmunol.164.12.6166 (2000).

79   Qian, B. Z. & Pollard, J. W. Macrophage diversity enhances tumor progression and metastasis. *Cell* **141**, 39-51, doi:10.1016/j.cell.2010.03.014 (2010).

80   Martinez, F. O. & Gordon, S. The M1 and M2 paradigm of macrophage activation: time for reassessment. *F1000Prime Rep* **6**, 13, doi:10.12703/P6-13 (2014).

81   <1471-2172-13-31.pdf>.

82   Lacey, D. C. *et al.* Defining GM-CSF- and macrophage-CSF-dependent macrophage responses by in vitro models. *J Immunol* **188**, 5752-5765, doi:10.4049/jimmunol.1103426 (2012).

83   Xie, N. *et al.* NAD(+) metabolism: pathophysiologic mechanisms and therapeutic potential. *Signal Transduct Target Ther* **5**, 227, doi:10.1038/s41392-020-00311-7 (2020).

84   Perez-Aso, M., Mediero, A., Low, Y. C., Levine, J. & Cronstein, B. N. Adenosine A2A receptor plays an important role in radiation-induced dermal injury. *FASEB J* **30**, 457-465, doi:10.1096/fj.15-280388 (2016).

85   Park, S. W. *et al.* Anthocyanins from black soybean seed coat prevent radiation-induced skin fibrosis by downregulating TGF-beta and Smad3 expression. *Arch Dermatol Res* **310**, 401-412, doi:10.1007/s00403-018-1827-7 (2018).

86   Yoo, H. *et al.* Gefitinib Inhibits Radiation-Induced Skin Fibrosis By Inhibition of STAT1 Expression. *International Journal of Radiation Oncology*Biology*Physics* **90**, doi:10.1016/j.ijrobp.2014.05.2237 (2014).

87   Horton, J. A. *et al.* Inhibition of radiation-induced skin fibrosis with imatinib. *Int J Radiat Biol* **89**, 162-170, doi:10.3109/09553002.2013.741281 (2013).

88   Liu, W. *et al.* Interleukin 1beta (IL1B) signaling is a critical component of radiation-induced skin fibrosis. *Radiat Res* **165**, 181-191, doi:10.1667/rr3478.1 (2006).

89   <Pentoxifylline does not spare acute radiation reactions in rat lung and skin.pdf>.

90   Yoo, H. *et al.* Pyruvate metabolism: A therapeutic opportunity in radiation-induced skin injury. *Biochem Biophys Res Commun* **460**, 504-510, doi:10.1016/j.bbrc.2015.03.060 (2015).

91   Horton, J. A. *et al.* Quercetin inhibits radiation-induced skin fibrosis. *Radiat Res* **180**, 205-215, doi:10.1667/RR3237.1 (2013).

92   de Andrade, C. B. V. *et al.* Radiotherapy-Induced Skin Reactions Induce Fibrosis Mediated by TGF-beta1 Cytokine. *Dose Response* **15**, 1559325817705019, doi:10.1177/1559325817705019 (2017).

93   Thanik, V. D. *et al.* A novel mouse model of cutaneous radiation injury. *Plast Reconstr Surg* **127**, 560-568, doi:10.1097/PRS.0b013e3181fed4f7 (2011).

94   Du, G. *et al.* Expression of REIC/Dkk-3 in normal and hyperproliferative epidermis. *Exp Dermatol* **20**, 273-277, doi:10.1111/j.1600-0625.2010.01244.x (2011).

95   Diep, D. B., Hoen, N., Backman, M., Machon, O. & Krauss, S. Characterisation of the Wnt antagonists and their response to conditionally activated Wnt signalling in the developing mouse forebrain. *Brain Res Dev Brain Res* **153**, 261-270,

doi:10.1016/j.devbrainres.2004.09.008 (2004).

96   Aslan, H. *et al.* Advanced molecular profiling in vivo detects novel function of dickkopf-3 in the regulation of bone formation. *J Bone Miner Res* **21**, 1935-1945, doi:10.1359/jbmr.060819 (2006).

97   Fjeld, K., Kettunen, P., Furmanek, T., Kvinnsland, I. H. & Luukko, K. Dynamic expression of Wnt signaling-related Dickkopf1, -2, and -3 mRNAs in the developing mouse tooth. *Dev Dyn* **233**, 161-166, doi:10.1002/dvdy.20285 (2005).

98   Brenner, M. *et al.* Long-lasting molecular changes in human skin after repetitive in situ UV irradiation. *J Invest Dermatol* **129**, 1002-1011, doi:10.1038/jid.2008.325 (2009).

99   Epperly, M. W., Epstein, C. J., Travis, E. L. & Greenberger, J. S. Decreased pulmonary radiation resistance of manganese superoxide dismutase (MnSOD)-deficient mice is corrected by human manganese superoxide dismutase-Plasmid/Liposome (SOD2-PL) intratracheal gene therapy. *Radiat Res* **154**, 365-374, doi:10.1667/0033-7587(2000)154[0365:dprrom]2.0.co;2 (2000).

100   Sasse, A. D., Clark, L. G., Sasse, E. C. & Clark, O. A. Amifostine reduces side effects and improves complete response rate during radiotherapy: results of a meta-analysis. *Int J Radiat Oncol Biol Phys* **64**, 784-791, doi:10.1016/j.ijrobp.2005.06.023 (2006).

101   Nakamura, R. E. & Hackam, A. S. Analysis of Dickkopf3 interactions with Wnt signaling receptors. *Growth Factors* **28**, 232-242, doi:10.3109/08977191003738832 (2010).

102   Mizobuchi, Y. *et al.* REIC/Dkk-3 induces cell death in human malignant glioma. *Neuro Oncol* **10**, 244-253, doi:10.1215/15228517-2008-016 (2008).

103   Yue, W. *et al.* Downregulation of Dkk3 activates beta-catenin/TCF-4 signaling in lung cancer. *Carcinogenesis* **29**, 84-92, doi:10.1093/carcin/bgm267 (2008).

104   Meng, X. M., Nikolic-Paterson, D. J. & Lan, H. Y. TGF-beta: the master regulator of fibrosis. *Nat Rev Nephrol* **12**, 325-338, doi:10.1038/nrneph.2016.48 (2016).

105   He, W. *et al.* Exogenously administered secreted frizzled related protein 2 (Sfrp2) reduces fibrosis and improves cardiac function in a rat model of myocardial infarction. *Proc Natl Acad Sci U S A* **107**, 21110-21115, doi:10.1073/pnas.1004708107 (2010).

106   Henderson, W. R., Jr. *et al.* Inhibition of Wnt/beta-catenin/CREB binding protein (CBP) signaling reverses pulmonary fibrosis. *Proc Natl Acad Sci U S A* **107**, 14309-14314, doi:10.1073/pnas.1001520107 (2010).

107   Konigshoff, M. *et al.* Functional Wnt signaling is increased in idiopathic pulmonary fibrosis. *PLoS One* **3**, e2142, doi:10.1371/journal.pone.0002142 (2008).

108   Trensz, F., Haroun, S., Cloutier, A., Richter, M. V. & Grenier, G. A muscle resident cell population promotes fibrosis in hindlimb skeletal muscles of mdx mice through the Wnt canonical pathway. *Am J Physiol Cell Physiol* **299**, C939-947, doi:10.1152/ajpcell.00253.2010 (2010).

109   Surendran, K., McCaul, S. P. & Simon, T. C. A role for Wnt-4 in renal fibrosis. *Am J Physiol Renal Physiol* **282**, F431-441, doi:10.1152/ajprenal.0009.2001 (2002).

110   Watanabe, M. *et al.* Immunological aspects of REIC/Dkk-3 in monocyte differentiation and tumor regression. *Int J Oncol* **34**, 657-663, doi:10.3892/ijo_00000191 (2009).

111   Mantovani, A., Garlanda, C. & Locati, M. Macrophage diversity and polarization in atherosclerosis: a question of balance. *Arterioscler Thromb Vasc Biol* **29**, 1419-1423, doi:10.1161/ATVBAHA.108.180497 (2009).

112   Zhang, Y. *et al.* Dickkopf-2 knockdown protects against classic macrophage polarization and lipid loading by activation of Wnt/beta-catenin signaling. *J Cardiol* **78**, 328-333,

doi:10.1016/j.jjcc.2021.04.010 (2021).

113   Wilson, M. S. & Wynn, T. A. Pulmonary fibrosis: pathogenesis, etiology and regulation. *Mucosal Immunol* **2**, 103-121, doi:10.1038/mi.2008.85 (2009).

7. Acknowledgements

Last but not the least, I would like to show the respect to the animals, which had to be involved in our experiment for the betterment of human kind.

Affidativ

Li Li

Surname, first name

Dachauer Straß 12B

Street

85764, Oberschleißheim, Germany

Zip code, town, country

I hereby declare, that the submitted thesis entitled:

DKK3 Driven Wnt Pathway in Radiation-induced Inflammatory and Fibrosing Skin Injury

is my own work. I have only used the sources indicated and have not made unauthorized use of services of a third party. Where the work of others has been quoted or reproduced, the source is always given.

I further declare that the submitted thesis or parts thereof have not been presented as part of an examination degree to any other university.

Munich,06.07.2023   Li Li
place,date   doctoral candidate Signature